PERFORMANCE STUDIES OF TEXTURED JOURNAL BEARING

A Thesis submitted to the Delhi Technological University, Delhi in fulfilment of the requirements for the award of the degree of

DOCTOR OF PHILOSOPHY

in

Mechanical Engineering

by

VIPIN KUMAR SHARMA
(2K15/PhD/ME/06)

Under the Supervision of

Dr. R. C. SINGH
(Professor)

Dr. RAJIV CHAUDHARY
(Professor)

DEPARTMENT OF MECHANICAL ENGINEERING

DELHI TECHNOLOGICAL UNIVERSITY

Shahbad Daultpur Bawana Road

DELHI-110042, INDIA

2019

DECLARATION

I hereby declare that the thesis work entitled "PERFORMANCE STUDIES OF TEXTURED JOURNAL BEARING" is an original work carried out by me under the supervision of Dr. R.C. Singh, Professor, Department of Mechanical Engineering, Delhi Technological University, Delhi, and Dr. Rajiv Chaudhary, Professor, Department of Mechanical Engineering, Delhi Technological University, Delhi. This thesis has been prepared in conformity with the rules and regulations of the Delhi Technological University, Delhi. The research work presented and reported in the thesis has not been submitted either in part or full to any other university or institute for the award of any other degree or diploma.

VIPIN KUMAR SHARMA

(Regd. No: 2K15/PhD/ME/06)

Deptt. of Mechanical Engineering

Delhi Technological University,

Delhi

Date: 10th August 2019

Place: Delhi

CERTIFICATE

This is to certify that the thesis entitled, "**PERFORMANCE STUDIES OF TEXTURED JOURNAL BEARING**" submitted by **Mr. Vipin Kumar Sharma** to the Delhi Technological University, Delhi for the award of the degree of **Doctor of Philosophy in Mechanical Engineering** is a bona fide record of original research work carried out by him under our supervision in accordance with the rules and regulations of the institute. The results presented in this thesis have not been submitted, in part or full, to any University or Institute for the award of any degree or diploma.

Dr. Ramesh Chandra Singh
Professor,
Department of Mechanical Engineering
Delhi Technological University,
Delhi, India

Dr. Rajiv Chaudhary
Professor,
Department of Mechanical Engineering
Delhi Technological University,
Delhi, India

Dedicated to

My Father (Sh. Mani Ram Sharma)

My Mother (Smt. Gayatri Sharma)

My Wife (Smt. Poonam)

&

My Sweet Lovely Daughter Baby Aradhya Sharma

ACKNOWLEDGMENTS

I would like to express my deep gratitude, sincere thanks and appreciation to my supervisors Prof. Ramesh Chandra Singh and Prof. Rajiv Chaudhary for their valuable guidance during this Ph.D. work. I am thankful from my heart for all the help, encouragement, and support you generously extended to me.

I would like to express, a sincere gratitude to Prof. R.S. Mishra, Chairman, DRC, Mechanical Engineering Department and Prof. Vipin, Head of the Department, Mechanical Engineering, Delhi Technological University, for their valuable help, motivation and extending all the necessary processing and experimental facilities during my research work.

Thanks are also due to Prof. R.K. Pandey, Prof. Surjit Angra, Prof. D.S. Nagesh, Prof. Reeta Wattal, Prof. Rajesh Aggarwal and Prof. Naokant Deo for serving my SRC committee and many critical help without which I would not be able to complete my thesis in time.

I am also grateful to Prof. Ranganathan M. S. and Prof. Naveen Kumar for all the motivation and their teachings, without that I would not be able to finish my thesis work.

My sincere thanks to all the faculty and staff members of Department of Mechanical Engineering (DTU), who supported me during my entire course work and research work. I am grateful to Mr. Rajesh Bohra, Mr. Tekchand, Mr. Manmohan and Mr. Rakesh Sharma (MAIT) for their technical and experimental support.

I am grateful to the management of at Maharaja Agrasen Institute of Technology, Delhi, particularly Dr. Nand Kishor Garg, Founder Chairman, Sh. Prem Sagar Goel, Chairman, Prof. M. L. Goyal, Vice Chairman (Academics), Prof. Neelam Sharma, Director and Prof. Vednath Mathur, Head, Department of Mechanical and Automation Engineering for the timely help and support in every possible way to finish this thesis work.

I would like to express my sincere thanks to Mr. Sidharth, Assistant Professor, MAIT, Mr. Ramakant Rana, Assistant Professor, MAIT, Mr. Sumit Chaudhary

(Research Scholar, DTU), and my students for their support and encouragement throughout this period.

I am also grateful to the expert examiners for improving the overall quality of the thesis.

I am short of words to express my sincere gratitude to my parents. Whatever I have achieved in my professional life; it is because of them. I cannot express in words their efforts to nurture me. I am also indebted to my brother Mr. Naresh and my sister Ms. Jyoti who always extended help whenever required.

I am unable to express my sincere gratitude in words for the affection, encouragement and support by my wife during the entire research work, without their support I could not have completed my work. They happily permitted me to focus all my attention on my research work and continuously provided me the encouragement to complete my Ph.D. Finally, I dedicate this Ph.D. thesis to my dearest Daughter Aradhya, for her love and care.

Last but not the least; I thank the Almighty for giving me strength to complete this work in all respects.

(Vipin Kumar Sharma)

Delhi
2019

ABSTRACT

The conventional journal bearing material contains varying amounts of lead (Pb) in it. Pb provides the anti-wear and anti-friction properties. However, Pb has hazardous effects on health and the environment and disposal of lead contained bearing and lubricant having lead particles from the bearing surface is an important issue which needs to be dealt with. Surface texturing of the bearing surface, the material of bearing surface, use of better lubricating conditions are some of the methods which could be utilized to reduce the wear and friction coefficient of the bearing material.

In this work, attempts have been made to improve the performance of a journal bearing. A lead-free bearing material is proposed which showed better tribological properties as compared to the conventional journal bearing material. Also, spherical surface textures were produced on the bearing inner surface to improve its performance.

Two copper based composites, Copper-Aluminium (Cu-Al), Copper-Phosphorous (Cu-P) and two aluminium based composite, Aluminium-Graphite (Al-Gr) and Aluminium-Flyash (Al-F) have been fabricated using the stir casting technique. Friction and wear properties of the fabricated materials have been studied using a pin on disc test configuration as per ASTM-G99 standards. The conventional lead-bronze bearing material (Cu-Pb) was also studied as a reference material and results of fabricated materials were compared with that of lead bronze material.

The Copper-Phosphorus material resulted in the least amount of wear as compared to other materials in this experimental study and Aluminium Flyash composite material resulted in the least value of the coefficient of friction, however, it exhibits maximum wear. The copper-phosphorous material exhibits a lower coefficient of friction value as compared to the conventional journal bearing material (Cu-Pb). Electric discharge machining methods have been used to generate spherical surface textures on the inner bearing surface. Experiments were performed for the conventional journal bearing and textured journal bearing using a journal bearing test rig. Frictional torque and fluid film pressure were measured for both the cases and results were compared. The textured journal bearing reduces the frictional torque significantly and improves the maximum fluid film pressure.

List of Publications

International Journals

1. R.C. Singh, Rajiv Chaudhary, **Vipin K. Sharma,** Fabrication and Sliding Wear Behavior of some lead-free Bearing Materials, Material Research Express, Vol. 6, Issue 6, **2019**, pp. 066533, (**SCIE, SCOPUS Indexed**) IOP Publishing.
2. **Vipin K. Sharma**, R.C. Singh, Rajiv Chaudhary, Experimental Study of Sliding Wear Behavior of the Casted Lead Bronze Journal Bearing Material, SAE Technical Paper 2019-01-0824, **2019**, (**SCOPUS Indexed**) SAE Publications
3. **Vipin K. Sharma,** R.C. Singh, Rajiv Chaudhary, Wear and Friction behaviour of Aluminium metal composite reinforced with graphite particles, International Journal of Surface Science and Engineering, Vol. 12 Issue 5/6, **2018**, pp. 419-432 **(SCIE, SCOPUS Indexed)** Inderscience Publication
4. **Vipin K. Sharma,** R.C. Singh, Rajiv Chaudhary**,** An experimental study of tribological behaviors of Aluminium- and copper-based metal matrix composites for bearing applications, Int. Journal of Materials Engineering Innovation (Accepted 17 October **2018**) (**SCOPUS Indexed)** Inderscience Publication
5. **Vipin K. Sharma,** R.C. Singh, Rajiv Chaudhary, Study of Starting Friction during the Running of Plain Journal Bearing under Hydrodynamic Lubrication Regime, SAE Technical Paper, 2018-01-0838, **2018 (SCOPUS Indexed)** SAE Publications
6. **Vipin K. Sharma,** R.C. Singh, Rajiv Chaudhary, Experiental Study of Tribological properties of casted aluminium bronze, Materials Today: Proceedings, Vol. 5 Issue (14), Part 2, **2018,** pp. 28008-28017 **(SCOPUS Indexed)** Elsevier Publication.
7. **Vipin K. Sharma,** R.C. Singh, Rajiv Chaudhary, Effect of flyash particles with aluminium melt on the wear of aluminium metal matrix composites, Engineering Science and Technology, An International Journal, Vol. 20 Issue (4), **2017**, pp 1318-1323, **(ESCI, SCOPUS Indexed),** Elsevier Publication
8. **Vipin K. Sharma,** R.C. Singh, Rajiv Chaudhary, Experimental Analysis of Journal Bearing Under Hydrodynamic Lubrication, International journal of advanced production and industrial engineering, Vol. 1 Issue 3, **2016**, pp.16-17 (ISSN: ISSN: 2455–8419)

International Conferences

1. Vipin K. Sharma, R.C. Singh, Rajiv Chaudhary, Analysis of leaded bronze hydrodynamic journal bearing: Experimental and Artificial Neural Network approach, New frontiers in engineering, science and technology-2018, January **2018**, pp. 731-735.(978-93-86238-41-2)

2. **Vipin K. Sharma,** R.C. Singh, Rajiv Chaudhary, Wear Testing of Al-Si Alloy Fabricated by Stir Casting, ISFT-2016**, 2016**, pp. 660-663 (ISBN: 978-93-84935-64-1)

3. Prem Kumar Aggarwal**, Vipin K. Sharma,** R.C. Singh, Modelling for the pressure distribution in fluid film of hydrodynamic journal bearing using SAE 20W40 lubricant, New frontiers in engineering, science and technology-2018, January **2018**, (ISBN: 978-93-86238-41-2)

4. Sumit Chaudhary, **Vipin K. Sharma,** R.C. Singh, Rajiv Chaudhary, Experimental Investigation of the Temperature Variation and Vibrations at Different Loads at the Periphery of Single Cylinder Diesel Engine, ISFT-2016, **2016**, pp. 660-663 (ISBN: 978-93-84935-64-1)

List of Contents

List of Figures

.

List of Tables

Chapter 1 Introduction

Hydrodynamic journal bearings are the most used machine components which are used to support the shafts. Turbines and engines directly depend on the performance on journal bearings for their high reliability. Usually, the supporting shafts of turbines and engines are subjected to high speed and load conditions. Under such conditions journal bearings are the one successful component to support the shafts, as the other bearings (Rolling element bearing) would likely to results in short lifespan.

The studies related to the journal bearings revolves around three categories. (1) measurement of friction as a function of bearing materials, (2) measurement of friction as a mean of lubricant oil, (3) measurement of friction around the bearing periphery.

The first ever work published on the performance of journal bearing was done by von Pauli (von Pauli, 1849). The friction was measured for a 120º partial journal bearings. The researchers tested 13 different bearing metals and a bearing alloy (91% Sn, 6% Cu, and 3% Zn) had the minimum friction coefficient as 0.0033.

Thurston (1879) provides the early work on the journal bearing friction by considering the effects of lubricating oils. The authors provided the early work on the journal bearing friction by considering the effects of lubricating oils. Goodman (1886) performed a number of experiments on lubricated journal bearings and concluded that the friction between the journal bearing system is due to interlocking and interference between the asperities.
Petroff (1883) attempts to correlate the friction calculations with the hydrodynamic theory of lubrication. With help from Margule's theory, Petroff proposed a formula for friction force (F).

$$F = \frac{\eta U}{h_{av}} \times (wetted\ \ area) \tag{1.1}$$

h_{av}=mean effective film thickness, η =viscosity, U = velocity

The third category of work comes from the Beauchamp Tower. Tower (1891) proposed a new tactic to the experimental study of lubricated contacts. A series of experiments were conducted for the lubrication of railroad bearings. A hole was drilled for feeding the lubricant in the bearings, however, lubricant tends to come out from that hole whenever the shaft rotates with high speeds. It was concluded that the pressure was generated by the rotating

shaft in the lubricant film. This work laid the foundation for further studies in the field of journal bearings.

During the operation of the journal bearing, the shaft rolls itself up in the bearing in a direction opposite to the desired rotation. This was due to the initial metal to metal friction between the shaft and bearing. As adequate lubricant was supplied, the wedge-shaped lubricant film forms up immediately which lift the shaft in steady-state position.

Friction and wear are the two most critical factors due to which a particular machine component fails. During the designing of the elements, these two are kept in mind by the designers. The material of the journal (shaft) and bearing, surface roughness values, operating conditions are some of the factors on which the wear and friction coefficient value in a journal bearing depend.

In journal bearings, the relative motion between the bearing and shaft is sliding in nature. It has surface contact and makes a lower pair.

1.1 Purpose of Lubrication

In most of the industrial applications, lubricating oils are used to prevent the friction between the tribo-pairs. These oils also helps in reducing the wear. A lubricating oil is a substance which is applied in between two parts to reduce or decrease the friction and wear. Apart from separating the two parts, lubricants also helps in lowering the temperature of the system and also takes away or removes the wear debris.

A lubrication oil is a balanced mixtures of different components. A typical lubricating oil contains nearly 90 % base stock and rests amount consists of various additives. Petroleum derived compounds are the commonly used base stock, however, liquid solutions obtained through chemical actions or edible / non edible oils can also be used as base stock.

The primary functions of the lubricating oil are to:

- Lubricating oil must keep the surface separated under all the operating conditions. Operating conditions like speed, load and temperature. This keeps the friction and wear values to least.
- Apart from lubrication, lubricating oil also should act as the cooling medium between the tribo-pairs.

- The properties of lubricating oil like viscosity, density does not get change with operation and remains same.

1.2 Types of Lubrication

- Hydrodynamic lubrication
- Hydrostatic lubrication
- Elasto-hydrodyanamic lubrication
- Boundary lubrication
- Solid Film lubrication

In hydrodynamic lubrication regime, material surfaces which carries the load are separated with the help of a thick lubricating oil film. This oil film avoids the metal to metal contact. This type of lubrication requires adequate amount of oil at all the time during the operation of the system. The geometric position and motion of the shaft pulls the oil into a wedge shaped region at a sufficient velocity and generates the pressure enough to separates contacting surfaces against the load on the system. For the analysis of hydrodynamic lubrication, basic laws of fluid mechanics are used. Hydrostatic lubrication is produced by providing the lubrication oil (air or water may also be used) to the load carrying region with the help of external agencies. The pressure applied by the external agencies should be high enough to separate the contacting systems. The velocity of the shaft does not greatly affect the performance of the system. Elastohydrodynamic lubrication phenomenon occurs when the lubricating oil is poured in between the material surfaces which are normally in rolling contact (rolling element bearings or meshing gears). The mathematical explanation of this requires the Hertzian theory of contacting stress along with fluid dynamic equations are required to completely explain this phenomenon.

During the operation, if the surface area is slow, reduction in velocity of the moving surfaces, an increase in applied load, lessening of lubricating oil are the possible reasons due to which the lubricating oil film between the mating parts gets thin which prevents the formation of full film lubrication regime. This type of lubrication is known as boundary lubrication. During this, the asperities are separated by several molecular dimensions in thickness only. The change from full film lubrication regime to the boundary lubrication regime does not happen abruptly. Firstly, a mixed region of lubrication is formed and as the surfaces come

closer to each other with time, the mixed region of lubrication changes to boundary lubrication.

The ordinary lubrication oils does not perform efficiently at extreme temperature conditions, a solid lubricant layer of molybdenum or graphite is generally used to separate the contacting systems. The graphite or molybdenum powders are efficient enough to work in elevated temperature conditions as well. This type of lubrication is called as solid-film lubrication

Based on the lubrication type, there are three categories of journal bearings, (1) hydrodynamic, (2) hydrostatic and (3) hybrid journal bearing.

1.2.1 Hydrodynamic Journal Bearings

In the hydrodynamic type of journal bearings, the clearance between the journal and bearing (shaft) is filled with lubricant. The bearing remains fixed and journal is located with some eccentricity with the bearing surface. With the rotation of the journal, the lubricating oil moves and creates a wedging section. This wedging section generates the pressure which is used to lift the journal. By this action of the lubricant, the applied external load can be buoyed by the lubricant oil film without metal to metal contact between the journal and bearing.

1.2.2 Hydrostatic Journal Bearings

In the hydrostatic type of journal bearing, a thick film of lubricant is made to form between the journal (shaft) and bearing material surfaces by continuously providing the lubricating oil at some pressures with the help of several flow control/restricter devices. Various restrictors along with several flow control devices which are generally used for these type of bearing are represented by Figure. The oil from the oil tank is pumped with help of a motor operated pump. This pressurized lubricating oil is made to pass through various restrictors and flow control devices to the spaces between bearing and shaft.

1.2.3 Hybrid Journal Bearings

The hybrid journal bearings use the mechanism of hydrodynamic lubrication system as well as a hydrostatic lubrication system. In the operation of hydrodynamic journal bearing systems, the starting and stopping friction are the main reasons of wear. In hybrid journal bearing systems, the wear which is produces during the starting and stopping duration of the journal bearing system is normally avoided. These bearings are also capable to tolerate loads above the designed loads as well

(a)

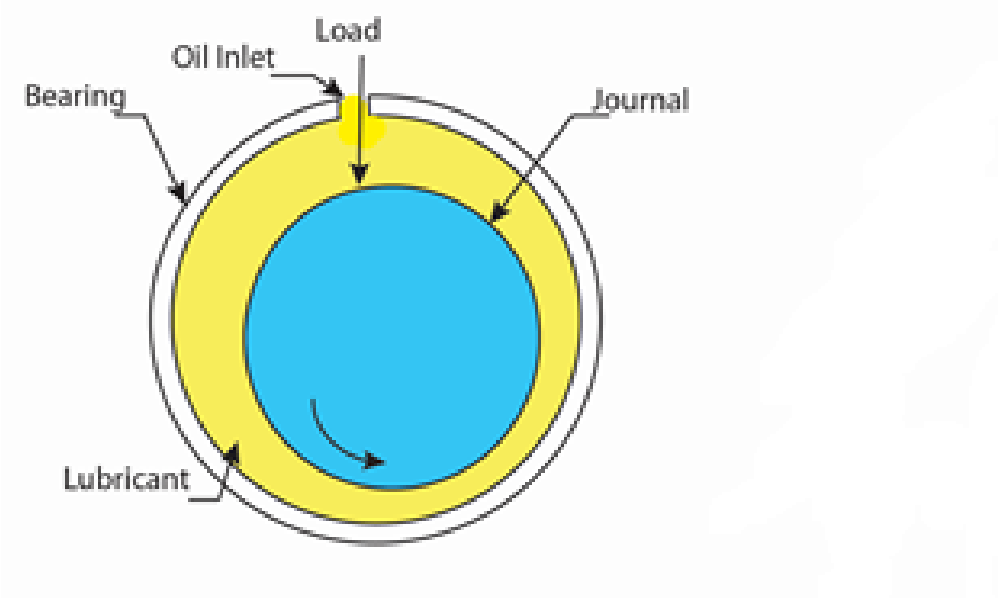
Load
Oil Inlet
Bearing
Journal
Lubricant

(b)

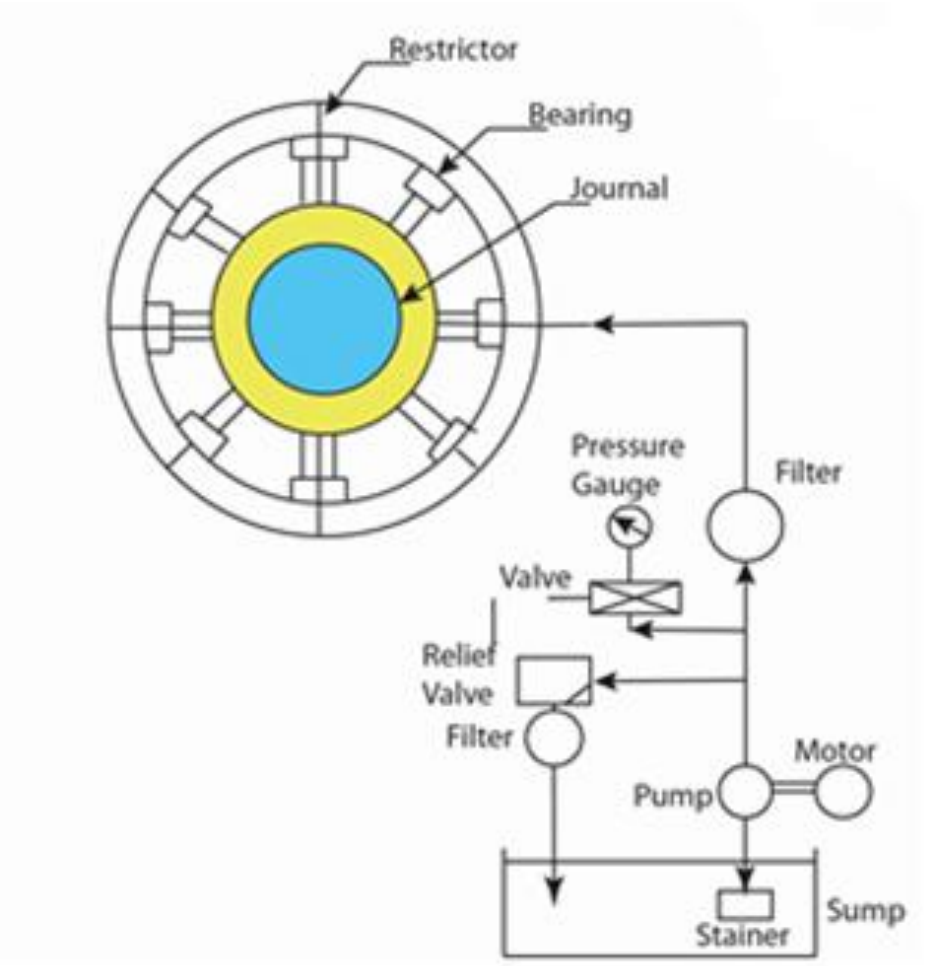
Restrictor
Bearing
Journal
Pressure
Gauge
Filter
Valve
Relief
Valve
Filter
Motor
Pump
Sump
Stainer

(c)

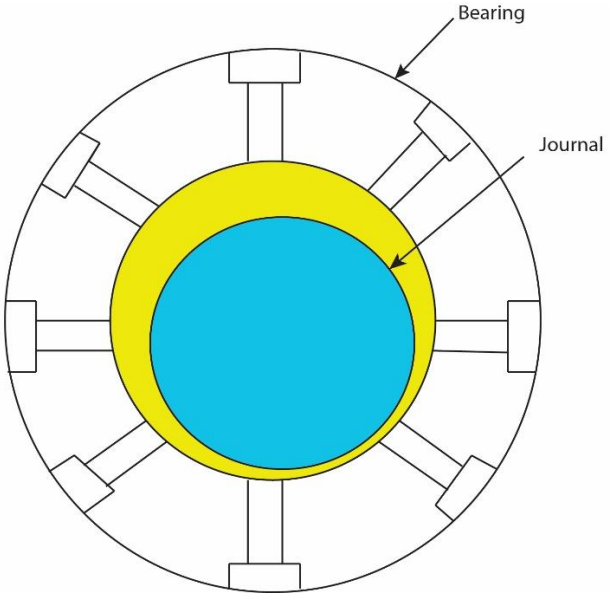

Figure 1.1: (a) Sketch of hydrodynamic journal bearing system (b) hydrostatic journal bearing (c) Hybrid journal bearing

1.3 Petroff's Equation

Petroff's equation explained the bearing friction by assuming that, the shaft and bearing are concentric. Petroff was the first who introduced the bearing friction. It defines the bearing friction in terms of dimensionless parameters. Equation 1.2 presents Petroff's equation

$$f = 2\pi^2 \frac{\mu N}{P} \frac{r}{c} \tag{1.2}$$

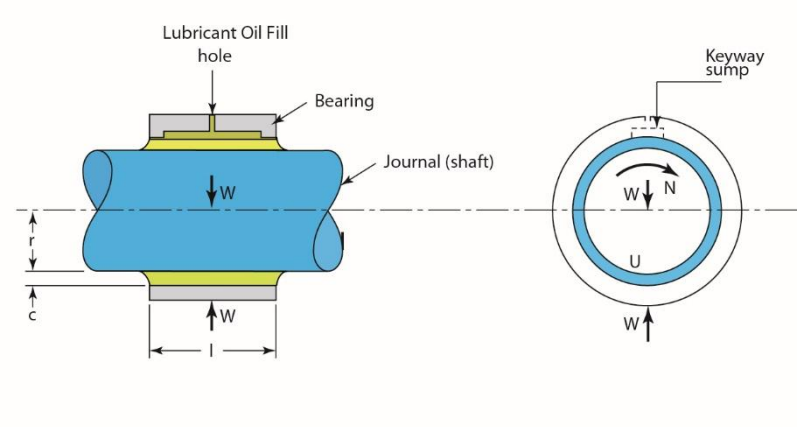

Figure 1.2: Presentation of concentric journal and bearing assembly

Further, friction torque (T_f) may be given as,

$$T_f = f \times w \tag{1.3}$$

1.4 Stable Lubrication

The transition or difference between the hydrodynamic and boundary lubrication can be explained with the help of a stribeck curve. Stribeck curve, presents the coefficient of friction with bearing characteristic number. This curve defines the stability of the lubrication and helps in better understanding of the hydrodynamic and boundary lubrication.

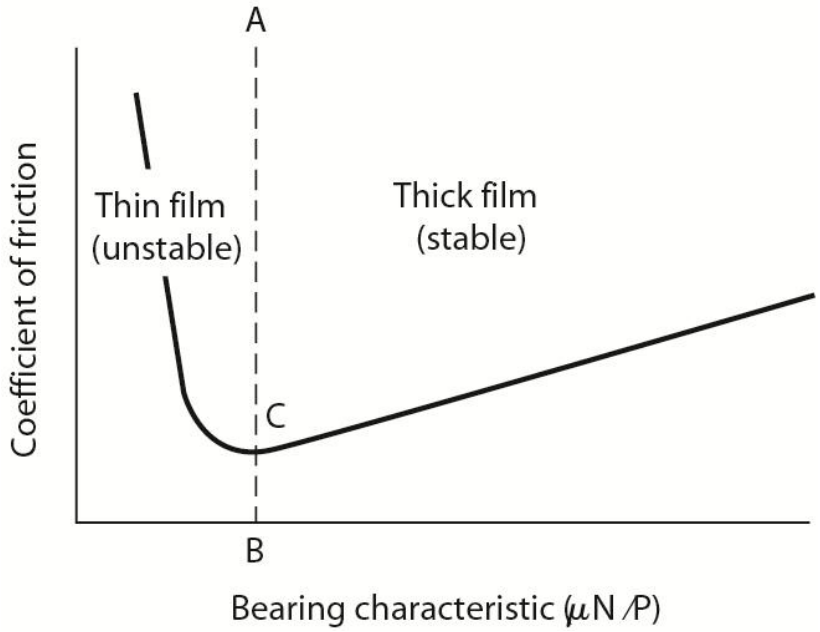

Figure 1.3: Stribeck Curve

In this curve, the left part of AB presents the thin film region lubrication region and right side of AB presents the thick film lubrication section. For the applications operating on the right side of AB, if there is some increase in temperature value, the viscosity values of the lubricant get a decrease. With this decrease in viscosity, the friction coefficient also gets decreases. During this, not much amount of heat is produces in shearing the lubricating oil film and hence the temperature of the lubricating oil film reduces. Therefore the region to the right of AB represents the stable lubrication region as the changes are self-correcting. On the other hand, on the left side of AB with increase in temperature viscosity gets decreased and hence the coefficient of friction further increase. This increase in coefficient of friction will generate more heat and will decrease the viscosity. Due to this the results will be get add up. Therefore this region presents unstable lubrication. Table 1.1 presents the features of different lubrication regimes.

Table 1.1: Features of different lubrication regimes.

Lubrication Regime	Bearing and Journal contacts	Film thickness range	Friction coefficient	Wear	Features
Thick Film	Contacts are only during start-up and stopping	10^{-3}-10^{-4}	0.01-0.005	None	Light applied loads and high journal rotation speed. The friction of coefficient is related to μN/[W/LD]
Thin Film	Intermittent dependence on surface roughness values	10^{-4} to 0.5×10^{-4}	0.005-0.05	Mild	High operating temperatures
Boundary	Surface to surface contact	To molecular level thickness	0.05- 0.15	Large	Heavy applied loading and slow speeds. Heat generation and friction coefficient does not depend on viscosity of the lubricating oil.

1.5 Formation of Thick Film

Figure 1.4 presents, the formation of thick film lubrication in journal bearing operation. During the starting condition when there is no lubricating oil in the between the clearance space, the bearing will be dry and shaft will try to climb on the right side. Now with the addition of lubricating oil into the system, the rotation shaft will move the oil around the periphery of the bearing in the rotating direction. The lubricating oil forces itself to a wedge-shaped section and pushed the shaft to the other side.

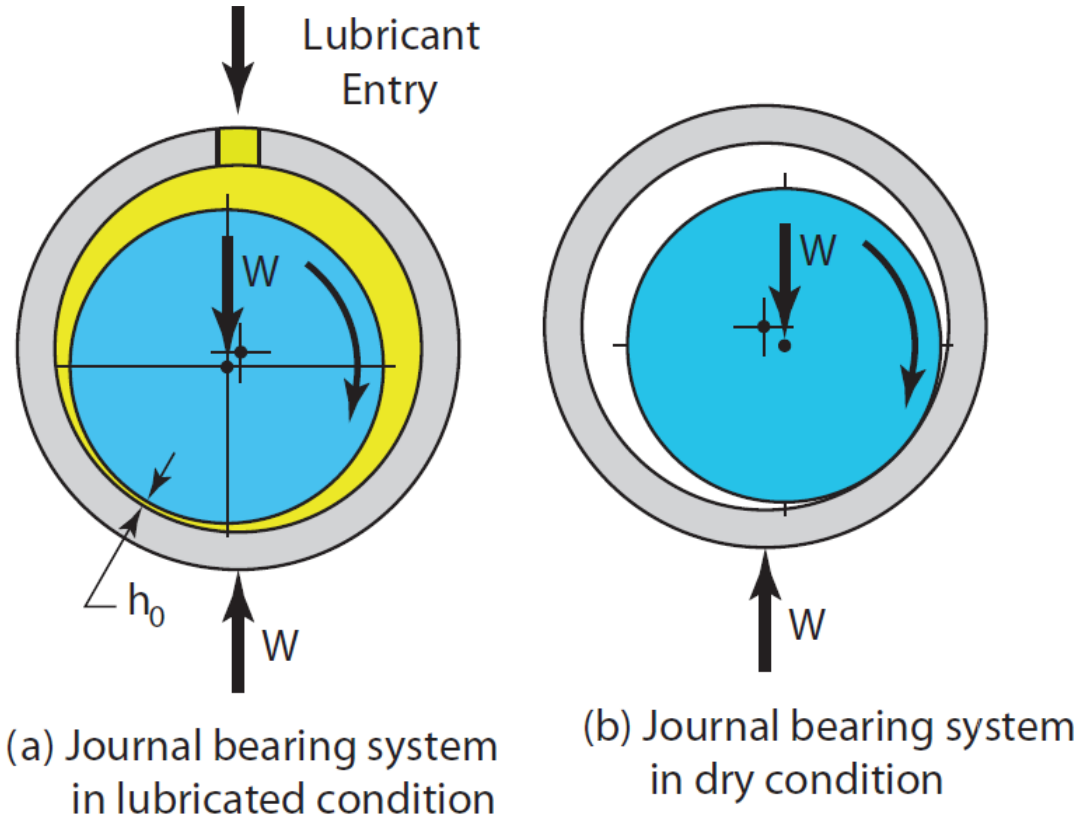

Figure 1.4: Journal bearing operation in lubricated and unlubricated condition.

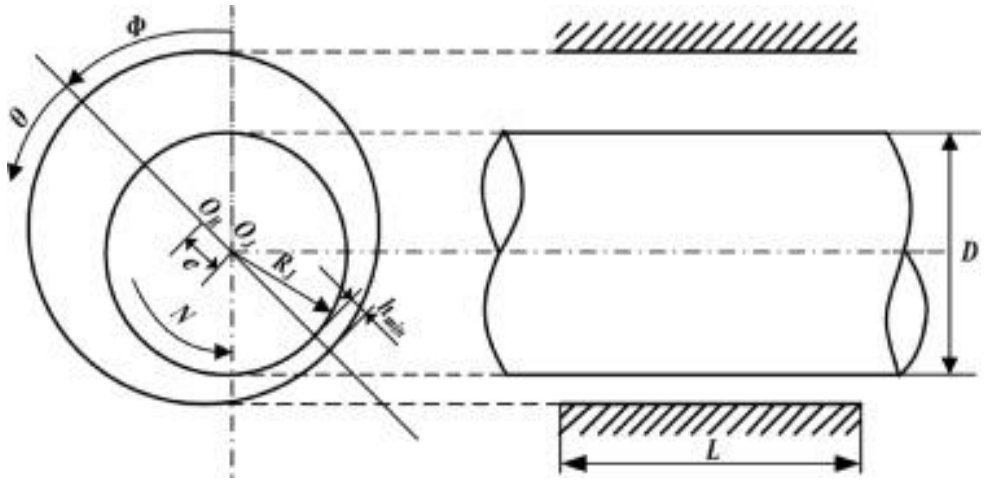

Figure 1.5: Basic Nomenclature of the journal bearing assembly

The Figure 1.5 presents the basic nomenclature of the journal bearing, 'O_j' and 'O_b' shows the journal center and bearing center. Symbol 'e' presents the difference between the center of journal and bearing. It is termed as eccentricity. The parameter 'h_{min}' shows the minimum film thickness. Rj is the journal radius and 'N' represents speed of the journal in revolution

per minute (rpm). 'L' is the bearing length and ratio of eccentricity to the radial clearance is known as the eccentricity ratio.

1.6 Journal and Bearing Configurations

1.6.1 Bearing Geometries

The cost and ease of producing the bearing geometry, working loading conditions, power loss during operation, dynamic properties, and ease of installation are some of the factors on which the choice of a particular bearing depends. The design of bearing varies from simple plain to complex titling pad bearings.

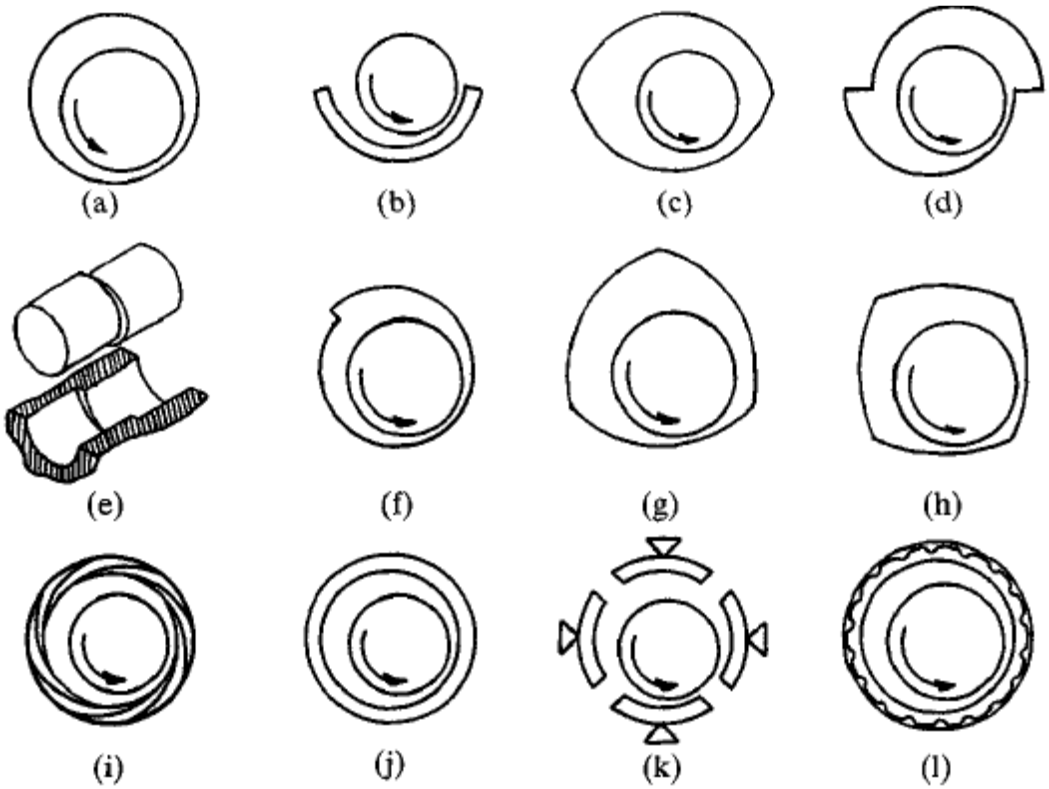

Figure 1.6: Shapes of bearings used for the journal bearing system (a) Full journal bearing profile (b) partial bearing; (c) elliptical bearing profile (d) offset type bearing; (e) rocking type journal bearing; (J) pressure dam type bearing; (g) three-lobe type bearing; (h) four-lobe bearing; (/) multileaf type bearing; (/) floating ring type bearing; (k) pivoted pad bearing; (/) foil type bearing.

Full bearing configurations are those in which the bearing surface completely surrounds itself around the journal (shaft) surface. These are easy to construct and are the most used bearings in rotating machinery. However, during the installation process, the circularity of the bearing distorts slightly. If the bearing surface only surrounds for 180^{o} or less, then it is termed as partial bearings. Partial bearings are used when the load is unidirectional only. These

bearings result in lower frictional force values and these do not require many tolerances during the manufacturing. If the radius of the bearing is more than the radius of journal, these type of bearings are known as clearance bearings and if the radius of bearing and journal are same it is termed as a fitted bearing.

Configurations in which two circular bearing half are machined and joined together are termed as elliptical/lemon bearings. These type of bearings are used in applications of slow and moderated speeds. In elliptical bearings, if the two halves of the bearing are displaced about the major axis. These are known as offset bearings. These bearings have high horizontal stiffness, which provides dynamic stability. Further, offset bearings allows a greater flow of the lubricating oil which in result reduces the overall temperature of the journal bearing system.

Journal bearing configuration in which shaft as well as bearing surfaces are separated axially into slices with the offset centerlines. This type of arrangement of shaft and bearing generates a dynamic rocking movement which in result produces a thick lubricating oil film. These type of bearing are called as rocking journal bearing.

When a step is machined from the bearing surface, the resulting bearing configuration is termed as a step, or pressure dam, bearing. This additional step in the bearing provides the extra hydrodynamic pressure when the lubricating oil rotates in the machines step. This extra pressure buildup improves the load carrying ability of the bearing and diminishes the problem of vibration during the operation of the journal bearing system.

Bearing configurations having three or more than three sectors are called as lobed or multi-lobed bearings. These bearings perform as a number of different partial bearings and are used in gas-bearing applications.

The multi-leaf journal bearings consist of a number of similar circular arcs or grooves. The operating features of a multi-leaf bearing does not depend on the loading directions for bearings having eight or more grooves.

In the floating-ring type bearing system, the lubricant oil film is separated in two by introducing a floating ring between bearing and journal. These bearings have relatively low frictional losses, low heat generations and provide greater stability. Pivot-type bearings have also been used as these can accommodate small variations of journal deflection or misalignments. A foil journal bearing has a thin compliant bearing surface which rests atop a number of different corrugations. With comparison to the conventional journal bearing

system, the foil bearings have thicker oil film, better load carrying capacity, low power loss, better vibrational stability, and endurance at higher operating temperatures.

1.6.2 Journal configuration

In the journal bearing system, it is expected that the journal surface should be a perfect circular. However, due to limitations in manufacturing and wear effects, the journal of different shapes and profile are used. These different shapes of the of the journal are presented in Figure 1.7 (a-c). The grooving in the journal surfaces has also been done to enhance the performance of the journal bearing setup.

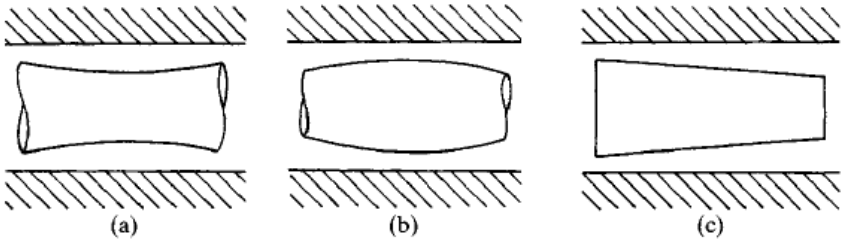

Figure 1.7: Journal shapes used in the journal bearing system (a) Hourglass (b) tapered type (c) barrel

1.7 Bearing Materials

Good anti-wear and frictionless properties are the basic requirements of the bearing material. Apart from them, embeddability, machinability, anti-seizure and corrosion resistance properties are also expected from the bearing material. Copper (Cu) alloy is the most used material for the bearing fabrications, as it offers good strength and corrosion resistance. By considering the various desired properties for a bearing material, copper alloy as tin bronze, phosphorous bronze, and lead (Pb) bronze materials are largely used. The alloying of Pb in Cu improves the sliding properties of the Cu. The Cu-Pb alloy system is generally characterized by partial solubility in a liquid state and insolubility in a solid state. The final structure, after the solidification process, has Cu and Pb crystals. Pb provides the soft phase to the copper which lubricates it under sliding applications. Besides having very good properties, the disposal of Pb is a difficult task. A substantial amount of Pb contents are released in the environment during the fabrication and working of machine components made up of Pb contained alloys. So attempts were made by researchers to minimize the usage of Pb contained alloys or to minimize the wastage which contains lead contents. Researchers had suggested replacing the conventional Cu-Pb alloy with Cu-Carbon fiber, Cu-graphite, and Cu-Aluminium. The disposal of lead in the Cu-Pb alloys is a big concern which needs to be dealt with. Lead contains inherent toxicity which causes chronic effects on animals and

humans as well. So the harmful effects related to the use of lead contained machine parts and disposal of it have been noticed in recent times and numerous studies have been performed in the field of the journal bearing materials.

1.7.1 Tribological Requirements

Good wear resistance, embed-ability, corrosion resistance, seizure resistance and low friction are the basic tribological requirement of the journal bearings.

1.7.1.1 Wear and Friction

In general, the properly lubricated bearing does get to wear very easily. It can operate without any damage for a long time. When operating under the hydrodynamic regime, the rheological properties of the lubricant used determines the friction. Under boundary and mixed lubrication regime, the tribological properties are calculated by the material of the journal and the bearing. The choice of optimized bearing design and bearing material helps in reducing this wear and friction. Apart from this, nowadays formulated lubricants with nano-particles are used to reduce the wear and friction. However, if the operating conditions are not controlled, this may lead to damage of bearing surface, as the shaft (journal) material is harder than the bearing material. Misalignment of journal, extreme operating conditions, and incorrect design cause the wear of bearing surfaces. With misalignment or faulty design of the journal bearing assembly, the clearance between the journal and shaft reduces which may result in damage of the bearing surface. The cavitation erosion is another big cause for the wear of the bearing surface. The cavitation region occurs in the journal bearing assembly when the continuity of the lubricant oil breaks. It occurs on the regions of bearing surface that has under the effect of low lubricant pressure.

1.7.1.2 Seizure Resistance

This type of failure in the bearing system occurs when it runs at extreme loads, speed, and temperature and under the oil starvation condition. In these conditions, the chances of the breaking of the lubricant oil film get increased. This may give rise to direct metal to metal contact. Due to this contact, severe adhesion of the bearing surface and journal occurs and result in damage to bearing and journal. Ideally, if a material has good wear resistance, it shall survive the metal contact with the counter surface in the situation of starvation of lubricating oil. Heavy wear, noise, and vibration are the after effects of the seizure. In lubricated conditions, scarcity of lubricant oil is the main cause of seizure in the journal bearing system. The metal to metal contact results in heavy wearing and increase in

temperature. The wear debris produces during this also helps in initializing the seizure. In dry conditions, loss of clearance, thermal expansion, and wear debris agglomeration are the main causes of seizure. Due to the higher friction, the clearance between the journal and bearing changes and interlocking between the mating parts takes place. This agglomeration of wear debris also increases the contact pressure which in the result, increases the torque required for the rotation of the shaft.

1.7.1.3 Embeddability

The ability of the bearing material to embed the wear debris particles and contamination so that, it does not damage the journal surface is called as embeddability. In journal bearings, the oil film thickness varies with the oil film pressure. There is a larger tendency to wear at the lowest oil film area. In the operation of the journal bearings, the wear debris travels with the lubricant. If the size of the wear debris or contaminations is smaller than the minimum oil film thickness, then the wear particle keeps on traveling with the lubricant. For the cases, where the size of the wear particle is greater than the least oil film thickness, the wear particle may damage the shaft surface. For preventing this, the bearing materials play a pivotal role. The presence of soft phases in the bearing material helps in providing the required embeddability properties of the bearing material. The lead (Pb) particles in Copper alloys and tin (Sn) in aluminium alloys helps provides the embed-ability to the materials.

1.7.1.4 Corrosion resistance

The lubricating oil used in the journal bearing systems tends to oxidize under high operating temperatures which causes deterioration of bearing and shaft properties. For lead contained bearing materials, the soft lead phases get leached away from the material which results in corrosion damage.

1.8 Organization of Thesis

The whole thesis work is divided into five chapters.

Chapter 1 – Introduction

This chapter deals with the history and introduction about the journal bearing performance. Different properties of the journal material were discussed along with its types.

Chapter 2 – Literature Review

This chapter describes the previous works carried in the field of the journal bearing analysis. In this chapter, previous works in the areas such as performance studies of journal bearing, journal bearing materials and textured journal bearing systems are reviewed. The gap in literature and the objectives of the present work were also discussed in this chapter.

Chapter 3 - Methodology and Experimentation

This chapter discusses the methodology and experimentation for achieving the objectives of the thesis. This chapter is divided into three parts. In the first part, two aluminium and two copper-based materials were fabricated using the stir casting method. Pin on disc experiments were carried out as per ASTM-G99 standards. In the second parts, a journal bearing tribo-system is fabricated, one without textures and one by incorporating the textured surface. Design and development of the surface textures on the bearing surface are also discussed. The experimental tests for both, conventional and textured surfaces were carried out. In the third part, the computational fluid dynamics module of the ANSYS software is used to model a journal bearing system.

Chapter 4-Result and Discussion.

This chapter presents the results of experimental work and ANSYS modeling. The results of computational fluid dynamics study, pin on disc experimentation and journal bearing experimentation with discussion were presented.

Chapter 5-Conclusions and Future Works

This chapter highlights the main conclusions of the work. Scope for future works was also discussed.

Chapter 2 Literature Review

This chapter presents the research findings in the field of journal bearings. The whole chapter is divided into three parts. The first part presents the works of the researchers in the area of the journal bearing performance. The second part includes research work from the field of bearing materials. The third part has recent works related to the effects of textured surfaces on the performance of journal bearings. After reviewing the research articles the possible gaps in the literature were discussed.

Based on the literature gaps and discussions with the experts from the field of the journal bearing research, objectives of the present work were selected.

2.1 Journal Bearing Performance

Bouyer and Fillon (2011) experimentally found out the effect of different shaft materials, bearing roughness, and journal rotational speed on the friction coefficient in a lubricated journal bearing system. It is reported that the friction coefficient during the start-up of the journal bearing system increases with the increase in surface roughness. Three bronze bearing with varying length and one steel bearing with babbit overlay were used to conduct the experimental study. The friction coefficient value almost remains constant between 0.16-0.20. Ahmad et al. (2014) experimentally found out the effects of oil groove location and lubrication supply pressure on the temperature and lubricant film pressure. Experiments were performed at different load and journal speeds. Authors reported that the temperature profile decreases when the oil groove is located in the converging section or minimum film thickness region.

Gao et al. (2014) utilized the concepts of computational fluid dynamics to evaluate the effects of eccentricity ratio on the pressure profile for a water lubricated journal bearing system. It is reported by authors that high and low eccentricity ratios are not preferred for designing the water lubricated journal bearing system. Eccentricity ratio of 0.6 and 0.7 are the better choices for a journal bearing system with water as lubricating oil. With this study, authors suggest the initial diameter dimension, to design an efficient plain journal bearing under water lubricated hydrodynamic lubrication.

Muzakkir et al. (2015) analyzed the effects of cylindricity and bearing clearance on the performance of a heavily loaded slow speed journal bearing system. A lubricity tester having block and disc system was used to estimate the sliding distance required to reach the steady

wear. A mathematically model was also developed to estimate the wear. This model gave the results with an error of about 8.8 % and suggests that wear in journal bearing system is a localized phenomenon which directly depends on the cylindricity.

Durak (2016) designed and developed a journal bearing test rig for the measurement of fretting wear in the journal bearing system. A micro vibration motor was attached with the shaft system to provide the vibrations of the amplitude ranging between 0-100µm. An AlSn20Cu bearing was used for the analysis and formation of fretting wear patterns are studied at different frequencies. An increase in remainder force, surface roughness and wear scar and decrease in friction coefficient were observed by the authors.

McCarthy and Glavatskih (2009), measured the friction coefficient during the dry starting condition. The friction coefficient and wear values were evaluated during the transition between the stationary state and moving state at the startup. A block ring test apparatus was used by authors for the investigation. Christensen and Tonder (1971) described the application of the hydrodynamic theory of lubrication of rough bearing surfaces. The analysis of a full journal bearing (with finite width) is done with the help of this theory. This paper mainly focuses on how the roughness influences the characteristics of the bearing and corresponding bearing response is obtained. The result shows that the effect of surface roughness on the characteristics of a journal bearing is small in most cases. The result of this experiment agrees with the hydrodynamic theory of lubrication of rough bearing surfaces. Near the hydrodynamic limit, roughness shows an appreciable effect. The expression is obtained from Reynolds's equation. Tzeng and Saibel (1967) studied the friction, pressure generation, load carrying capacity under the effect of surface roughness of the journal bearing surfaces. The surface roughness is represented as a probability density function and evaluated experimentally. With the surface roughness the friction force between the journal and bearing assembly increases, however, the increase in the load carrying capacity is very significant. It is reported that, a very finished surface leads to less satisfactory results from the hydrodynamic lubrication theory. Wang et al. (1997) studied the phenomenon of mixed lubrication in a finite journal bearing having large eccentricity ratios. This study was based on the effects of bearing deformation, surface finish and asperity interactions. In this study, authors utilized the average Reynolds equation to analyse the effects of surface roughness on lubricant flow. The FEM-based influence-function method was considered to calculate the deformations under hydrodynamic pressures. The results showed that the maximum average

pressure, corresponding to the highest eccentricity ratio was approximately 40 MPa at 1500 rpm. In most of the cases, the journal bearing was operating under a mixed lubrication regime without any seizure.

Poddar and Tandon (2016) experimentally studied the vapour cavitation of journal bearing using vibration, acoustic emission, and oil film photography. Their set-up consisted of a journal bearing rig with transparent sleeve, a bronze bearing insert and LED illuminator. Their study found the cavitation to be of a vaporous type. The acoustic emission results confirmed the occurrence of vapour cavitation due to the generation of the elastic transient wave. From the vibration results, it was found that the vapour cavitation played a significant role in dampening of rotor vibrations. Harnoy (1995) develops an analysis for the time-variable friction during the start-up of a journal in a lubricated-sleeve bearing. A dynamic friction model has been developed from the theory of unsteady lubrication. A stribeck curve is also developed between the friction vs. Steady velocity and hysteresis curve is obtained in case of oscillating velocity. The result shows that friction can be reduced by high start-up acceleration. A reduction in the maximum friction force and friction energy losses is obtained when bearing support is flexible. High start-up acceleration can't be achieved in every bearing. This paper indicates various alternatives to increase the torsional stiffness of the shaft which provides flexible bearing support. Desai and Patel (2005) studied about the pressure distribution analysis in hydrodynamic journal bearing for various loading conditions and various operating parameters like materials, types of lubricant, size, clearance, rotational speed, supply pressure range etc. In the experimental work, the test bearing was located between two anti-friction bearings. The bearing is then tested under different parameters like type of lubricant, loading conditions and speed etc. in the last they have compared the experimental result to the theoretical values and results are found satisfactory. Abhijeet et al. (2015) studied the variations in vibrations of journal bearing due to different lubrications, which has a significant impact on the stability, performance on an operational point of view. The research investigated the impact of viscosity on the stability of plain hydrodynamic journal bearing. As part of this research, experimental data was collected for different combinations of lubricant viscosity, shaft speed and load. The study after analysis concluded that lubricant viscosity has an evident effect on vibrations of the system. Thinner oils show fewer vibrations at higher speeds, while thicker oils show less vibrations at low speeds. A numerical and experimental approach has been developed to study the vibrations of the journal bearing.

Keogh et al. (1997) used the CFD based design techniques to predict the bearing thermal conditions. They were applied to a generic two-axial groove circular bearing. Two-dimensional parameters which incorporated the lubricant shearing, convection, conduction, and viscosity-temperature variations were taken into account. The numerical solutions obtained on CFD were based on FVM approach. These parameters were varied using CFD computations to obtain a design chart for maximum bearing shell and journal temperature. The design charts are efficient and without numerical complexity. Dhande and Pande (2016) study about implemented a fully three-dimensional CFD analysis and multi-phase flow phenomenon for stimulation of hydrodynamic journal bearing considering the realistic deformations of the bearing with Fluid-Structure Interactions (FSI) along with cavitation. In this, a new numerical method comprising CFD and FSI methodology with optimization is proposed where both inertial as well as cavitation effects are considered. It is obtained that the pressure build up in journal bearing is lower with cavitation as compared without cavitation. The peak pressure increases with an increase in both shaft speed as well as eccentricity ratio. The computation time also reduces. Vijayaraghavan and Brewe (1998) studied the rate of viscosity variation on the performance of journal bearing. In this study, they utilized the Roeland model on viscosity-temperature-pressure which characterizes the viscosity profile of a lubricant when viscosity values are known corresponding to two unique temperatures and pressures. To incorporate the cavitation effects and distribution of fluid properties across film thickness, THD numerical model was used. A high viscosity lubricant was used for the study and performance parameters and pressure distribution are determined. The results showed that the effects of rate of viscosity variation are diminished if the lubricant supply temperature is lower than the temperature at which the viscosity of the lubricants is same. Santos et al. (2012) studied hydrodynamic journal bearing by applying the ideas in Generalized Integral Transform Technique (GITT) to solve the Reynolds equation. This approach is an Eigen function expansion methodology for solving multiphysics problems. Extensive parametric analysis was done and the results were compared with the GITT approach to show its consistency. The GITT approach was successfully employed in the analysis and can be extended to take into account the dynamic cavitation, bearing deformations and heat exchange.

Some authors also developed software models to predict the behavior of the system during start-up. Krithivasan and Khonsari (2003) modeled a finite element model for the journal

bearing system and predict the seizure of the journal during startup conditions. Ettles et al. (2003) generates some design models for the thrust bearings and suggested the technique of jacking oil lift during the shut-down and start-up of the thrust bearing to prevent its seizure. The starting friction also causes a rise in temperature of the oil film. Wang et al. (1997) compare the fast and slow start-up conditions for the measurement of oil film temperature. The amount of temperature rise of the oil film in case of a fast start-up was low as compared to slow start-up conditions. Pistner (1996) conducted an experimental study of the start-up friction of the shoe bearing of a hydraulic pump. The temperature of the thrust pad increases very fast during the initial stage of the running i. e. start-up, which is results, induces the rupture of the lubricant film. This problem of sudden temperature rise could be minimized by preheating the thrust pad before using for the actual working or supplying the lubricating oil at a bit higher temperature. Similarly, the use of mineral and synthetic oils can also minimize the friction and wear of the elements. There is a number of different methods which are used by researchers to reduce the friction force and wear from the journal bearing tribopair.

A polymer liner was incorporated by Linjamaa et al. (2016) in a hybrid journal bearing and various elastic and thermal deformations of the surface of bearing were evaluated to enhance the performance of the bearing. Finite element modeling technique was used by authors to evaluate the parameters. To improve the load carrying capacity and coefficient of friction improvement Bompos et al. (2016) proposed a multistep journal bearing. Overall there was an improvement of 38 % in coefficient of friction and 9.7 % in load carrying capacity of the multistep bearing as compared to the plain journal bearing. Khatri and Sharma (2016) used FEM for solving the Reynolds equation. Power law was used for shear stress-strain relation. Textured and untextured bearing surfaces were studied and textured resulted in better stability. Kim and Jeon (2008) experimentally found out the effects of engine oil viscosity change on the engine oil seat frictional torque. It is reported by authors that, engine oil seat frictional torque decreases with low viscosity engine oil.

2.2 Journal Bearing Material

One feasible solution to reduce the wear from the bearing is to change the bearing material to one which shows better wear resistance as well as good machinability, embed-ability, and anti-seizure properties. Lead bronze is mostly used for the fabrication of journal bearings because of its very good anti-friction properties. The lead element in the bronze helps in providing the anti-friction properties. However, the disposal of lead contained bearing and lubricant having lead particles from the bearing surface is an important issue which needs to be dealt with. The lead contains inherent toxicity which causes chronic effects on animals and humans as well. So the harmful effects related to the use of lead contained machine parts and disposal of it have been noticed in recent times and numerous studies have been performed in the field of the journal bearing materials. A brief review of research articles on the wear and friction analysis of different lead-free bearing materials is presented here.

Al-bronze materials are also used as the bearing material [W. Boltan (1981)]. Aluminium bronze (Al-bronze) is an alloy of copper which consist of up to 12 % of Al, Ni, Mn, and Si are also present as the secondary alloying elements. High wear resistance, strength, corrosion resistance are some properties which make the Al-bronze use in many mechanical applications. The addition of Nickel (Ni) greatly increases the wear resistance of Al bronze. The formation of an intrinsic thin aluminium oxide film helps in protecting the Al bronze material from any wear and corrosive effects. There are various types of Al bronze materials, the materials having less than 8% Al are called as single-phase alpha alloys and the other one which contains aluminium in the range of 8-11 % are called as duplex alloys. Al-bronzes are generally used as bearing materials where any other materials would fail rapidly. As Al bronze is used for heavy working equipment's, so it is important to know the wear behavior of the Al-bronze material as well. The wear studies of bronze alloys have been reported extensively in the past.

Al-Bronze material having 10% Al is used for the casting process and it gives high corrosion resistance and high strength [Schmidt (1992)]. This alloy (10% Al) also has better comprehensive properties, and it is the widely used alloy in its family (Al-Bronze) [Li et al. (2006)]. Al-bronze material keeps their strength at high temperature as well. Phosphorous bronze is the potential copper alloy which has good corrosion resistance, wear resistance and machinability. These properties of phosphorous bronze make it suitable for bearing applications. Gebretsadik et al. (2015a) studied the tribological performance of tin-based

plated bearing in boundary as well as mixed lubricating conditions and compared with the conventional lead-based overlay bearing material. Authors used a block on ring test method for the analysis. It is reported that tin-based overlay shows comparable tribological properties for longer test durations. In mixed lubricating condition, tin-based overlay exhibits better wear resistance as compared to lead-based overlay.

In another research article by Gebretsadik et al. (2015b) Polyamide-lmide overlay with graphite and MoS_2 and Al-Sn materials were tested for tribological properties and compared with lead-based materials. The Polyamide-lmide overlay with graphite and MoS_2 resulted in better wear and friction properties as compared to Al-SN and Pb based materials. The Pb based material also resulted in the maximum amount of wear as well.

For the applications of journal bearings, steel is the most used material for journal (shaft) part of the bearing assembly. So the new journal bearing material should also have better adherence properties concerning steel. It is reported by Li et al. (1996) that, materials like Al, Cu, and Zn have very low adherence to steel. It indicates that an alloy of Al-Cu-Zn may be possibly used to make bearings. Authors (Li et al.) developed a Cu-14 Al-X alloy and reported less wear rate and coefficient of friction when tested against 1Cr18Ni9Ti steel. When the Al bronze alloy is tested against steel material for wear and friction, it reduces the coefficient of friction, however, the wear rate increases [Shi et al. (1996), Blau (1984)]. During the experimentation, the complex Al-bronze phases got heat-treated and may produce different results. Chmura and Gronostajski mixed the granular aluminium chips and aluminium bronze alloy (8% Al) to develop a composite material for bearings. Authors reported that with the increase of aluminium in bronze the wear intensity tends to decrease [Chmura and Gronostajski (2006)].

Yan et al. (2018) performed the scratch tests using the nano-indentor for evaluating the sliding wear nature of Cu-Al and Cu-Ni nano-twinned metals. The wear and hardness of Cu – Al increases with an increase in Al contents in Cu. Also, the Ni content in Cu improves the wear behavior. Saud et al. (2015) investigated the effects of Mn or Ti on the microstrure and corrosion behavior of Cu-Ni-Al alloys. The alloys with 0.7% Mn or Ti resulted in highest strain recovery as compared to other compositions. Panagopopoulos et al. (2012) investigated the friction behavior of leaded (α+β) brass against stainless steel. A pin on disk tribometer was used for the experimentation. Distilled water and NaCl solution was used as the lubricating medium and results were compared with the commercial SAE 80 W lubricant.

It is concluded by authors that, aqueous solutions may be used for improving the tribological properties of (α+β) brass. The aqueous solution helps in making a protective oxide layer which prevents the wearing.

The Cu-Al alloys also behave excellently to the heat treatment processes. Ding et al. (2018) evaluated the stress corrosion cracking susceptibility of the heat treated Cu-Ni-Al alloys. The heat treatment significantly improved the microstructure of the copper alloys. The stress corrosion cracking susceptibility also increases with the heat treatment process. The maximum stress corrosion cracking susceptibility was obtained with annealing heat treatment process. Song et al. (2013) reported that the corrosion behavior of Cu-Ni-Al was closely related to the microstructure. During the tribological testing of material in NaCl solution, it was observed by authors that the finely homogeneous microstructure of the material did not allow the easy penetration of the chloride solution and makes a dense protective film which in result improves the corrosion resistance. The hard faces like β and k phases can be generated by using the heat treatment process. These phases provide the necessary corrosion resistance to the alloy.

Wu et al. (2015) observed the improvement in the mechanical and corrosion resistive properties of the Cu-Ni-Al alloys with the heat treatment process. For further improving the surface properties and corrosive resistance of the Cu-Al alloys, Qin et al. (2018) used the chromium implantation on the Cu-Al alloys. The chromium content rapidly forms a coating on the Cu-Al surface and enhances the corrosion resistance. Using the similar technique Luo et al. (2017) applied the double layers of Ni-Cu and Ni-Al-Cu on copper alloys. The modified Ni-Cu layer on the material improved the corrosion resistance by growing a protective film of $Ni(OH)_2$ and Cu_2O.

Wert et al. (1993), studied a series of copper-aluminum alloys for different mechanical properties. The wear is found to be linearly related to the compressive stress induced during the wear process.

Aluminium bronze has been developed by Yuanyuan et al. (1996), by optimizing the microstructure, introducing special elements and controlling the parameters of the casting process. Equey et al. (2001), studied bronze materials for different surface roughness values and alloy microstructures. Gao and Cheng (2008), fabricated an aluminium bronze material using hot rolling. Equal channel angular extrusion (ECAE) was subjected to elevated temperatures. The effects of ECAE were evaluated by Authors for microstructure and

tribological properties. It is reported that ECAE improves the wear resistance of the alloy. Feyzullahoglu and Sakiroglu (2010) developed aluminium based journal bearing alloys by metal mold casting and were investigated for tribological performances. Wear and friction behavior of developed Al-Si, Al-Sn, and Al-Pb alloys was investigated using a pin on disc machine. Authors found that Al-Si alloys have the lowest friction coefficient values, highest hardness value, and superior tribological properties as compared to other developed alloys. Al-Si-Pb alloys were produced by Pathak et al. (1997) and tested for various anti-friction and anti-seizure properties. The lower amount of Si (5-11.5 %) results in the seizure of the materials. Alloys having (11.5-15%) Si content improves the anti-seizure properties of the alloys. Similarly, Pathak and Mohan (2003) fabricated Al-Sn and Al-Pb alloys and compared for various mechanical properties. The addition of Sn and Pb both decreases the coefficient of friction for the aluminium base alloys, however, Al-Pb alloy performed better as compared to Al-Sn alloys. Gao et al. (2011) developed a tin/bronze based coating and applied it on the bushing of the bearing surfaces. The friction and wear tests were performed and results were compared with a lead-bronze bushing of the bearing. The bearing coated with tin/bronze coating represents better tribological properties as compared with the lead/bronze bearing. Voong et al. (2003) evaluated the tribological properties of the Cr-bearing steel and Al-Si alloys with two lubricants. Pin on reciprocating plate type system was used for the friction and wear studies.

Zhang et al. (2016) studied the tin-copper overlay, tin-nickel and nickel barrier overlay for the diesel engines bearings. Tribological properties of the prepared overlay material were found out using the ring on disc tribometer at 0.013 m/s sliding speed and 12 MPa load for 100 m of sliding distance. The tin-nickle overlay shows the highest hardness and lowest coefficient of friction values. Tin-nickel has a desirable combination of hardness and frictional resistance which provides better seizure resistance to the bearing materials.

Sharma et al. (1998) used the liquid metallurgical technique to cast ZA-27/graphite journal bearing materials. The prepared materials were tested using a bearing test rig in dry, lubricated and semi-lubricated condition. It is reported by authors that graphite particles in ZA-27 help in reducing the friction coefficient of the material. The composite materials run with low friction coefficient even in a semi-lubricated and dry condition as well. The unreinforced ZA-27 alloy also gets jammed at much lower loads as compared to the fabricated composite materials.

To solve the jamming problem of metallic bearings, Kim et al. (2004) fabricated a hybrid composite journal bearing having carbon fibre reinforced phenolic composite liner with backing. In the developed composite material, carbon fibre provides the self-lubricating properties and phenolic resin have very good thermal resistance. Pin on disc tests were performed at several velocities and pressure values to check the reliability of the developed material. Kaplan and Yildiz (2003) fabricated the aluminium bronze (Cu4Ni9Al4Fe) material by using sand casting and die casting method. The change in microstructure and mechanical properties due to the fabrication methods. It was observed by authors that the metallographic structure of the aluminium bronze was heterogeneous in die casting, whereas it is homogeneous in sand casting method. The heat treatment of aluminium bronze also helped in increasing the hardness and tensile strength.

Thapliyal and Dwivedi (2016) evaluated the tribological behaviour of friction stir fabricated nickel aluminium bronze alloy. Pin on disc experiments were performed using a full factorial design. The results obtained for friction stirred alloy were compared with the casted Ni aluminium alloy. It is reported that, sliding velocity, load and specimen temperature greatly affects the wear rate of the material.

Patel et al. (2017) evaluated the effect of ferro-fluids on the performance of a journal bearing. Two combinations of the material of shaft and journal were used in the analysis. In the first combination, a ferrous shaft and an AISI-410 steel bearing was used. In the second combination, a ferrous shaft and a brass bearing was used. Experiments were performed at different load and rotational speed values. After the analysis, it is concluded by authors that the combination of ferrous shaft and brass bearing resulted in better performance as compared to the ferrous and steel shaft bearing combination.

Mathavan and Patnaik (2016) prepared and investigated the wear and friction behavior of Al-Si, Al-Si-Cr, and Al-Si-Ni bearing alloys. The experiments were performed on a pin on disc machine as per ASTM-G99 standards. SAE 1050 steel was used as the counter surface for the pin on disc experiments. It is reported by authors that, Al-Si-Ni resulted in maximum value of coefficient of friction and Ai-Si had minimum coefficient of friction.

In the recent past graphite has also been successfully used by researchers to fabricate the aluminium matrix composites for bearings, pistons, bearings, and impellers. The graphite content helps in improving the machinability and wear resistance. Liu et al. (1997) performed the wear tests for Al-Si-Graphite composites. 1.55 wt % of graphite content was used for the

fabrication of composite. The surface of the composite was treated with laser beams and wear resistance was evaluated between the laser beam treated ans as cast matrix composites. The laser beam treated composite resulted in better wear resistance. Baradeswaran and Perumal (2014) fabricated the aluminium-graphite composite with 5, 10, 15, 20 wt % of graphite particles. The wear and friction properties of composite material were evaluated. It is reported by authors that, the presence of 5 wt % graphite can provide superior wear particles to aluminium, however lower that 5 wt % graphite particles is need to be evaluated. Akhlaghi and Bidaki (2007) prepared aluminium graphite composites with 5-20 wt % graphite flakes. Experiments were performed in dry and impregnated conditions. Aluminium graphite composite having 5 wt % resulted with better tribological properties.

Chen and Huang (2013) used the hot pressing technique to prepare Al-Gr composites. The graphite particle helps in increasing the thermal conductivity of the composite. Sahoo et al. (2016) prepared aluminium-graphite composite using the heat-assisted pressing technique. The surface mechanism properties were evaluated and the aluminium-graphite material resulted in five times more hardness as compared to the aluminium alloy. Singh et al. (2001) tested the wear behaviour of aluminium – silicon alloy with graphite reinforcement. 10 wt. % graphite particles were reinforced in the aluminium-silicon matrix. Sliding wear tests were conducted at 0.2–1.6 Mpa pressure and 1.89, 3.96 and 5.55 m/s sliding speed conditions using a pin on disc setup. Authors reported that the Al-Gr composite exhibits low wear rates as compared to aluminium silicon alloy at the operating conditions. Also increasing the load on the pin sample increases the wear rate of the composite and increasing sliding speeds decreases it except at maximum pressure value.

Basavarajappa et al. (2007) evaluated the wear rate of the glass epoxy polymer composites with graphite as the secondary filler. 10% vol. of graphite particles were used with SiCp. Pin on disc experiments were performed by authors at various sliding distances, speeds, and loading conditions. The graphite particles helped in increasing the wear resistance of the fabricated composite. Panda et al. (2016) used the thermo-graphites for preparing the composites. Authors prepared two composites, one with 10% natural graphite and other with 10% thermo-graphite material. It is reported by authors that the composite with thermo-graphite particles works betters than the normal graphite contained composite material at several conditions. However, the difference between the performance of composites with thermo-graphite and normal graphite was not clear at low pressure and velocity values.

The other reinforcement agents which are generally used with matrix of aluminium are, SiC (Lee et al. (1992), Izciler and Muratoglu (2003), Candan et al. (2001), Sahin (2003)), Copper (Dinaharan et al. (2017)), alumina (Al-Qutub et al. (2006), Yang (2003)), TiC (Shamsipour et al. (2016)), lead (Sastry (2010)), Coated B4C (Shabani et al. (2012), Mazahery and Shabani (2012) and uncoated B_4C (Rahimipour et al. (2013)).

2.3 Surface Textures

In the last few decades, operating characteristics of mechanical components have becomes very extreme. This has reduced the lubricating film between the mating components to the dimensions of surface roughness. Numerous research is going on to improve the performance of mechanical systems by incorporating surface modification. Surface texturing is one of the most used surface enhancement methods. Intentional grooves of various shapes are generated on the mating parts which help in improving the performance of the mechanical systems. In recent time surface texturing has been utilized by a number of researchers for improving the friction and wear behavior of the tribo-pairs. It is reported that these microcavities act as a reservoir for the lubricating oil and provides the necessary lubrication for the tribo-pairs in mixed or boundary lubrication regime. In hydrodynamic lubrication regime, extra pressure is generated by the textured surface which consequently reduces the friction coefficient and wear between the mating parts [Scaraggi et al. (2014), Zhang et al. (2014)]. In some cases, these textures also act as debris entrapping areas and minimize the third body abrasion (Wang et al. (2013)). A textured surface also has less contact area as compared to a non-textured one, which may reduce the stiction and hence reduce the wear and increases the durability (Costa and Hutchings (2007)). For the fabrication of surface textures, there are four possible mechanisms of obtaining the dimples. (a) Adding material: the desired amount of material are added at the appropriate areas (b) removing material: small depressions are created by extracting the material (c) moving material: the material from the required areas are redistributed and dimple is obtained by using the plastic deformation (d) self-forming: wear resistant area are formed on specific areas and a dimple is produced by wear between the surfaces

In a hydrodynamic journal bearing system, the lubricating film operates in converging and diverging regions. The fabrication of surface textures in these converging and diverging gaps is a challenging task. Due to this difficulty, very few articles are published on the friction and

wear measurement of textured surface which were based on the experimental studies. Most of the experimental studies were performed on the commonly used wear and friction testing machines, pin on disc and ball on the disc. Tala-Ighil et al. (2011) investigated the effects of spherical and cylindrical surface textures on the performance characteristics of hydrodynamic journal bearings. Full textures and partial textures were considered on the surface on journal bearing surface. Four cases on spherical surface textures were considered by authors and Reynolds equation was solved using the finite difference method. In another research cylindrical surface textures were created (Texture height= 15 μm, length=2 mm and texture aspect ratio= 0.0075) and 25 different combinations of the textured surfaces were studied considering full and partial texturing. It is reported that full texturing is completely ineffective and partial one improves the performance of the bearing.

Lu and Khonsari (2007) investigated the textured journal bearings by considering different sizes of textures and by using two different methods for the fabrication of textures. Authors used, chemical etching and machining methods to produce the dimples. Dimples were produced by varying the dimple diameter as 2mm and 4mm, dimple depth as 0.165mm and 0.448mm and bur diameter as 6.223mm and 9.373 mm. During the mixed lubrication regime, the full textured bearing performed better as compared to the partial textured bearing. For hydrodynamic lubrication regime, the dimples surfaces produce the extra pressure which separated the journal and bearing surfaces and reduces the coefficient of friction.

Kango et al. (2013) numerically compared the effects of surface textures of spherical shape and of micro-grooving on the coefficient of friction temperature generation in journal bearing. The authors took three cases of the different number of surface textures having spherical dimples were considered. The first case had one texture with four dimples, second with five textures with four dimples each and ten textures with four dimples each. For grooved bearing, transverse grooves and longitudinal grooves were used. A numerical study was conducted at different eccentricity ratios. Authors concluded that surface textures/grooves improve the output performance of the journal bearing system. With comparison to surface textures, micro-grooves reduces the coefficient of friction significantly.

In another research by Kango et al. (2012) sinusoidal, spherical and dimple surface textures were incorporated in the bearing inner surface and the governing equations by considering

the surface textures were solved using the finite difference method. In this numerical study, it is reported that surface textures enhance the bearing performance significantly.

Ausas et al. (2007) used the Reynolds equation and p-theta model as proposed by Elrod and Adams (1974) to examine the journal bearing performance with full textured with rectangular dimples. The considered textured has different depths. Authors reported that for textured surfaces, a Reynolds cavitation equation underestimates the cavitation regions in the journal bearing. So one needs to use mass conserving techniques for solving textured surface areas for journal bearings.

Brizmer and Klingerman (2012) used the parametric study on the full textured and partial textured bearing surfaces. Author considered the textured surfaces for infinitely long as well as finite length journal bearings and reported that full textures reduce the load carrying capacity with very marginal improvement in attitude angle for the considered range of eccentricity ratios (0-1). For finite bearings the full textures result in significant reduction in attitude angle, however, the load capacity reduces. For partial textured surfaces, the load carrying capacity and attitude angle improve for low eccentricity ratios. Full higher eccentricity ratios, full texturing and partial texturing both were not able to improve the performance factors.

Fowell et al. (2012) analyzed the effects of a textured surface in hydrodynamic bearing using the numerical techniques. Regularly spaced rectangular textures were considered for the study.

Khatri and Sharma (2016), numerically found out the effects of surface textures and non-Newtonian lubricant on the performance factors of a journal bearing. The Reynolds equation was solved using the finite element method. A power law model was used to draw the shear stress-strain diagram for the lubricant. Three cases with textured surfaces were considered for the evaluation. Bearing surface with full texturing (0^o-360^o) and partial texturing (0^o-180^o and 180^o-360^o) were considered for the numerical analysis. It is reported by authors that frictional torque values reduces significantly for the textured bearing. The lowest frictional torque values were obtained for fully textured bearing surface followed by (180^o-360^o) and (0^o-180^o).

Sinanoglu et al. (2005) developed a neural network and analyse the pressure development of journal bearing in different surface textures (trapezoidal and saw profile) of the shaft and also with various rotational speeds (1000-2000 rpm).

The effects of the compound and simple dimple surface textures on the performance of journal bearing were studied by Meng (2015), two-layer pores were used by authors to generate the dimples on the bearing surface. A rectangular-spherical shape compound dimples were used in the analysis. Fluid-solid interaction (FSI) method along with Navier strokes equation was solved for the analysis of the dimple effects. The compound dimple resulted in better tribological properties like low friction coefficient and increases the load carrying capacity as compared to the simple dimple. The change in the viscosity of the lubricating oil also influences the starting friction torque greatly.

Qiu and Khonsari (2009) used the theories of "Floberg–Jakobsson–Olsson cavitation" with a "mass conservative algorithm" to precisely expect the conduct of cavitation in flat surfaces improved with dimples. The dimple shape for the analysis was assumed to be circular in shape. It is reported in their work that, if cavitation did not occur, the Reynolds equation and solution of Navier–Stokes equation resulted same for estimation of pressure in a dimple.

Shinde and Pawar (2017) used the partial grooving of the bearing surface to improve the performance of the journal bearing assembly. Authors used the COMSOL Multi-physics software for the numerical analysis of the grooved bearing. The maximum lubricant film pressure, capacity, frictional torque and power were evaluated and for 90-180 partial grooving, it is reported that maximum lubricant pressure increased by 81.9 % and load carrying capacity by 75.9 %, however, there were no improvement in frictional torque and power loss. The bearing surface with 90-360 partial grooving resulted in maximum decrease in power loss and frictional torque. Computational fluid dynamics (CFD) study has been conducted by Cupillard et al. (2007) for evaluating the effects of deep and shallow textures. Simulations were performed using the mesh deformation technique with CFD. High load condition with 125 N load and deep grooves (d = 1.15 mm) were used in the area of maximum pressure and, low load of 200 N with shallow grooves (d = 45 μm) are used in the area of maximum film thickness. For low loading condition, the frictional force reduces with textures and textures in maximum pressure area resulted in maximum reduction in friction force as compared to the use of thin viscous lubricant.

Etsion (2004) evaluated the effects of surface textures on the trobological parts. Laser texturing methods were used to produce surface textures. It is observed that each micro texture acts as an individual hydrodynamic bearing, in the case of mixed lubrication and fully flooded lubrication. In experimental tests the friction was reduced with laser surface texturing.

Hsu et al. (2013) studied the effects of roughness and magnetic field on the performance of short journal bearings. The performance factors include loading capacity, the coefficient of friction and attitude angle. A concentric wire was used with the shaft of the journal bearing system to evaluate the magnetic field effects. The combined effects of longitudinal surface roughness and magnetic field enhance the maximum oil film pressure which in result improves the performance of the journal bearing system. On the other hand, the transverse roughness had negative effects on the friction coefficient.

2.4 Literature Gap

It is observed from the literature review that, limited research has been conducted for experimentally examine the performance of textured journal bearings. As far as the lead contained materials of the bearing are concerned, attempts have been made by several authors to minimize the lead contents in the journal bearing material. In this work, these two prime factors are considered and investigated to enhance the performance of the journal bearing systems. The main points observed by studying the literature are mentioned below.

- The partial texturing to the bearing surface is found to have positive effects on the performance of the bearing system, however, the improvements in the performance factors is not very high. The performance also gets decreases with increase in the eccentricity ratio. The full texturing of the bearing surface has proved to be detrimental. In some cases, the full texturing resulted in enhancement of bearing performance. So contrary results have been observed in the experimental findings.
- The optimal shape of the textures and size of the textures greatly depends on the operating conditions and eccentricity ratio.
- The location of the textures also plays a very important role. However, contrary results have been reported and more research is needed to be carried out in this area.
- Attempts have been made by researchers to find out the tribology properties (e. g. Wear, frictional, and lubrication effects) independently and then incorporate to journal bearings. The simultaneous effect of all (wear, friction and lubrication effects) has not been incorporated to journal bearings.
- Most of the work related to surface texturing of the journal bearing are based on theoretical investigations, and very little amount of experimental work has been reported. So this area of the journal bearing research is needed to be explored more.
- Very few attempts have been made to replace the lead bronze material of the bearing.

In the present study, attempts has been made to find out the tribological properties of the journal bearing materials using a pin on disc setup. Two aluminium and two copper-based materials were fabricated using the stir casting method. Later the frictional torque and pressure distribution around the periphery of the untextured and textured journal bearing were evaluated on a journal bearing test rig using various lubricants at different speed and loading conditions. A computational fluid dynamic model is also proposed to evaluate the performance parameters of the untextured and textured journal bearing.

2.5 Objectives:

The presented research work has incorporated the following analyses:

1. Theoretical studies for performance behaviours of conventional and textured journal bearing.
2. Tribological studies of different bearing materials for performance of journal bearing for experiment.
3. Experimental studies for performance behaviour of conventional and textured journal bearing under flooded and starved condition

Chapter 3 Methodology and Experiments

3.1 Fabrication and Processing of Materials

Journal bearings are used in subsystems of different power trains and engines. These bearings are mostly operated in hydrodynamic lubrication regimes as low pressures are generated in them with compared to rolling element bearings. The performance of a journal bearing depends on its working conditions. The speed of the journal and load on the journal are the two main parameters which affect its performance. Besides these, the lubricant oil nature, material of bearing and surface roughness values of journal and bearing are the other factors. For selecting the bearing materials, several materials were fabricated and processed for evaluating the tribological properties.

In the recent past, experimental as well as theoretical research is going on to select an appropriate material and design for the better performance of the journal bearing system. It is evident from previous literature that, leaded bronze material is the commonly used material for the bearing of a journal bearing system. The antifriction nature of the lead contents in the bronze help in providing the antifriction properties to the material. Apart from antifriction, conformability, embeddability, wettability and hardness are some of the desired properties of bearing material.

3.1.1 Material and Testing

Generally, the foremost criteria for the performance evaluation of a journal bearing material are the minimum wear of the two mating tribopairs and no mechanical failure, seizure cracks during or after its operation. The lubricant used in between the journal and bearing system helps in reducing the coefficient of friction by providing the hydrodynamic lubrication and also by providing the boundary lubrication.

3.1.2Measurement of Wear and Friction

Wear and friction coefficient between the tribo-pairs are measured by a number of different methods. Some of the famous methods include, ball on disc, pin on drum, and pin on disc. In the present thesis work, pin on disc method was used to evaluate the wear and friction parameters. The experiments were performed as per ASTM-G99 standards (Anil et al. 2017, Davim and Marques 2001, Davim et al. 2001, Petrica et al. 2017). In pin on disc method, a pin of required material who's wear and friction properties are to be evaluated, is made to slide on a much harder counter disc. The disc is securely held on a chamber which is further connected with a motor. This motor helps in rotating the disc at a specified speed. The pin is

held against the disc with the help of holder, which is further connected with one end of a bell crank lever. The other end of the bell crank lever is connected with a loading pan through wire and pulley system. The dead weights applied on the loading pan are transferred to the pin with the help of bell crank lever in 1:1 ratio.

Two sensors, namely wear and friction sensors are installed on the machine for detecting the wear from the pin and, the friction force between the pin and disc surfaces. The wear sensor detects the change in length of the pin in micrometer units.

A pumping system is attached with the pin and disc chamber for the continuous supply of the lubricating oil. A Lubricating tank is used to store the lubricating oil. The pump lifts the oil from this tank and supplies at the interface of pin and disc with the help of a tube. A measuring scale is also attached with the pin on disc platform to varying the track distance of the pin on disc surface. The disc rotates with specified speed. In the present work, the tip of the pin was in the form of a non-rotating flat surface.

The pin on disc machine consists of a motor which rotates the disc at variable speeds using the rheostat position. The speed can be varied from 200 to 2000 rpm. For the loading purpose, the weights are placed on a flat pan and transmitted via wire, pulleys and a bell-crank mechanism. After each run of the experimental plan, wear of the pin in the form of mass loss was evaluated by measuring its weight before the start and after the experimental run using a precise weighing balance which has 0.0001g accuracy.

The wear from the pin surface is also recorded by a wear sensor in micrometer (μm) units. From the data of wear loss, wear volume and specific wear coefficient (Ka) was calculated to assess the wear from the pin samples.

$$K_a = V_{wear} \Big/ F_{load} \times S \tag{3.1}$$

Where, V_{wear} [m3] is the measured wear volume, F_{load} [N] is the applied load and S [m] is the sliding distance.

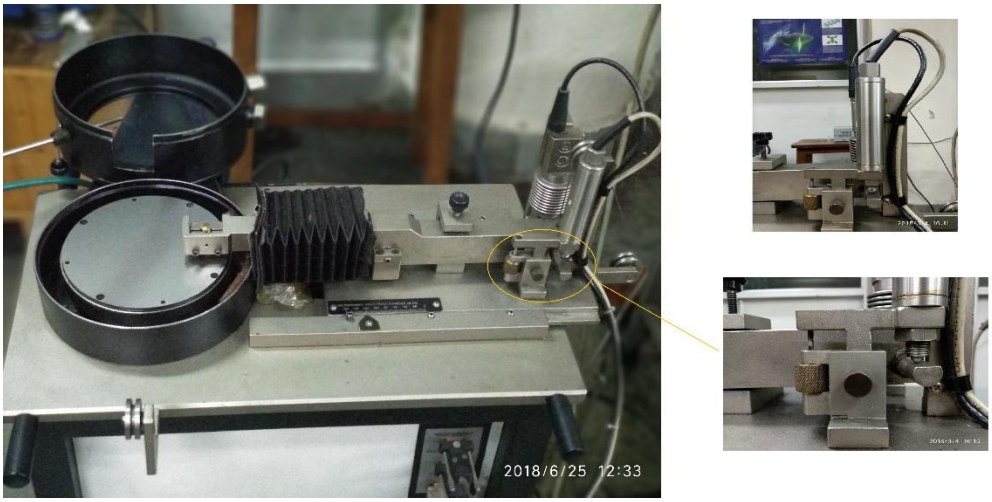

Figure 3.1 (a): Pin on Disc Tribometer

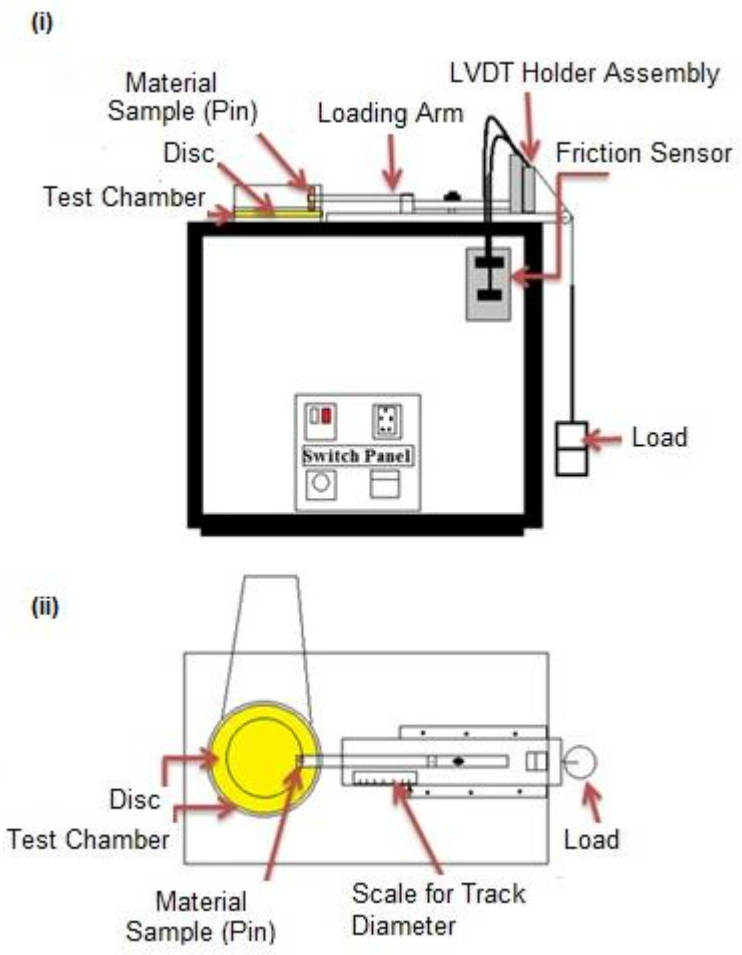

Figure 3.1 (b): Sketch of Pin on disc tribometer (i) Front View (ii) Top View

3.1.3 Measurement of Hardness

The Vickers hardness test method was developed by Smith and Sandland in 1924 In case of Vickers test, the required calculations of the hardness measurement are independent of the size of the indenter used. This quality makes this hardness method a most versatile method for all the materials. The unit of hardness obtained from this method is expressed as the Vickers Pyramid Number (HV).

A Fischer made microhardness tester was used in the present investigation for the measurement of hardness of the fabricated materials.

The hardness measurement was done as per ASTM E-384 standards (ASTM E-384 standards, (2017)). In this test, the test surfaces were cleaned and placed perpendicularly to the indenter. For obtaining the indentation load is applied very smoothly on the surface. A diamond indenter of square base pyramid shape was used to indent on a surface of the specimens at a load of 3000 mN for 20 seconds. To obtain the quality of tests, the load should be accurately applied on each measurement.

The hardness measurement instrument measures the diagonals of the indentation and calculates the Vicker hardness number. The Vicker hardness number is defined as the ratio of the load applied by the indenter to the pyramidal contact area of the indentation. In this work for each specimen, three hardness values were measured and an average of three was taken for the analysis.

Figure 3.2: (a) Vickers hardness tester

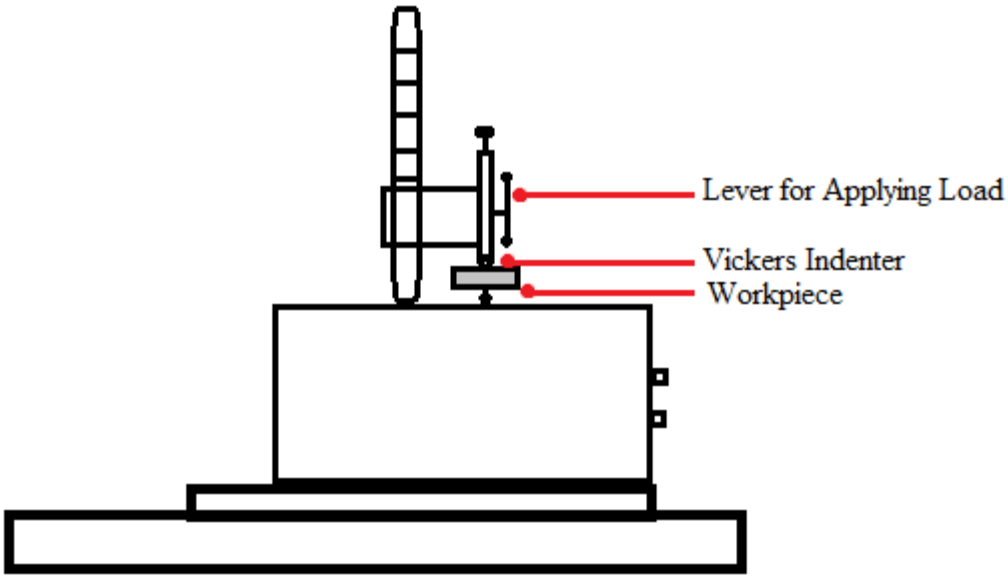

Figure 3.2: (b) Schematic presentation of Vickers hardness tester

3.1.4 Fabrication of Materials

There are numerous technique for the fabrication of composite materials. The choice of a particular fabrication method depends on the material and design specification of the product to be made. Liquid state, semisolid and powder metallurgy are the famous fabrication techniques used to produce aluminium and copper composite (Baradeswaran and Perumal 2014, Vettivel et al., 2012, Kandave et al., 2017). Many researchers investigated the effect of different fabrication method on the properties of the composite materials (Wang and Rack, 1991, Taya et al., 1991, Bhansali and Mehrabian, 1982). Stir casting method is the mostly used fabrication method (Rohatgi et al., 1998). The low operating cost and high production rate makes the stir casting as the economical method. Formation of clusters and agglomeration of reinforced particles are the problems which should be dealt properly to prepare a sound composite with stir casting method (Mazahery and Shabani, 2014). Materials were manufactured with the help of a stir casting process. Stir-casting is the process of melting the material with continuous stirring and immediately pouring the melt into a preformed cavity, then cooling it and allowing it to solidify. In conventional casting, the particles often tend to form agglomerates, which can be only dissolved by vigorous stirring at high temperature. The stir casting set up (Figure) consists of a furnace, crucible and a rotor attached to the motor.

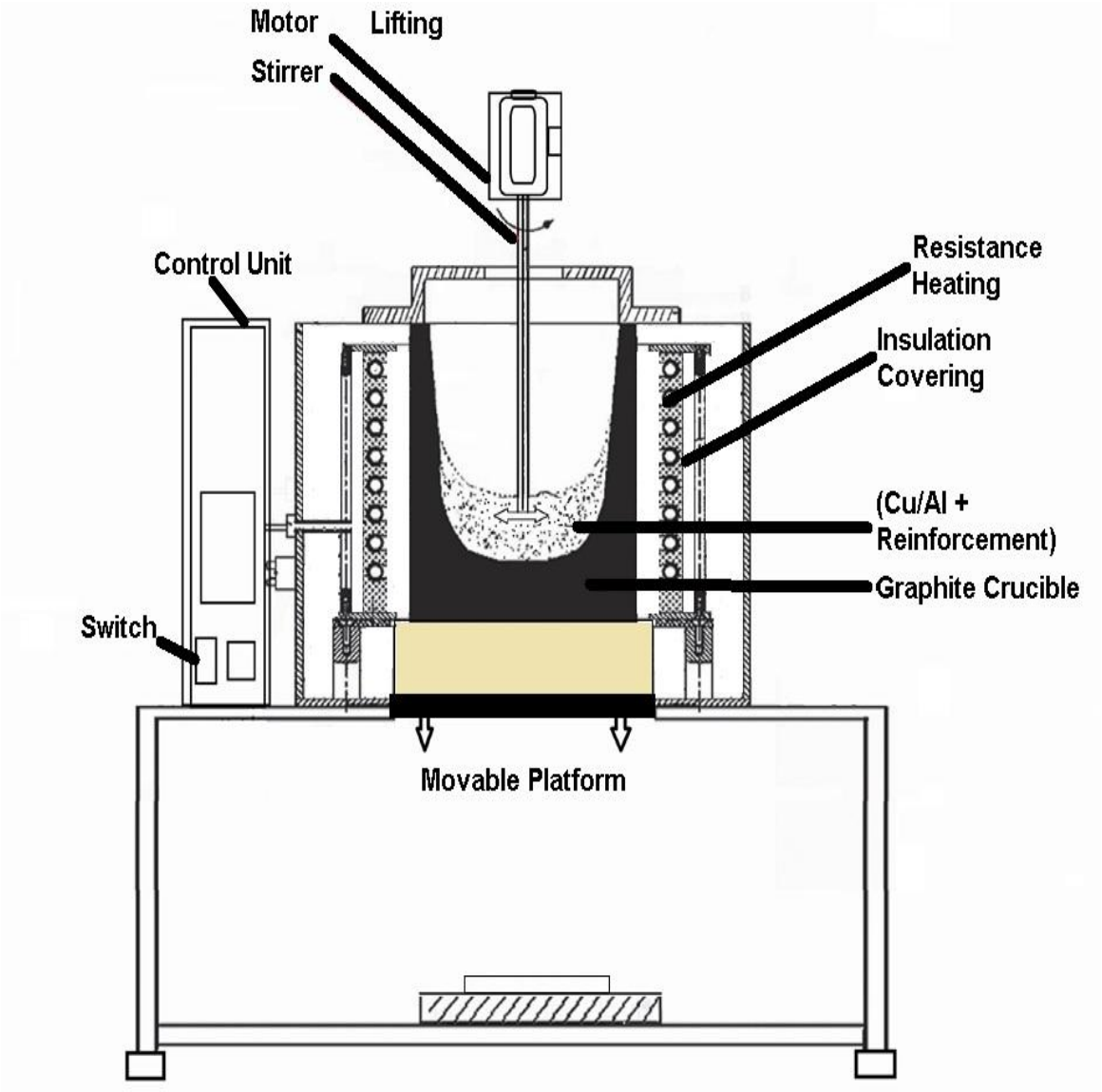

Figure 3.3: Stir casting setup used for melting the fabrication of materials

3.2 Conventional Journal Bearing Material-Leaded Bronze (Cu-Pb)

The leaded-tin bronzes are used in industrial applications since the 20th century. The lead contents of the bronze provide the necessary anti-friction and anti-seizure properties. The distribution of lead particles in the copper matrix helps in achieving these properties.

The lead content remains almost insoluble in copper. The two metals remain insoluble in molten state. When the molten mixture of lead and copper freezes with time, the copper freeze first and lead particles freezes as globules. By the equilibrium phase diagram of the lead and copper, it is seen that lead has 0.003 % solubility in copper matrix. In the microstructure of the lead copper material, the lead particles replace the Tin particles which results in diminishing the strength of the material. The introduction of lead in copper also

believed to reduce the hot hardness/shortness of the material. Based on these conclusions, the lead contents are used in the range of 1-10% for most of the industrial applications.

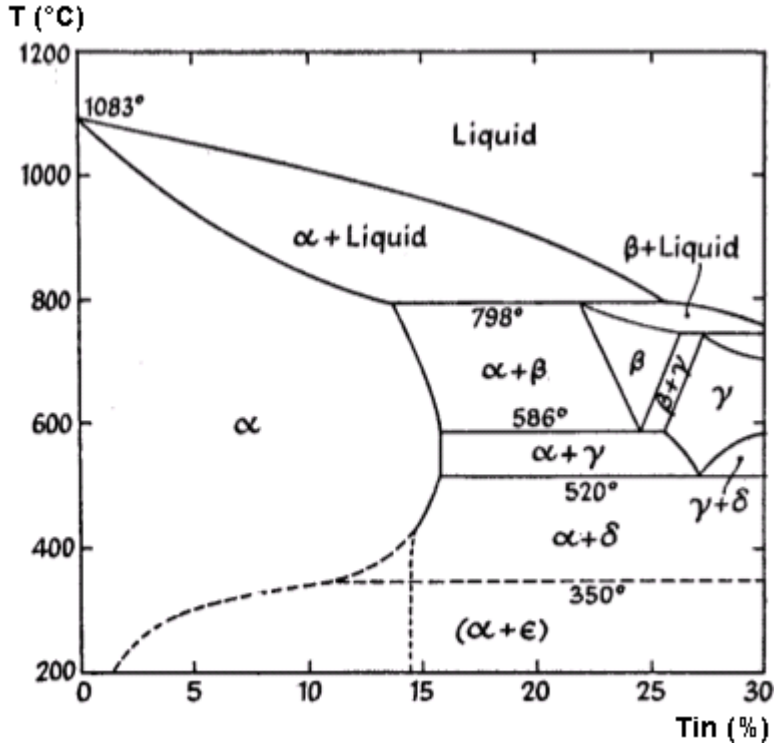

Figure 3.4: Constitutional Diagram for Copper Tin alloys

The presence of free lead globules in the copper matrix provides the inherent solid lubrication between the mating parts. These lead particles layer gets transferred to the steel shaft and provides the necessary friction resistance. This low shear strength lead film layer also reduces the overheating of the shaft and bearing interface.

During the optimal running conditions, the lead globules come to the mating surfaces and make a very soft and anti-friction layer. This layer prevents the seizure between the mating parts (Prasad et al. (1996)). However, the boundaries between the lead particles and copper matrix also act at weak sections, which could lead to cracks. These cracks progresses and may fracture the material. On the other hand, the lead contents are hazardous to the environment. The disposal of lead contained bearing and lubricant having lead particles from bearing surface is an important issue which need to be dealt with proper care. The lead contains the inherent toxicity which causes chronic effects on animals and humans as well.

The Cu-Pb material was casted using the stir casting process. The amounts of Nickel and Tin added in the melt were in the account of desired wt% of alloying elements. For Cu-Pb, copper was first melted at 1100° C and Tin and Lead were added after melting the copper in the crucible. The melt was continuously stirred for the homogenous mixing of the elements. After the complete melting, the melt was superheated to a temperature to 50°C above the pouring temperature.

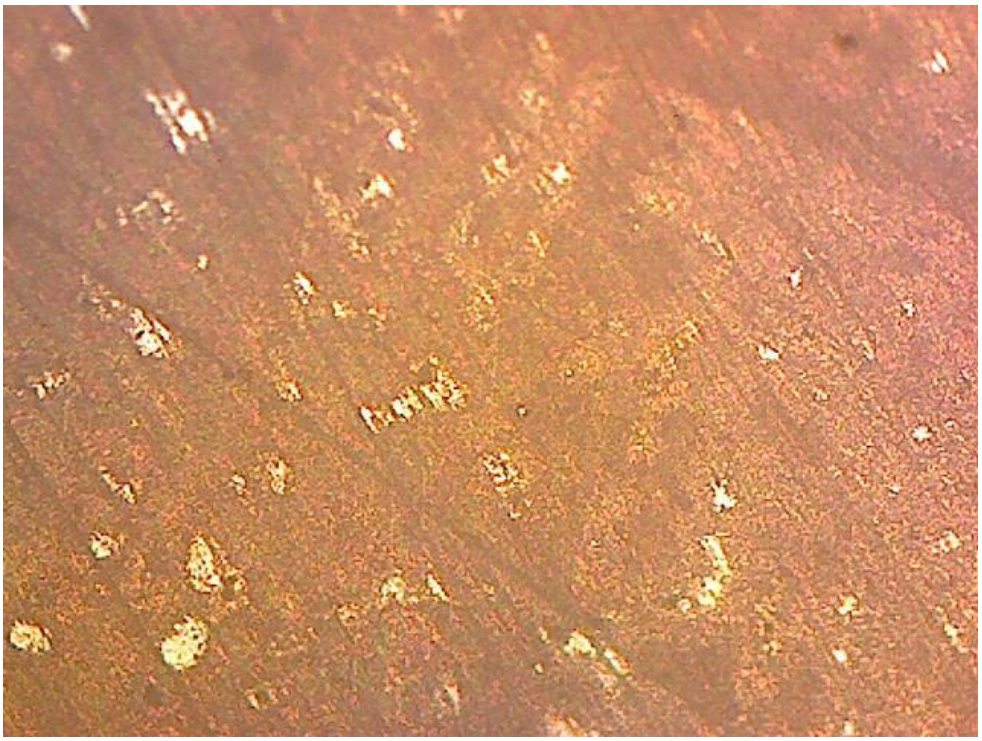

Figure 3.5: Microscopic image of Cu-Pb material at 20X magnification.

3.3 Aluminium Bronze (Cu-NiAl) Material

The addition of aluminium in the copper matrix increases the strength and corrosion resistance appreciably. The phase diagram of alminium bronze indicates the presence of alpha phase solid solution with the 8% addition of aluminium in copper. At above 9% aluminium, the beta phase also gets formed in the copper matrix. The presence of aluminium also improves the hardness of the materials and hence makes it brittle. The introduction of Nickel and Iron helps in improving the ductility. These elements prolong the alpha field in the matrix.

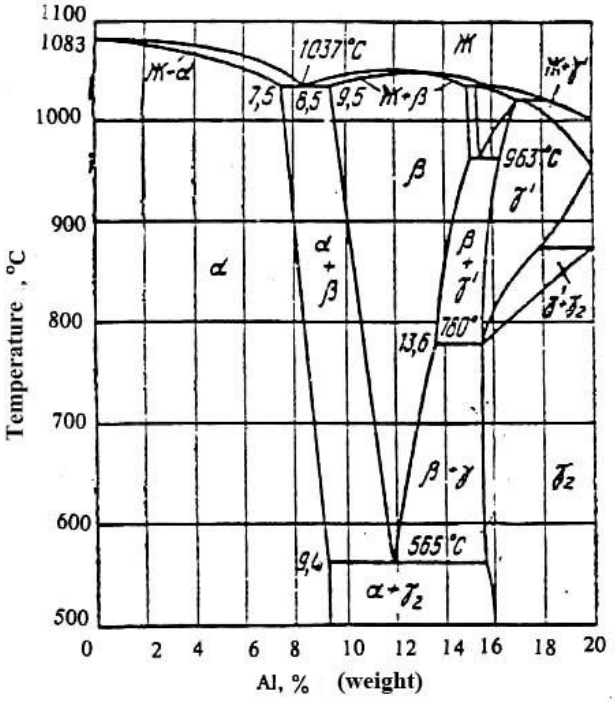

Figure 3.6 : Copper-Aluminium equilibrium diagram.

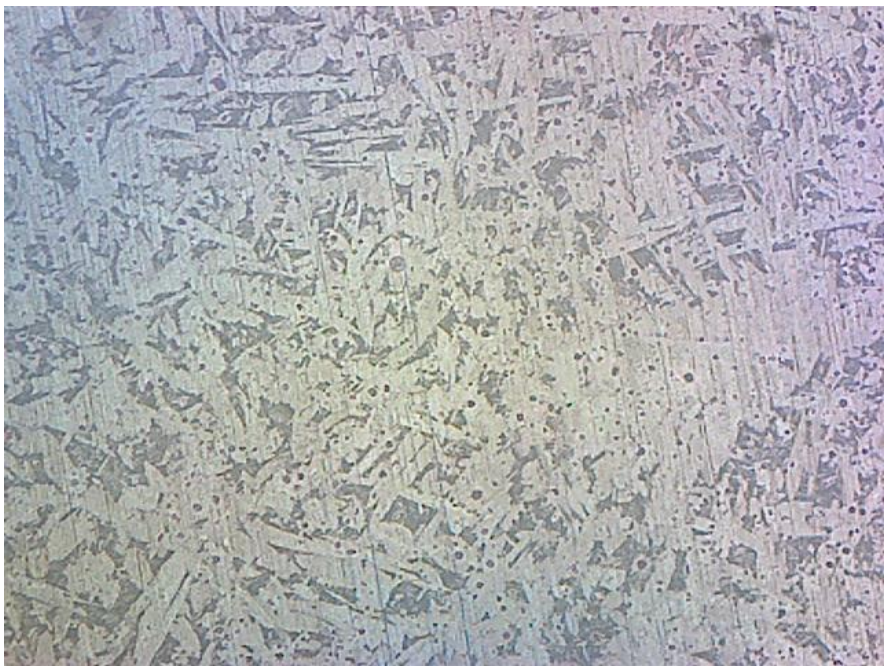

Figure 3.7: Optical microscopic image of Cu-NiAl material 20X magnification.

3.4 Phosphorous Bronze

Phosphorous bronze (Cu-PAl) contains tin and phosphorous as the alloying elements in the copper matrix. The presence of tin provides the strength and corrosion resistance and

phosphorous helps in making the material more wear resistive. The spectroscopic analysis of the prepared materials is given in Table 3.1.

Table 3.1: Chemical composition of copper composites

wt. %	Sn	Pb	Si	Al	P	Zn	Mg	Mn	Ni	Cu
Cu-Pb	6.8	1.2	0.018	-	-	-	0.0001	0.0018	0.29	Bal.
Cu-NiAl	0.0478	-	0.150	9.2	-	-	0.0012	0.3340	4.0	Bal.
Cu-PAl	4.2	0.05	-	0.25	0.30	0.30		-	-	Bal.

Figure 3.8: Optical microscopic image of Cu-PAl at 20X magnification

3.5 Aluminium Flyash Composites

The aluminium metal was melted in the crucible which was heated to a temperature of about 900°C, while the reinforcement material (flyash) was added externally in a fixed proportion of 2-4-6 % weight. Aluminium and flyash were mixed with the help of a specially designed stirrer, at a rotational speed of 100 rpm with the aid of the rotor forhomogeneous mixing.

Table 3.2 Elemental percentage in various specimens

Element	Sample 1 (low flyash 2 % wt)	Sample 2 (Medium flyash 4 % wt)	Sample 3 (High flyash 6 % wt)
Si	9.901	10.296	10.35
Fe	1.202	1.313	1.2266
Cu	0.6284	0.6703	0.694
Mg	0.0723	0.097	0.876
Zn	0.5841	0.6021	0.636
Ni	0.106	0.1155	0.1157
Pb	0.400	0.3177	0.2937
Al	86.886	86.355	86.30

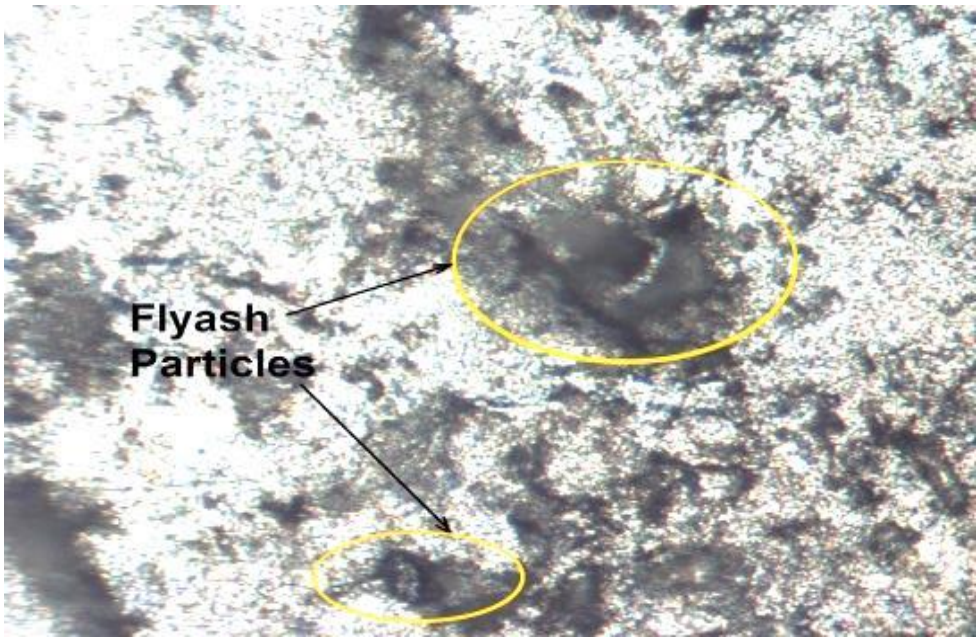

Figure 3.9: Optical microscopic image of Aluminium Flyash composite (2% wt) at 20X magnification.

3.6 Aluminium Graphite Composite

Commercially available Aluminium and graphite powders were used in the investigation. The aluminium was melted in a crucible and graphite particulates were added externally to the melt. The graphite powder particles of size 0.1 mm were used for the fabrication of the composite. A specially designed stirrer having blades of 9cm length in plus sign was rotated

with the help of a rotor to mix the aluminium and graphite. For the uniform mixing the stirrer was rotated at a speed of 100 rpm.

Table 3.3: Composition and basic properties of graphite used for composite

Element	Unit	Value
Graphite	wt.%	99.9
Particle diameter	mm	0.1
Density	g/cm^3	1.8

Table 3.4: Chemical composition of Aluminium Alloy

Element	wt. %
Si	0.1697
Mg	0.6492
Zn	1.0259
Ni	0.1207
Cu	1.2
Fe	0.4102
Al.	Bal.

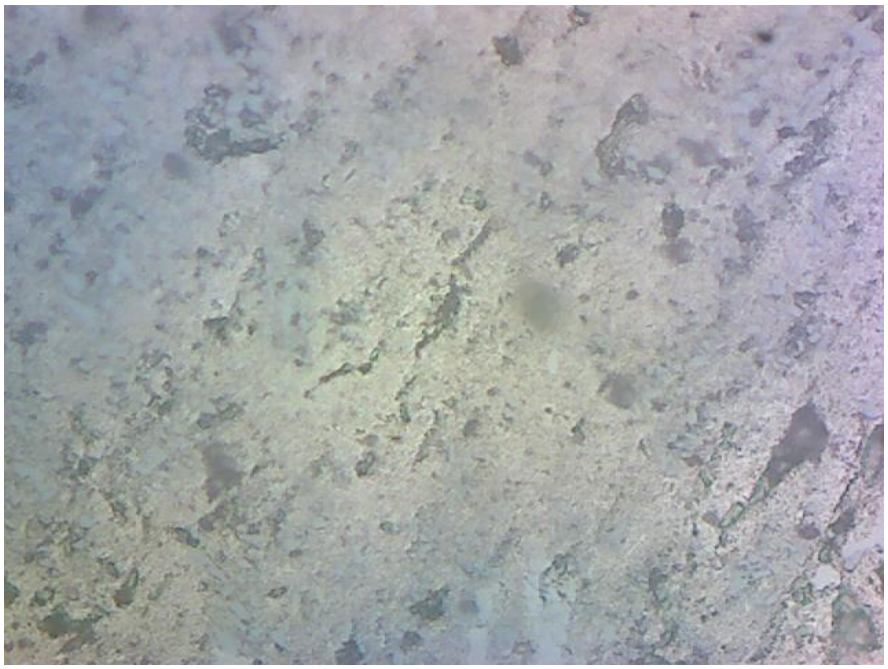

Figure 3.10: Optical microscopic image of Aluminium Graphite composite (2% wt) at 20X magnification.

3.7 Counter Surface Material

For the pin on disc studies, mild steel disc (C-0.16 %, Mn-0.80 %, Si-0.40%, S-0.03%, Ph-0.03%) were used for the investigation of the wear and friction properties of the fabricated materials.

3.8 Lubricating Oil

For wear and friction tests a commercially available Shell made SAE 15W-40 lubricating oil was used. A viscometer was used to measure the viscosity and density of the lubricating oil as per ASTM D-445 (ASTM Standard D445 (1970)), D-4052 standards (ASTM Standard D4052 (1984)). The lubricant had 106.39 mm^2/s at 40ºC and 13.6 mm^2/s at 100ºC. The density of the used lubricant was 0.83 g/cm^3.

3.9 Wear and Friction Testing

The wear and friction testing of the prepared materials was done in two phases. In this first phase, dry sliding tests were conducted for Al-F and Al-Gr materials. The input factors used for the testing of the aluminium composites (Al-F and Al-Gr) are given in Table 3.5. For each experimental run, three observations were obtained and the average of three was taken to draw the graphs. The one material which yields better tribological properties was selected for further investigation.

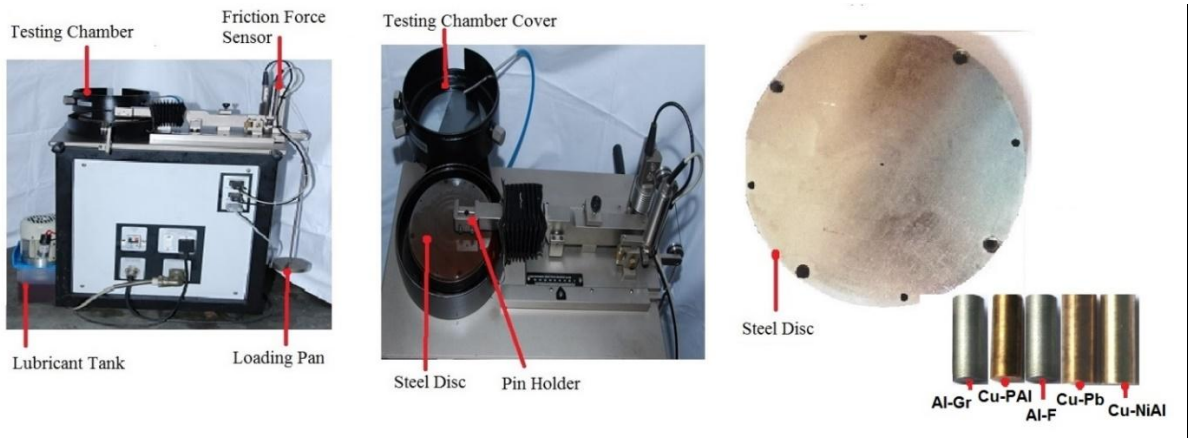

Figure 3.11: Pin and disc specimens for the dry sliding wear test

In this study, the Al-F material exhibits lower values of coefficient of friction as compared to the Al-Gr material. In the second phase of pin on disc testing, the copper-based materials, Cu-NiAl, and Cu-PAl were tested for various operating conditions. Table 3.6 presents the testing conditions for copper composites. The hardness value for the aluminium composites was

much less as compared to the copper composite. So to obtain wear in copper composite a much larger load/pressure values were used. After getting the desired results, the selected copper and aluminium composites tribological nature was compared at common testing conditions as mentioned in Table 3.7.

Table 3.5: Wear and friction parameters for aluminium composite

Test Condition	Values
Speed (m/s)	4.39
Load (N)	9.81
Track Diameter (mm)	90
Pin diameter, Height (mm)	10, 30
Disc diameter, height (mm)	165, 10
Sliding distance (m)	2000
Temperature (°C)	22
Humidity (%)	50
Lubricating condition	Dry

Table 3.6: Wear and friction parameters for copper composites

Test Condition	Values
Speed (m/s)	4.39, 5.18, 5.97
Normal Pressure (Mpa)	0.31
Track Diameter (mm)	120
Pin diameter, Height (mm)	10, 30
Disc diameter, Height (mm)	165, 10
Sliding distance (m)	4000
Temperature (°C)	22
Humidity (%)	50
Lubricating condition	Dry, Starved, Fully Flooded

Table 3.7: Experimental testing conditions for the comparison of wear and friction for selected aluminium and copper composite materials.

Test Condition	Values
Speed (m/s)	4.39
Normal Pressure (Mpa)	0.31
Track Diameter (mm)	120
Pin diameter, Height (mm)	10, 30
Disc diameter, Height (mm)	165, 10
Sliding distance (m)	4000
Temperature (°C)	22
Humidity (%)	50
Lubricating condition	Dry, Fully Flooded

3.10 Hardness Tests

The tribological behavior of the materials is directly related to its hardness and fracture toughness. However, in this work, the study is limited to the determination of hardness using Vickers hardness measurement method and further research needs to be carried out for the clear understanding of the effect of fracture toughness on the tribological behavior of the material. The hardness (HV) of the prepared specimens is listed in Table 3.8. The Cu-Al exhibits maximum hardness value of 243.6 HV followed by 212.9 HV for Cu-PAl material. The conventional Cu-Pb has a hardness value of 116.6 HV. The presence of aluminium particles in Cu-Al and Cu-PAl helped in achieving the more hardness to the copper matrix. The Al-F and Al-Gr materials have hardness value in the range of 92-97 HV.

Table 3.8: Vicker hardness values for prepared specimens

Material	**Hardness (HV)**
Cu-Pb	116.6
Cu-NiAl	243.6
Cu-PAl	212.9
Al-F	96.5
Al-Gr	92.6
Mild Steel	379.8

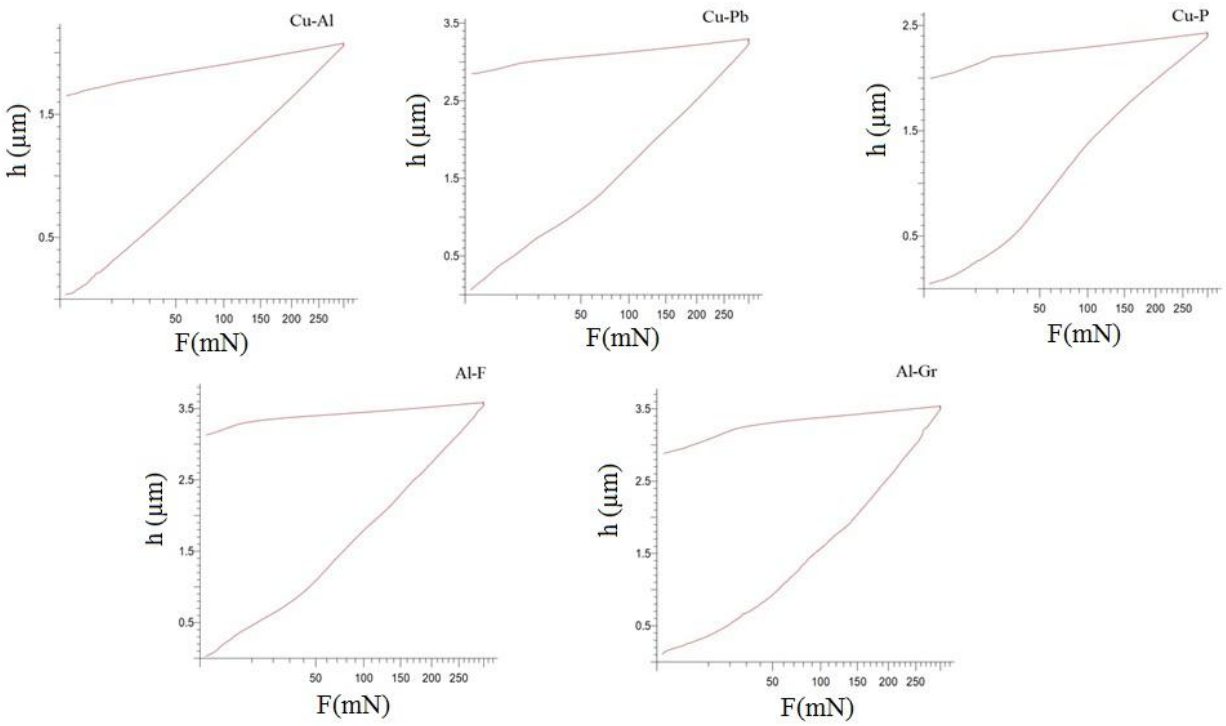

Figure 3.12: Loading and unloading diagrams for the measurement of Vicker hardness

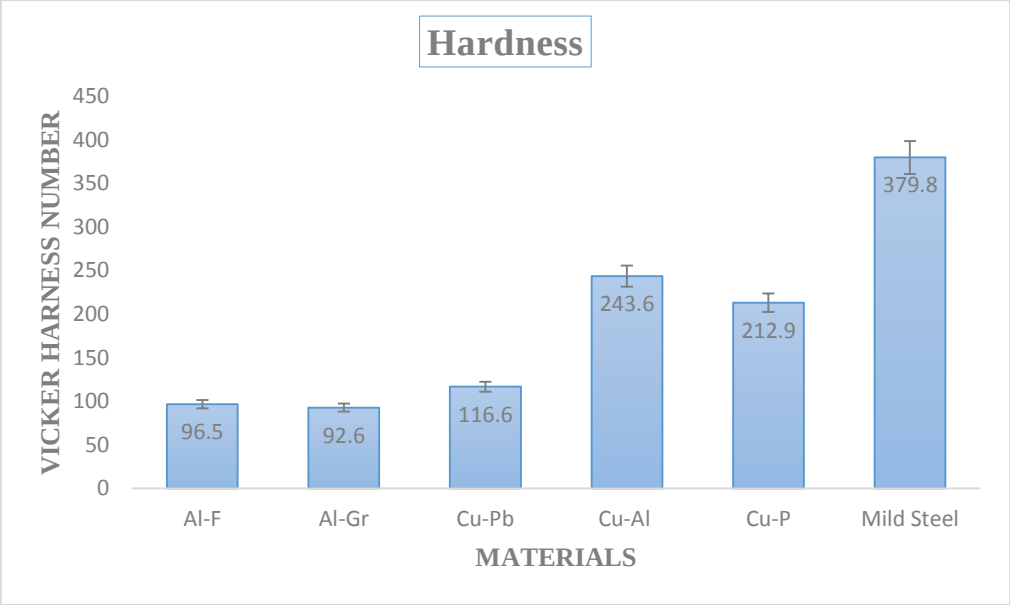

Figure 3.13 : Vicker Hardness Number for fabricated materials.

3.11 Journal bearing test Rig Experiments

A journal bearing has a cylindrical component around a rotating shaft. It is used to support the radial load or used to guide for the smooth and efficient transfer of torque. The space between the bearing and shafts is filled with lubricating oil. In hydrodynamic lubrication technique, as the shaft starts to rotate, it tries to climbs the bearing surface and as the rotational speed of the shaft is further increased, the lubricating oil forces itself into a wedge-shaped region. This wedging action of the lubricating oil helps in generating the pressure within the system. In the present work, in order to find out the pressure and frictional torque, a journal bearing rig TR-660 was used. Figure 3.14 (a) represents the basic parts of the test rig and Figure 3.15 shows the location of pressure sensors. Journal bearing test rig is a sturdy versatile apparatus, easy to operate with provision to measure pressure at a different angular position on the bottom half of journal bearing. The journal is mounted horizontally on a shaft supported on self-aligned bearings, the shaft is rotated with by a motor with timer belt. A loaded bronze flawless bearing freely slides over the journal and as it rotates bearing is formed, radial load is applied on bearing by pulling it upwards against journal by a loading lever. Ten numbers of sensors were fixed on the circumference of bearing with their terminal ends ending in the junction box. The permissible error in the measurement of pressure was ± 1 % Mpa. A friction sensor was used to measure the frictional torque with a permissible error of ± 1% Nm. The journal is driven by belt & two-step pulley arrangement and speed required is set on software. Radial load & journal speed were varied to suit the test conditions.

The test rig is capable of measuring the friction torque and pressure generation for a maximum shaft speed of 8000 rpm and a load of 3000 N (maximum). A hydraulic system is used to supply the lubricating oil at a constant flow. The maximum lubricant oil pressure provided by system is 0.25 Mpa. SAE 10W 40, SAE 15W 40 and SAE 20W 40 lubricating oils were used for the experimentation and each experiment was performed three times with measurement of frictional torque for accurate analysis of it. Table 3.7 provides the details of the journal bearing setup and input parameters of the experimentation.

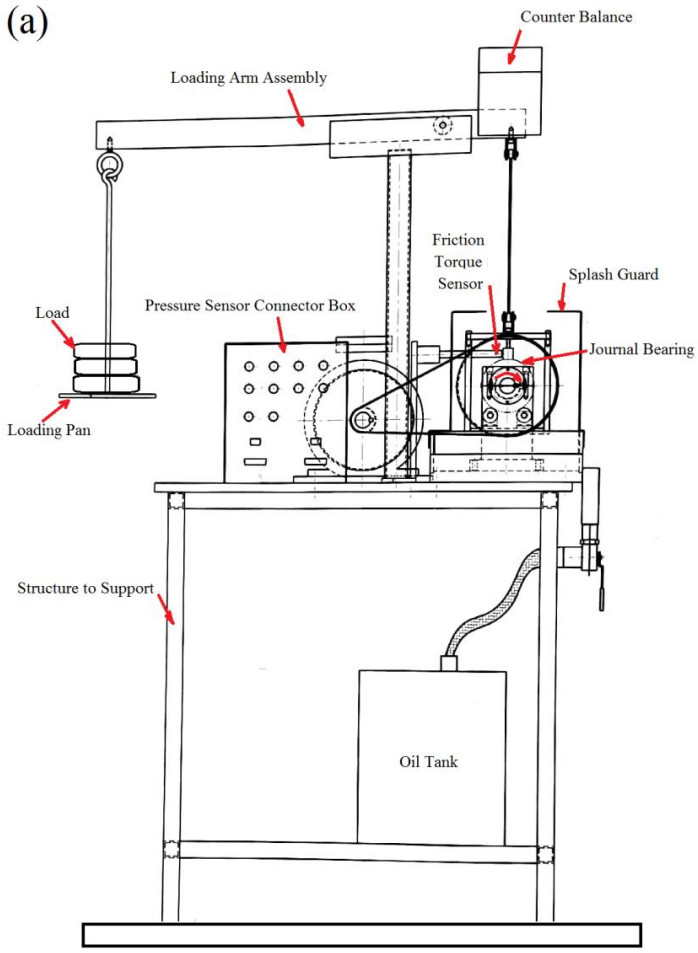

Figure 3.14: (a) Schematic of Journal bearing set-up

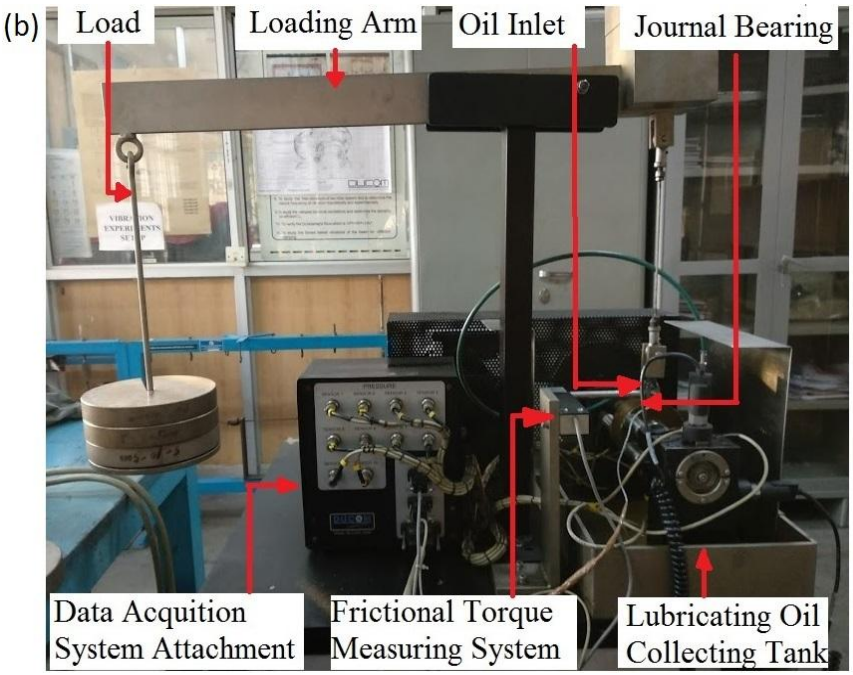

Figure 3.14: (b) Journal bearing experimental set-up.

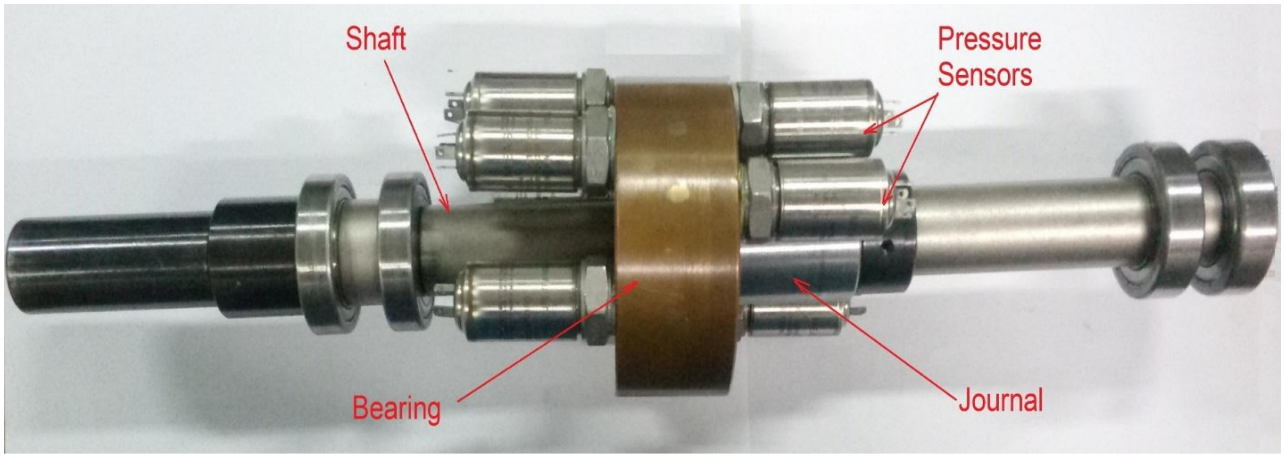

Figure 3.15: The Assembly of journal and bearing for the experimental test rig.

Table 3.9: Main bearing characteristics, lubricant properties and operating conditions.

Parameter	Symbol	Unit	Value/Range
Geometrical bearing characteristic			
Bearing diameter (Nomial)	d	*mm*	22.035
Outer Bush diameter	D	*mm*	40.01
Bearing length/diameter ratio	l/d		1
Bearing diameter clearance	C_d	*mm*	0.0027
Oil properties			
Lubricating Oil			SAE 10W-40/SAE 15W-40/SAE 20W-40
Dynamic viscosity at 40° C	μ_{40}	Ns/m^2	86.10/106.39/110.067
Density	ρ	g/cm^3	0.816/0.831/0.895
Operating conditions			
Rotational Speed	N	*rpm*	900, 1150, 1400, 1650, 1900, 2150
Applied load	W	*N*	250, 500, 750, 1000
Supply conditions			
Oil supply pressure	P_f	*kPa*	0.5
Oil supply temperature	T_f	*T*°	30

3.11.1 Measurement of Friction Torque

The Figure 3.16 represents the journal bearing with all the sensors. Friction torque, pressure, and temperature sensor were calibrated before using for the experimental work. Frictional torque measurement unit consists of an arm which is in contact with the journal bearing assembly. The data acquisition system which connects the sensor measures the startup torque. For the measurements of friction toque, all other pressure probes were removed in order to get the minimum disturbances from the other components.

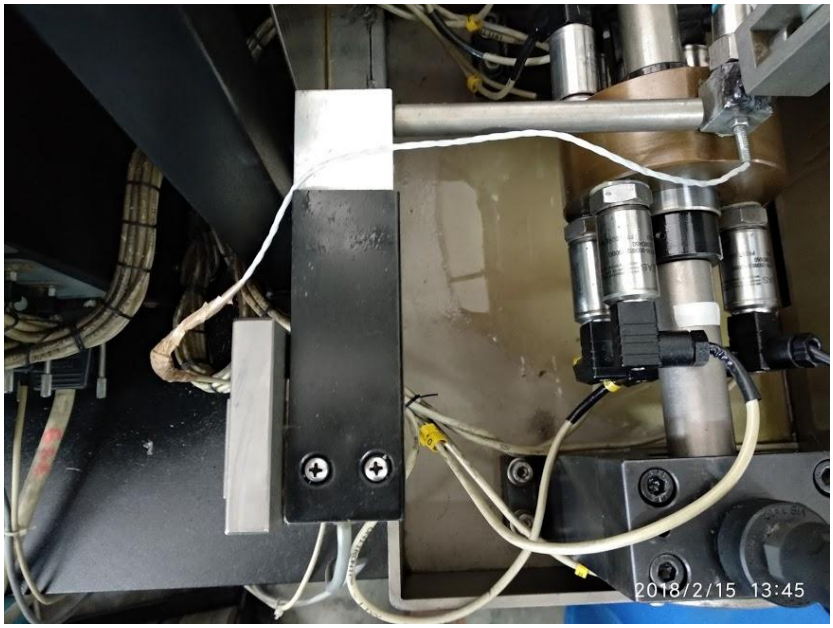

Figure 3.16: Location of friction force transducer

3.11.2 Measurement of Oil Film Pressure

During the running of the journal, the eccentricity between the journal and bearing generates a wedging section in the clearance space between the journal and bearing. This wedging section creates a pressure on the journal surface, which in result lifts the journal and helps in providing the smooth rotation of it. For the measurement of fluid film pressure, a total of ten (10) pressure sensors were used around the periphery of the bearing surface. Figure 3.17 presents the location of pressure sensors.

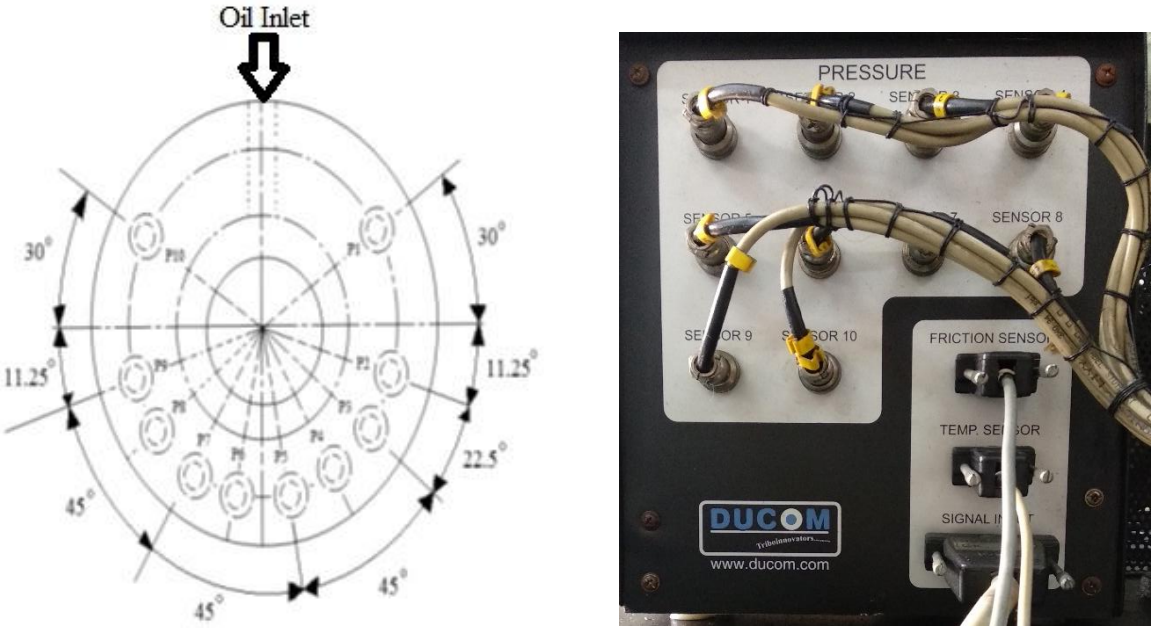

Figure 3.17: Location of pressure sensors, with its acquisition system

Figure 3.18: Untextured Bearing

3.12 Texturing Method-Electric Discharge Machining (EDM)

The bearing inner surfaces were textured using the electrical discharge machining process. Half spherical textures were fabricated with varying cross-sectional area and number of dimples.

From the literature review, it is found that it is very difficult to texture the inner surface of the bearing. Chemical machining is the most used texturing method adopted by researchers. The time consumption in printing the maskant and etching process are the main drawbacks of this method. In the present work , Electrical discharge machining process is utilized to produce the textures on the bearing surface. A specially designed electrode was prepared to produce

the spherical dimples on the bearings. This section also cover the fabrication process of the electrode along with the texture generation on the bearing surface.

3.12.1 Machine and Methods

In the electric discharge machining process, a thermal spark is generated between the electrode and the work-piece in some die-electric medium. The work-piece and electrode both should be made of conductive material. This thermal spark dissociates the ions of the die-electric fluid and liberates the high energy on the working surface which in result softens the material. The dissociation of the ions produces a pressure wave and removes the soft material and material debris from the working area.

The location of the spark generation is determined by the slightest gap between the electrode and the work-piece. During the machining process, the spark duration is generally in micro-second (µsec), however, the temperature of the area which is to be removed is very high. With this temperature, the spark partly melts the material and partially vaporizes. The final geometry obtained on the work-piece is the replica of the electrode shape. The intensity of thermal spark directly depends on the current value. With an increase in current, the electrons will strike with greater velocity and hence liberate more thermal energy at the work-piece surface.

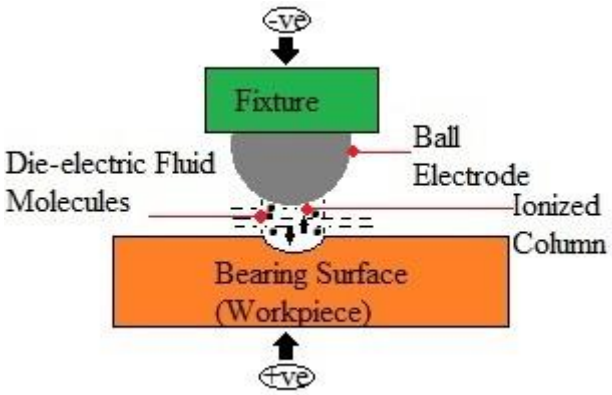

Figure 3.19: Schematic diagram of the electric discharge machining principle

The die-electric fluid in the process isolates the work-piece and electrode surfaces. Apart from this, it also helps in cooling the electrodes and removes the unwanted debris from the machining area and prevents the short-circuiting due to the debris.

For achieving the desired accuracy and shape of the machined work-piece, the gap between the electrode and work-piece should be maintained constant. This is achieved by connecting

the electrode with a servo system. Servo system controls the movement of the electrode and maintains constant gap between the two. Smoother surface, greater accuracy and absence of any mechanical stresses on the work-piece are some of the main advantages of using the EDM process.

In the EDM processing, the shape of the electrode is replicated onto the work-piece surface. In the present work, 7 half spherical dimples of 2 mm diameter and 0.5mm depth are prepared on the inner surface of bearing. For this 7 spherical hardened steel balls of 3mm diameter were attached on a specially designed fixture for making the electrode. The balls were attached on the fixtures by creating a counterbore on the fixture surface of 3 mm diameter and 1.5 mm depth. The balls are fixed on these counterbore with the help of adhesives. The straightness of all the ball surfaces were checked and maintained in level. Figure 3.20 below represents the fabrication process of the electrode.

(a) (b) (c)

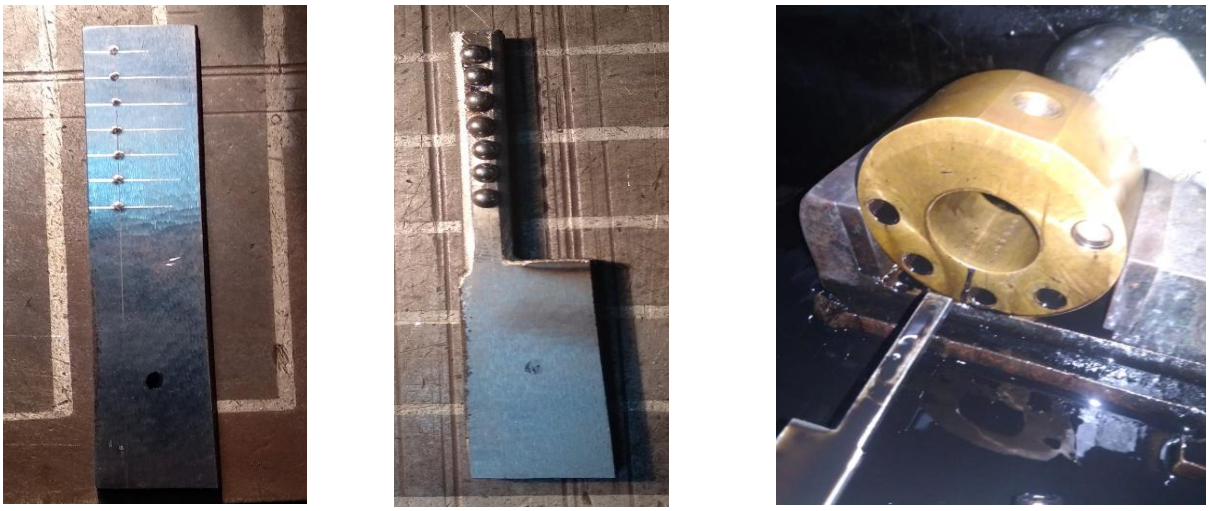

Figure 3.20: (a) Flat fixture for holding the ball (b) The prepared electrode (c) Electric discharge machining set up and positioning of electrode and work-piece.

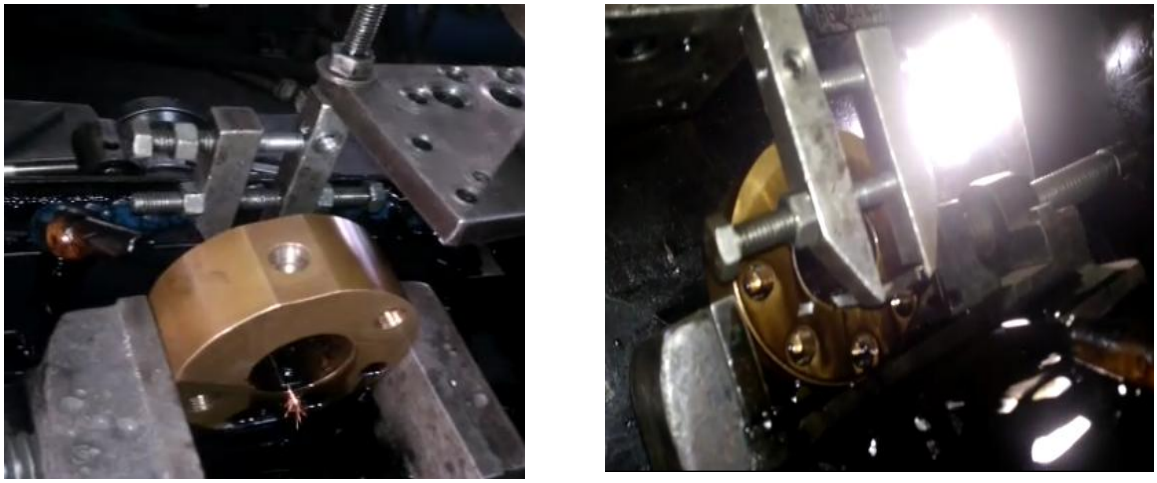

Figure 3.21 : Representation of EDM operation on bearing surface.

Table 3.10: Geometrical dimensions of the bearing

Input Parameter	**Numerical Value**
Bearing Diameter	40
Bearing Length	40
Clearnace (mm)	0.027
Dimple Diameter (mm)	2.3
Dimple Depth (mm)	0.5
No. of Dimples in circumferential direction	5
No.of Dimples in Axial Direction	7
Area Density (%)	0.997 %
Total number of dimples	35

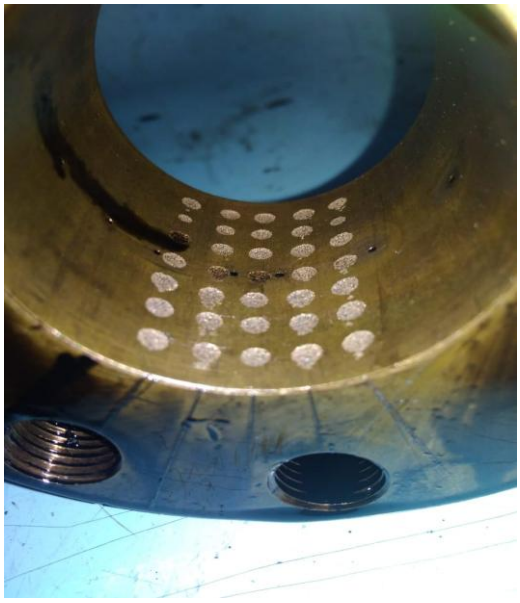

Figure 3.22: Textured journal bearing surface

3.12.2 Lubricating Oils

The performance of a journal bearing system is directly linked with the properties of the lubricating oil. For the experimental investigation, three different grades SAE 10W-40, 10W-15 and 20W-40 were used. The viscosity and density of the oils were measured with the help of "Automated Kinematic Viscometer" and a "U shaped oscillating apparatus" respectively.

(a) (b)

Figure 3.23: (a) Density meter (b) Viscometer

3.13 Computational Fluid Dynamics (CFD)

In this study, a plain journal bearing system and a textured journal bearing system are studied. For maintaining the similarity in the results, the dimensions of the two different bearing geometries are not changed throughout this work. For both geometries, 3 D models are investigated. The dimensions of the journal bearing system are kept same as that of the experimental setup.

3.13.1 Governing Equations

The analysis of CFD model are based on the fundamental equations of fluid dynamics. The continuity equation, momentum equation and Navier-Stokes equations.
The continuity equation presents the conservation of mass. The momentum equation is an equation of conservation for surface forces and volume and "Energy Equation" gives the relationship between the internal energy and other energies related to the fluid.

3.13.2 Simulation Model

A three-dimensional model is developed by using the CFX module. The basic sketch and geometric modeling of the fluid film is created using the SolidWorks software, then the geometry is transferred to ANSYS 19. Further, operations of meshing, model properties and results and analysis are performed using the ANSYS 19.

The basic steps of the performance analysis are presented in Figure 3.24. For analyzing the journal bearing system, it is assumed that, the flow is laminar, the lubricant properties are constant for the complete analysis and a steady state operation is considered.

The parameters used in journal bearing modeling and analyses are:

The diameter of journal (D) = 40.00 mm,

Clearance (radial) = 0.0027mm,

L/D ratio = 1,

Lubricant viscosity=106.39 mm^2/s,

Density=886 kg/m^3,

Angular velocity=8.75 rad/s.

The first step in the modeling of the journal bearing system is the geometric modeling. The clearance between the journal and bearing is filled with lubricant film. This lubricant film is modeled using the design modular. The thickness of this film is kept at 0.027 mm. the top layer of the lubricant layer is named as the "bearing" as it will be in contact with the bearing surface.

The inner part of the lubricant film is named as "journal". For simplifying the geometrical parameters, one side of lubricant oil film is considered as an "inlet" and the other one as an "outlet" (Figure 3.25).

After the design modeling step, next is the meshing of this lubricant film. Meshing defined as the discretization of the continuous body. With this discretization divides the body into finite number of elements. The lubricant film meshed with 40065 Nodes and 118348 elements (Figure 3.26).

The boundary conditions, lubricant properties and material of the components are defined in the "setup" section of the CFX module.
The governing equation for the analysis of the lubricating oil film was solved by assuming the steady-state flow. The gravity forces were not considered in the analysis and operating pressure was set at 101325 Pa.
Based on the geometry of the journal bearing, standard laminar with enhanced wall treatment was is selected as the viscous model along with the energy equation.

The boundary conditions as "pressure inlet" and "pressure outlet" were selected with gauge pressure at zero Pascal. The outer surface of the lubricating oil film is treated as the bearing and inner as the journal.

The bearing surface was modeled as "stationary wall" and journal surface as the "moving wall". An angular velocity equal to the speed of the journal was given to the journal surface of the model.

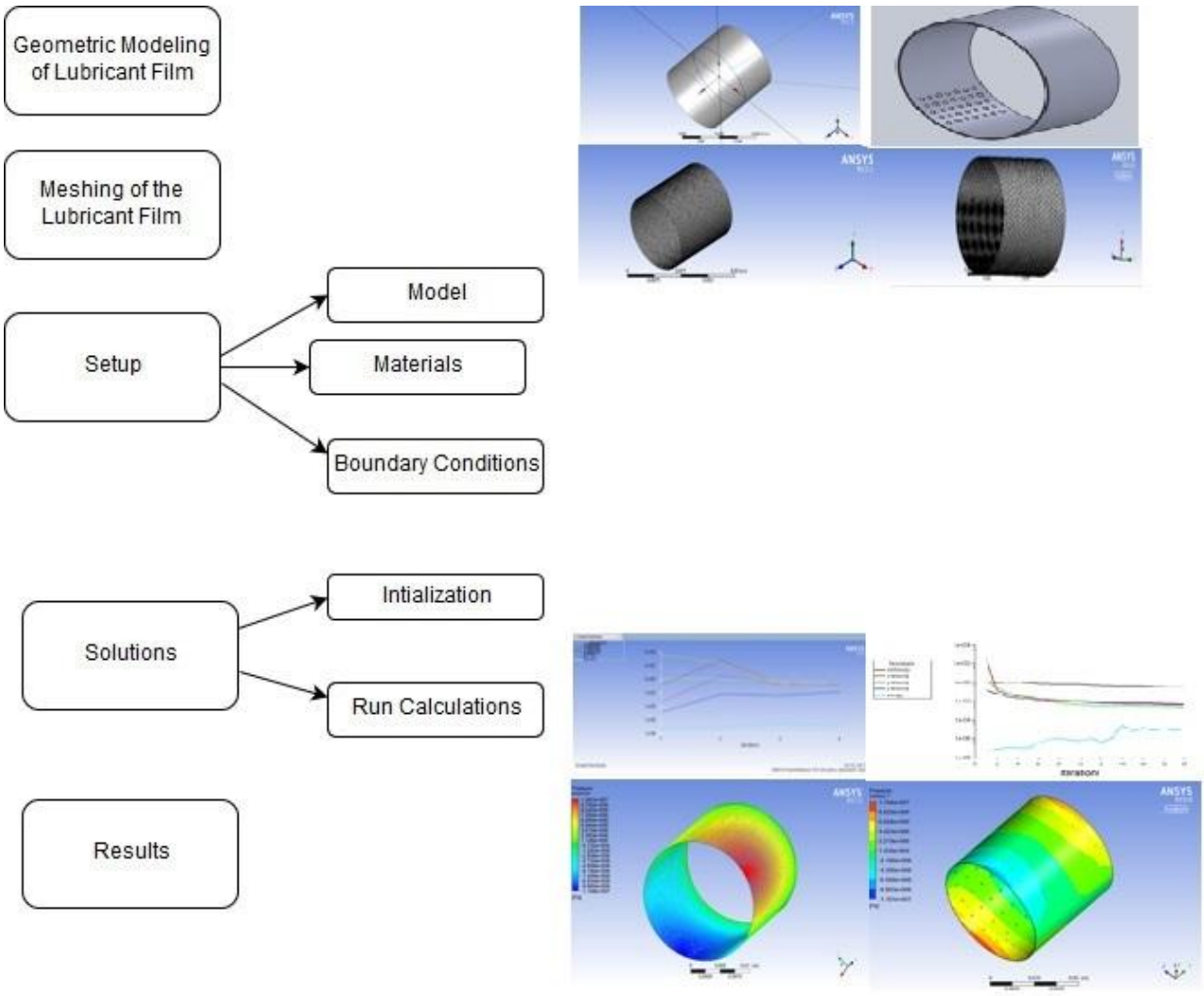

Figure 3.24: Flowchart for the modeling and analysis of lubricant film.

During the analysis of the meshed surface, the size of meshed gets changed with time. To include these changes in the analysis, the dynamic mesh condition was also selected. Dynamic mesh with the "smoothing" option was selected. After incorporating all the boundary conditions, the model was initialized and the solution is iterated for detecting the convergence in the system. For the numerical analysis, pressure based solver was chosen and the coupling between the velocity and pressure is treated by using the SIMPLE algorithm. All other options were kept as default.

Figure 3.25 presents the modeled lubricating oil film. It is modeled using the geometric modeling option from the FLUENT software. After modeling the geometry, the whole geometric surface was mesh into a number of small segments using the meshing technique (Figure 3.26)

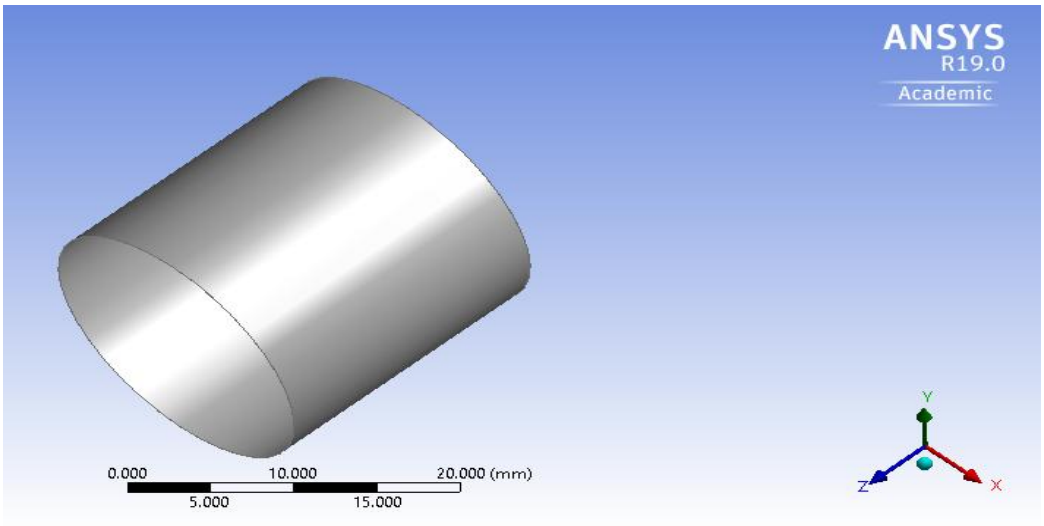

Figure 3.25: Geometry of lubricant oil film.

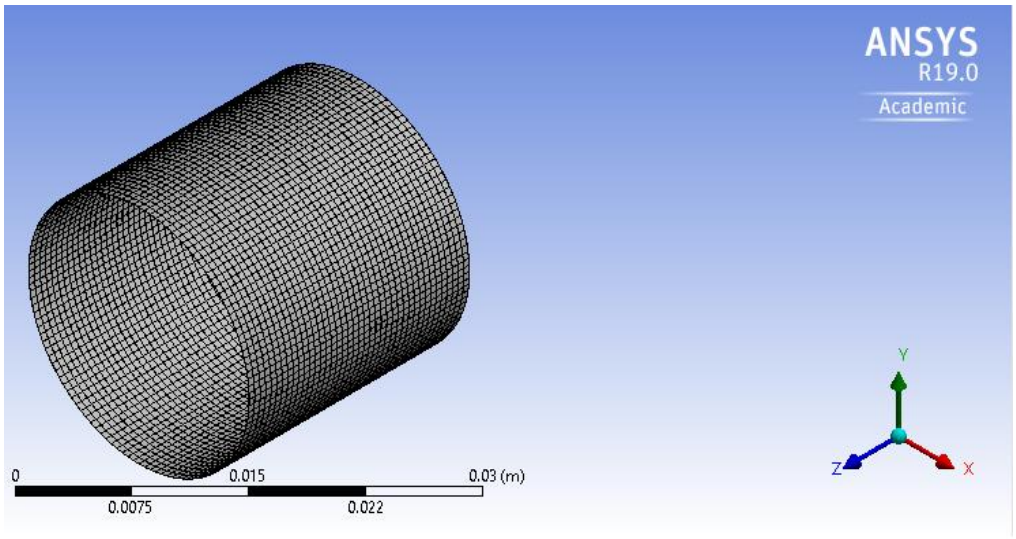

Figure 3.26: Meshed lubricant fluid film.

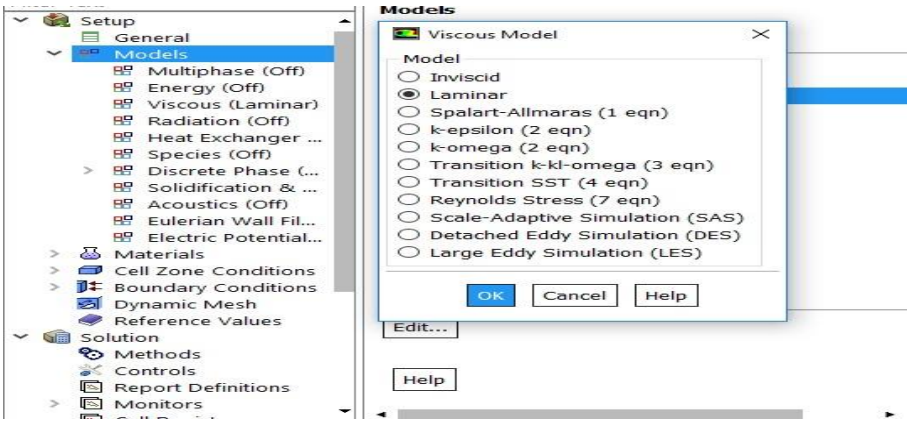

Figure 3.27: Selction of viscous model

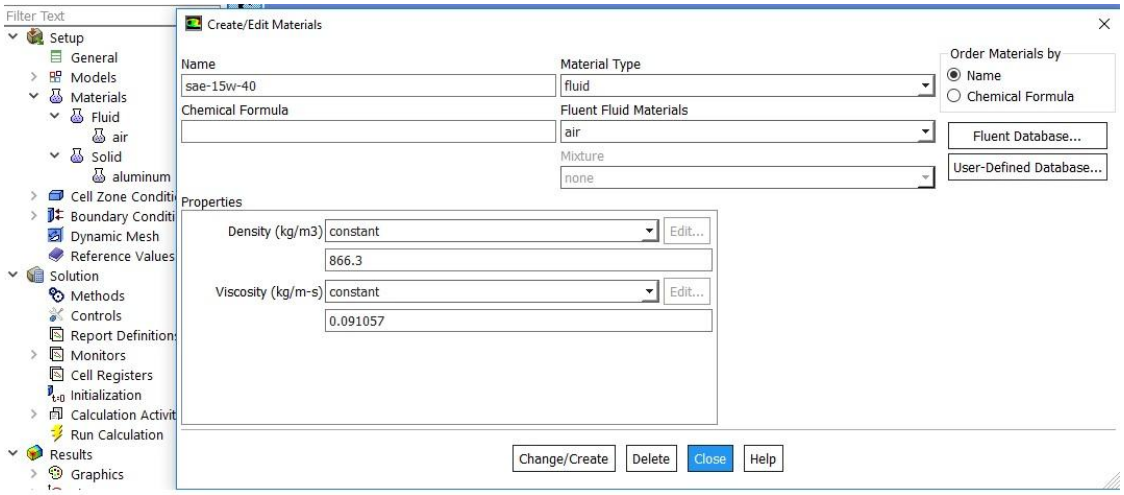

Figure 3.28: Properties of lubricating oil used.

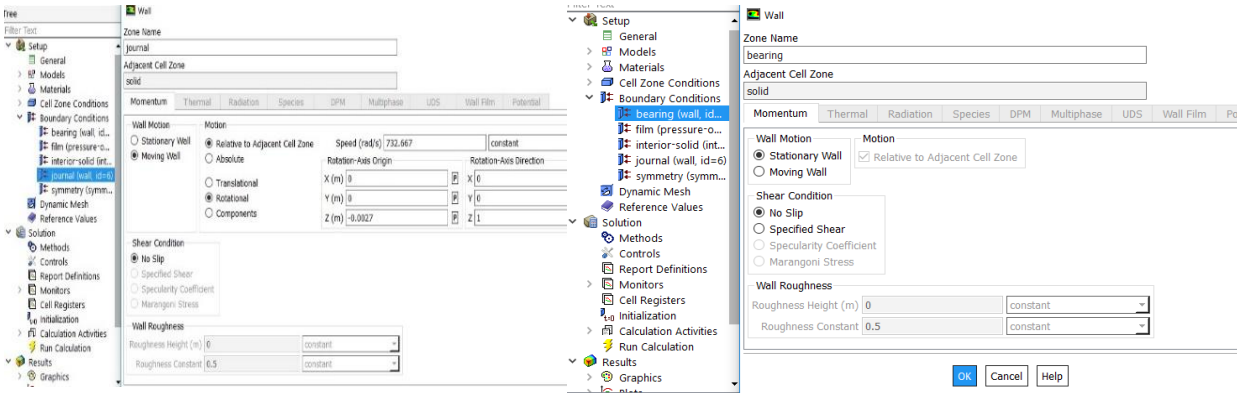

Figure 3.29: Boundary conditions for lubricating oil film.

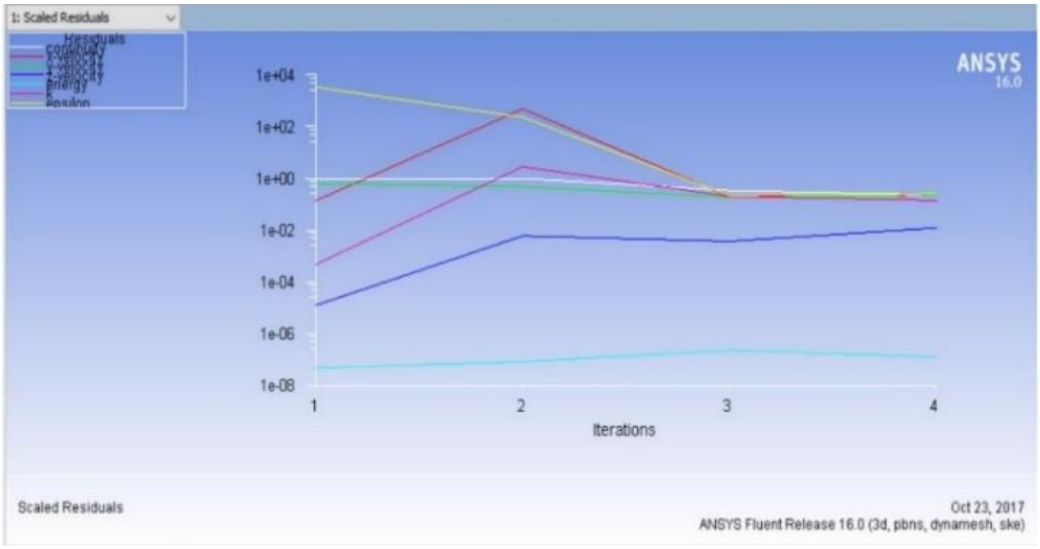

Figure 3.30: Converging results

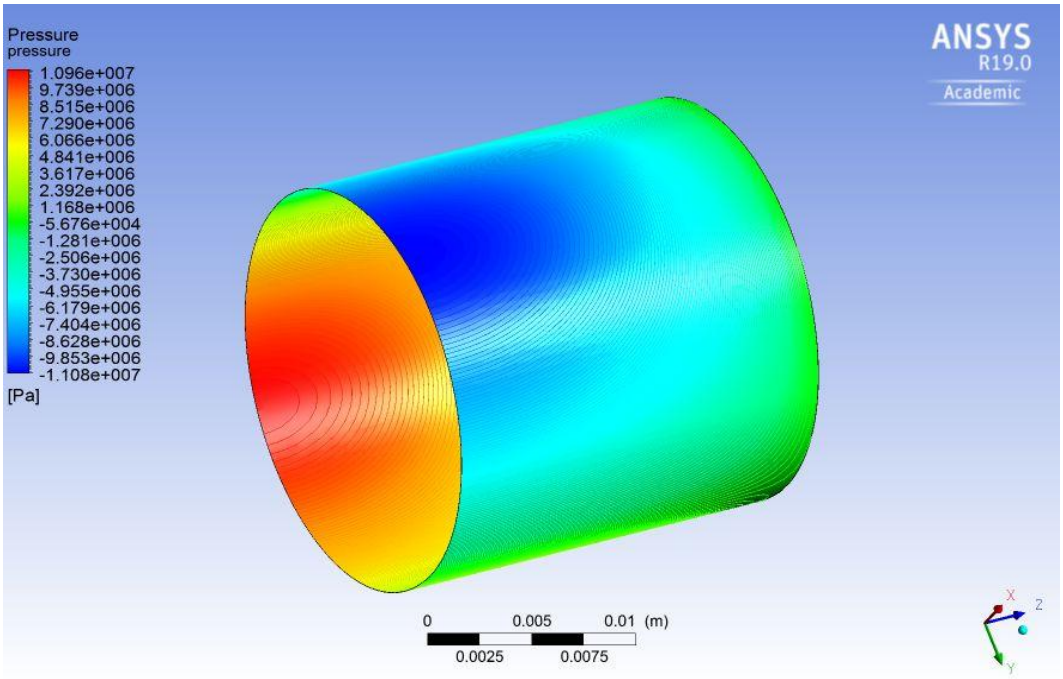

Figure 3.31: Pressure profile for lubricant fluid film

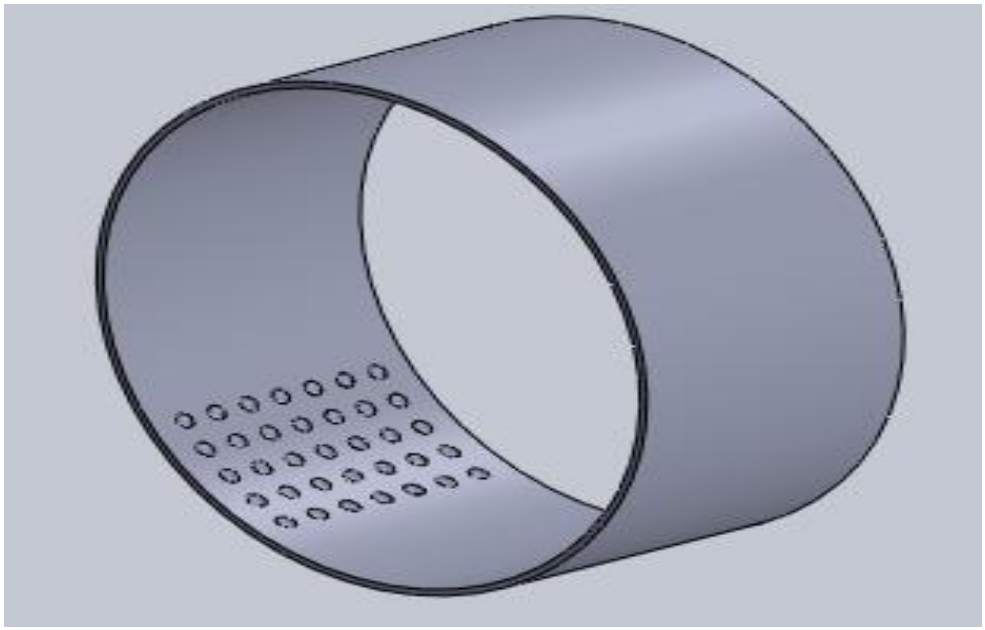

Figure 3.32: Textured fluid film profile

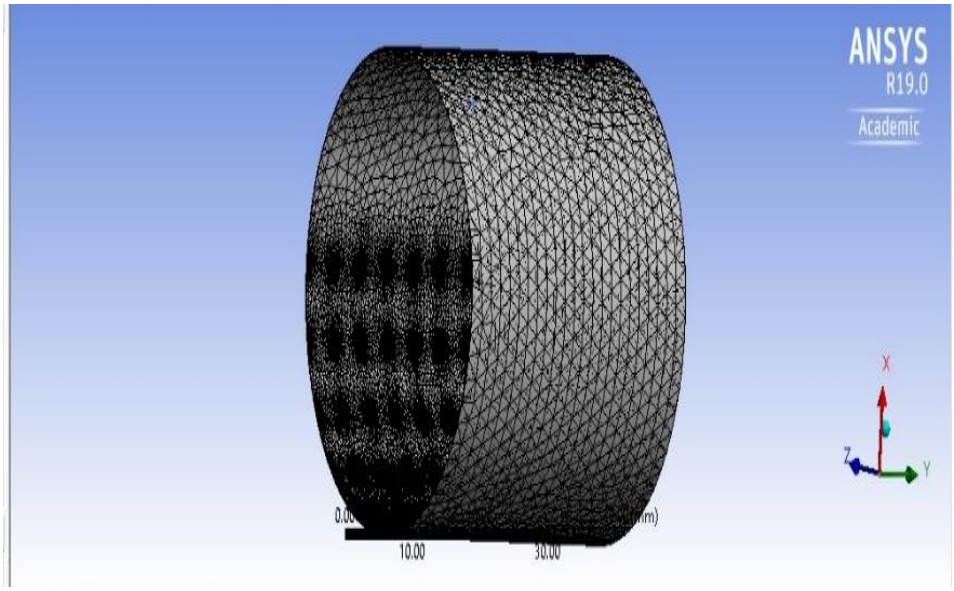

Figure 3.33: Meshed fluid film

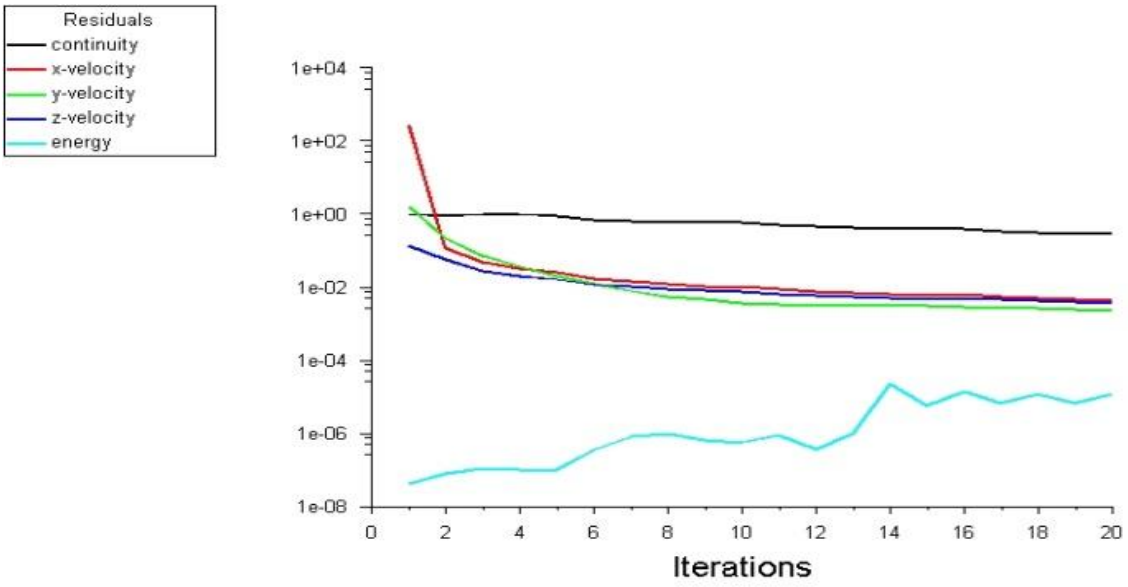

Figure 3.34: Converging results

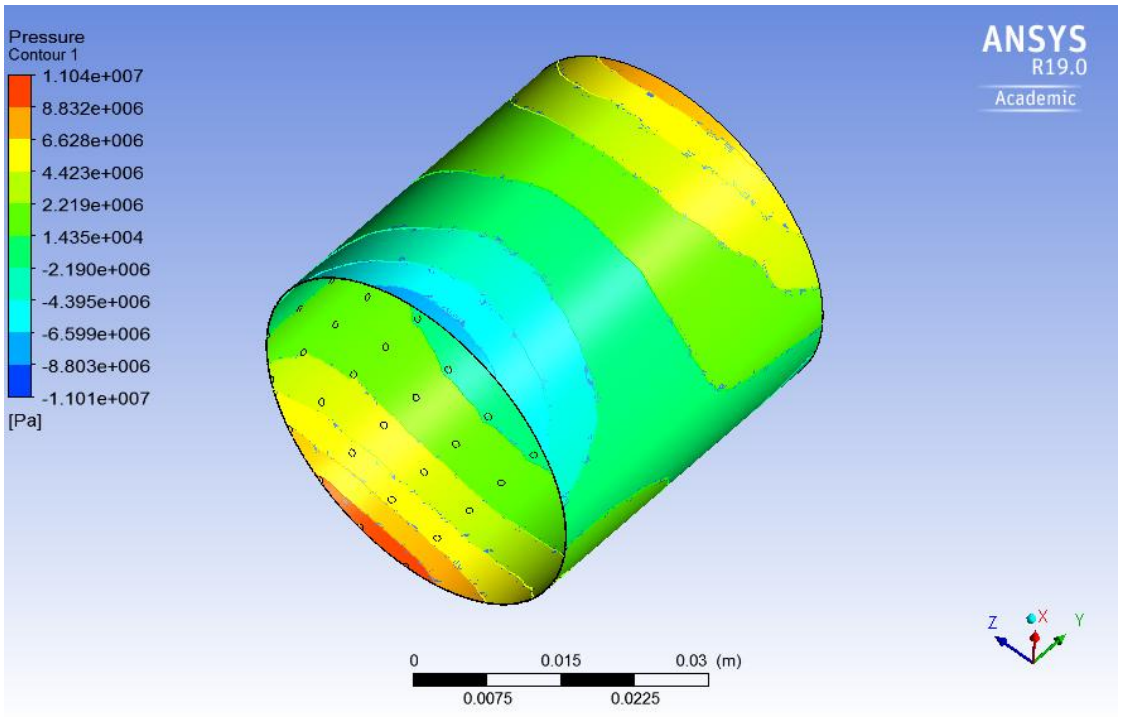

Figure 3.35: Pressure profile

Chapter 4 Results and Discussion

This chapter presents the results of the objectives of this thesis work. Graphs and tabular values are used to presents the results. Section 4.1 presents the wear and friction test results for the fabricated materials. In this, the optical micrographs, pin on disc testing results and scanning electron microscope and electric dispersive analysis results have been explained. In section 4.2 the results obtained from the journal bearing test rig with considering the surface textures have been plotted and explained for the frictional torque and maximum oil film pressure generation. The last section, 4.3 presents the results of the ANSYS modelling.

4.1 Wear and Friction Testing

Two aluminium matrix composites with flyash and graphite as the reinforcing elements have been prepared using the stir casting method. These prepared composites were tested for the proper mixing of reinforcing elements and tribological properties. 2 %, 4% and 6% by weight amount of flyash and graphite were used to fabricate the material. These two aluminium composites were compared for the tribological testing and best one between these was selected for the further investigation.

4.1.1 Aluminium Flyash Composite

The weight loss of the aluminium composite reinforced with different flyash contents is represented in Figure 4.1. It is quite clear that the weight loss of the composites decreases as the flyash contents in the composite increases. The flyash contents present in aluminium matrix resist the destructive action of the wear tests and hence increases the wear resistance of the composites. For sample1 (2% Flyash), Sample 2 (4 % flyash) and sample3 (6 % flyash), the amount of wear obtained are 0.415×10^{-6}, 0.405×10^{-6}, and 0.366×10^{-6} $mm^3/N.m$ respectively. The nature of wear was mostly abrasive.

The coefficient of friction is plotted with respect to sliding time. Data was accumulated for the coefficient of friction with the help of frictional sensor which is linked to the pin on disc machine through computer software. It can be seen from Figure 4.2 that the coefficient of friction is maximum for a sample having a high content of flyash for the initial stages and

lowest for a sample having medium flyash content. It is observed that the coefficient of friction in the medium flyash content sample is less as compared to the other two samples. In composites, the reinforcement in the composite supports the applied load which in result decreases the contact area between the pin and disc surface. Hence Sample 2 resulted in less coefficient of friction as compared to sample 1. It can also be seen from Figure 4.2 that as the flyash content further increases from 4% to 6%, the coefficient of friction increases with sliding time. A large number of flyash particles come in contact with the counter disc and these particles start destructing itself, and thus increase the coefficient of friction. So higher amount of flyash contents are not desirable for obtaining the low coefficient of friction values, although higher amount yield lowest wear rate. The flyash particles are lighter in weight and it wears themselves and protects the aluminium surface from wearing. Also an Al_2O_3 layer prevents the further wearing.

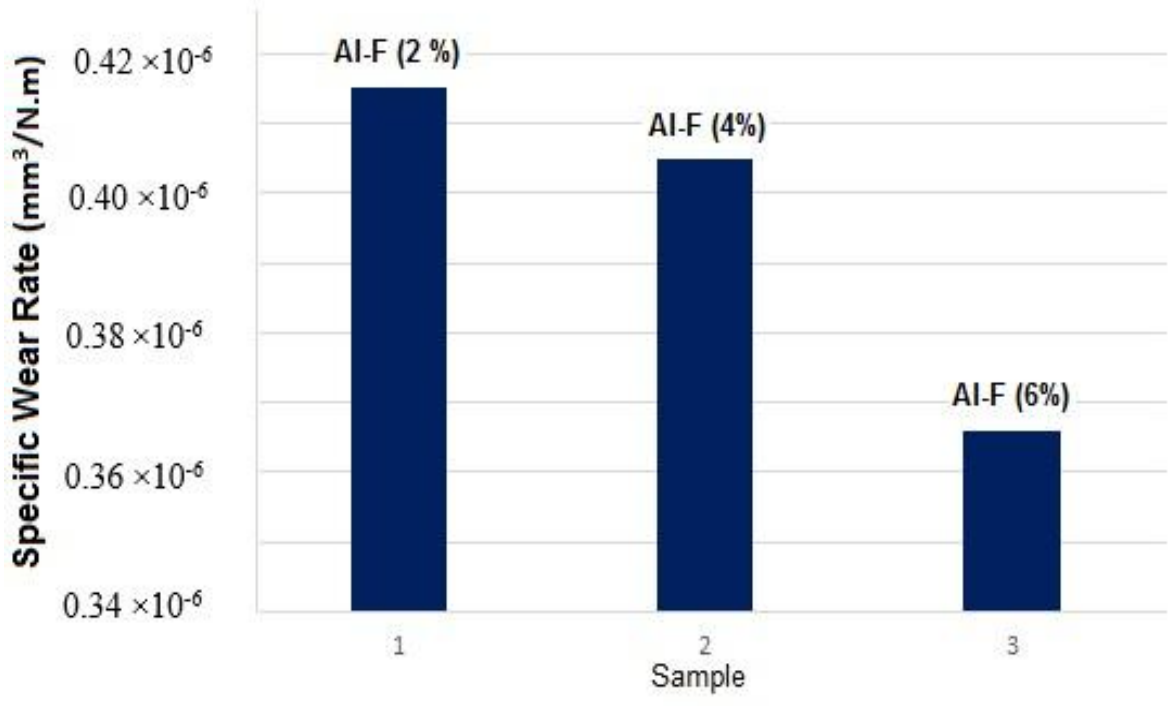

Figure 4.1: Variation of Wear for low, medium and high content flyash specimens

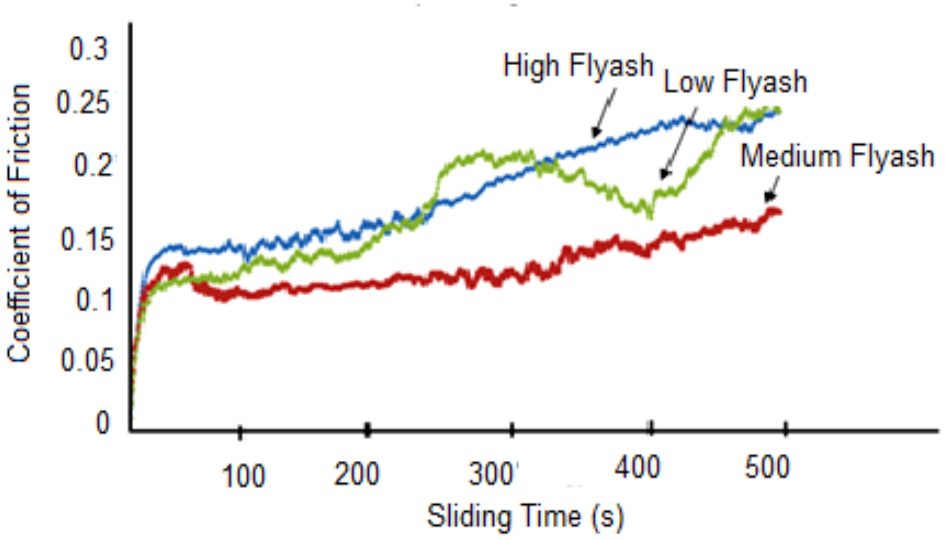

Figure 4.2: Coefficient of frictional with sliding time

4.1.1.1 Surface Analysis

The performance of the aluminium matrix composite depends on the uniformity of the reinforced particles in its matrix. Agglomeration and sedimentation of the reinforced particle results in the fabrication of non-homogeneous composite. To determine the distribution of flyash particles and the presence of the porosity in the composite an optical microscope was used. For optical micrographs, the three samples surfaces were cleaned properly. The cleaned samples were then inspected under a microscope and images have been obtained (Figure 4.3(a), 4.3(b), 4.3(c)). It is seen that for all samples the flyash particles are evenly distributed in the aluminium matrix. Figure 4.3 (b) and (c) also represents the accumulative nature of the flyash particles as their amount increases. Later SEM analysis of the wear area on the composite was also done to understand the different mechanisms of wear during the frictional and wear testing of the composite.

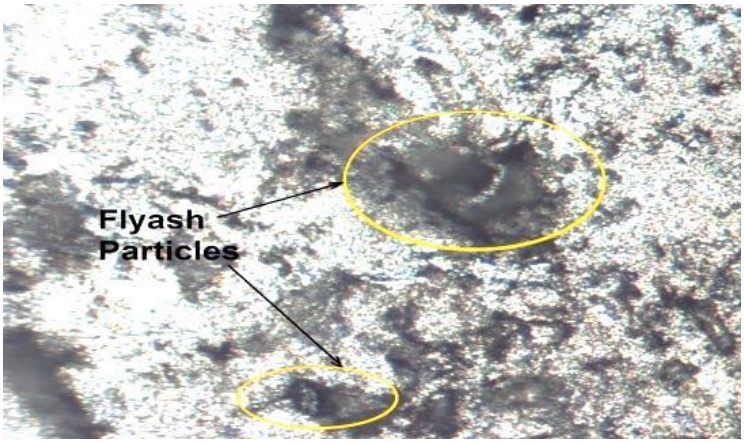

Figure 4.3 (a): Micrograph for low flyash sample

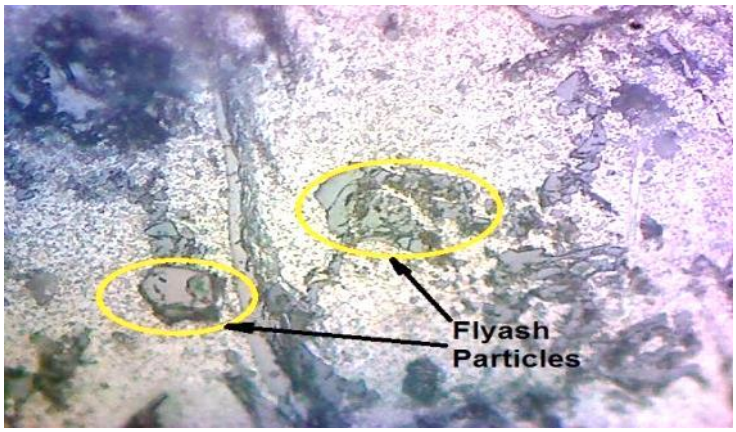

Figure 4.3 (b): Micrograph for medium flyash sample

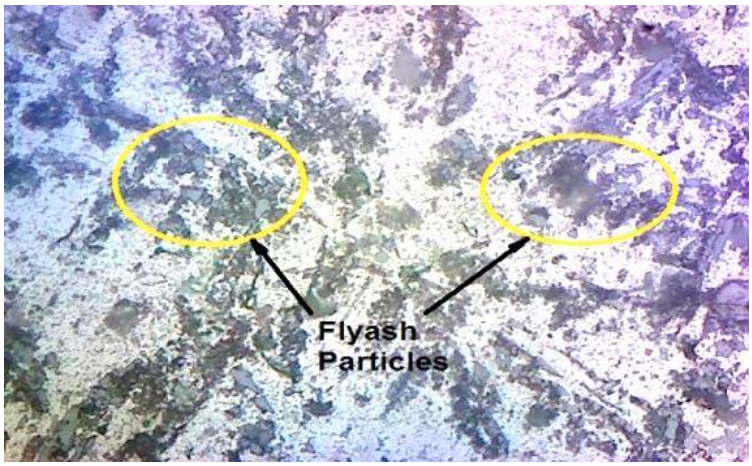

Figure 4.3 (c): Micrograph for high flyash sample

The SEM analysis was done using a scanning electron microscope (HITACHI E 3700N) at 1000 magnification. The obtained SEM images of the different samples are presented in Figure 4.4(a), (b), (c).

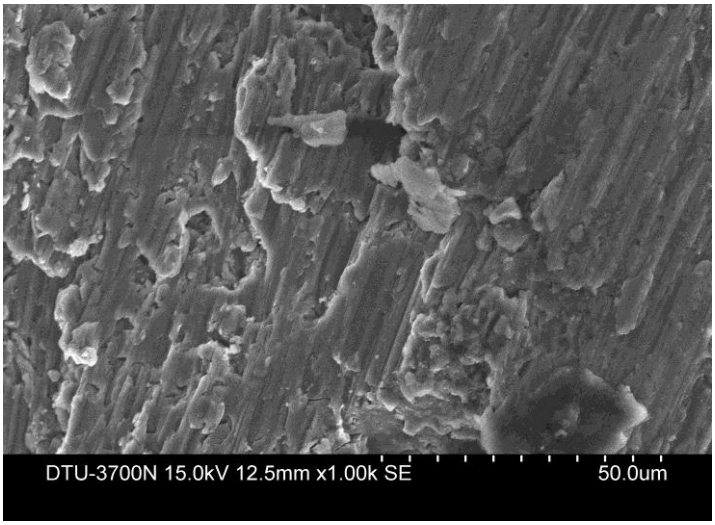

Figure 4.4 (a): SEM images of 2% flyash sample.

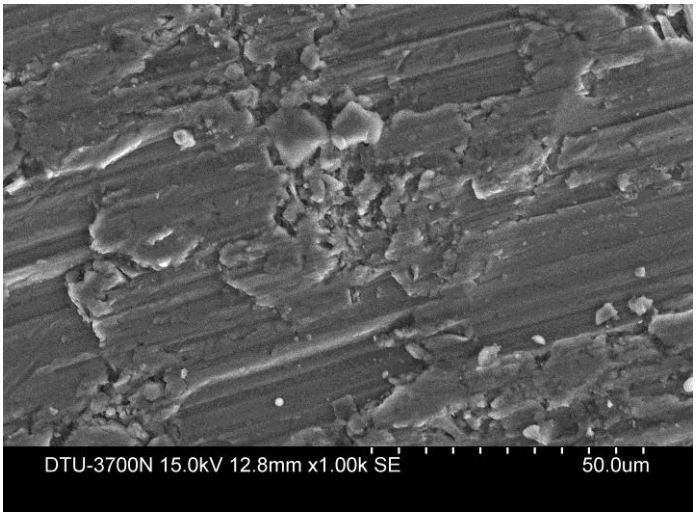

Figure 4.4 (b): SEM images of 4% flyash sample.

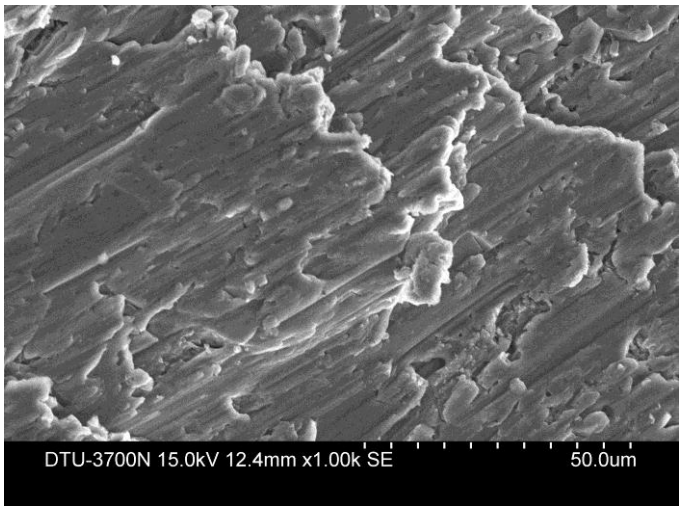

Figure 4.4 (c): SEM images of 6% flyash sample.

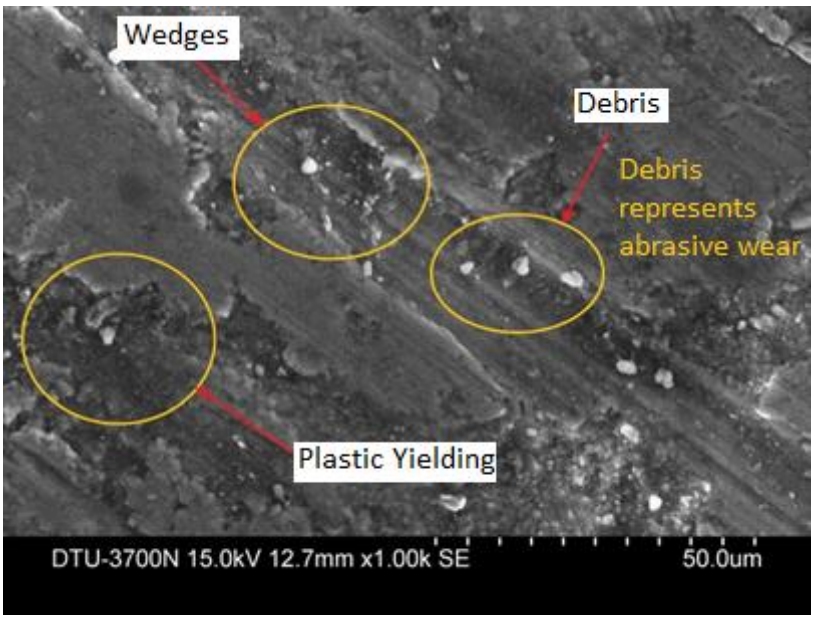

Figure 4.5 (a): SEM images of 2% flyash sample after wear test.

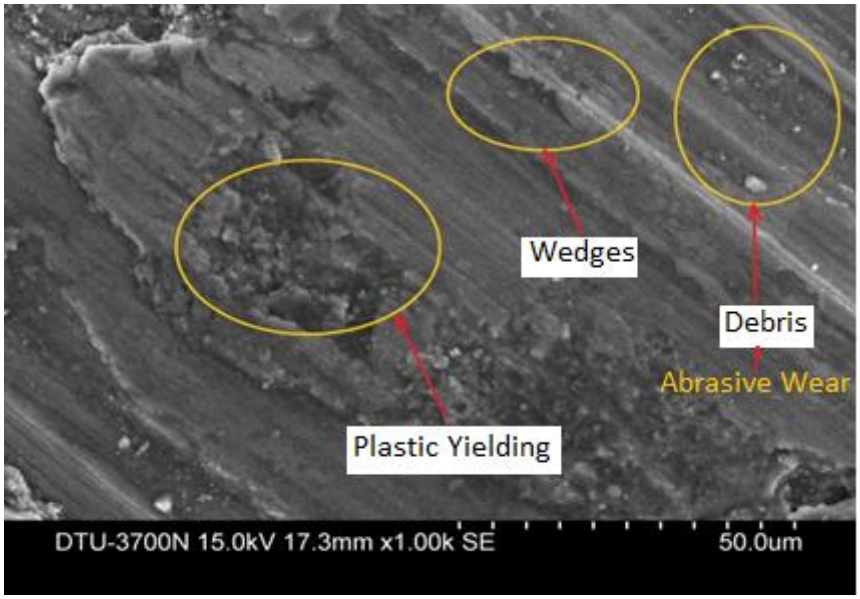

Figure 4.5 (b): SEM images of 4% flyash sample after wear test

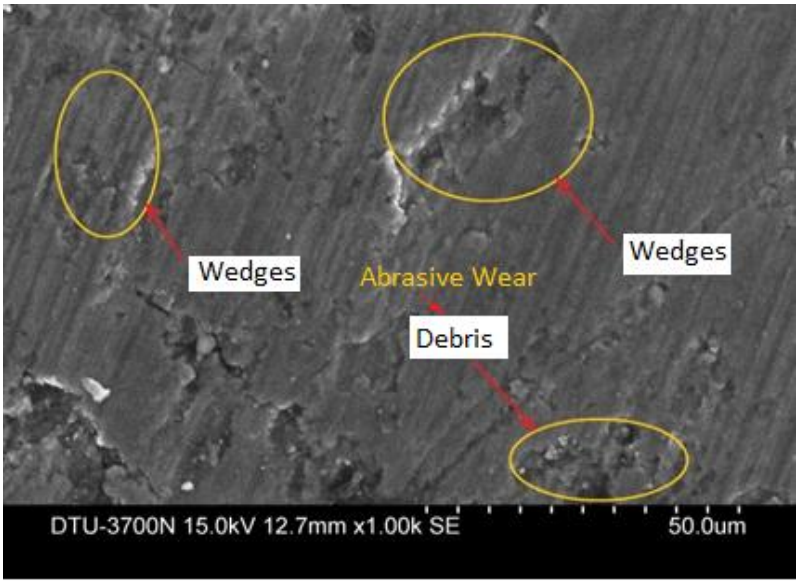

Figure 4.5 (c): SEM images of 6% flyash sample after the wear test

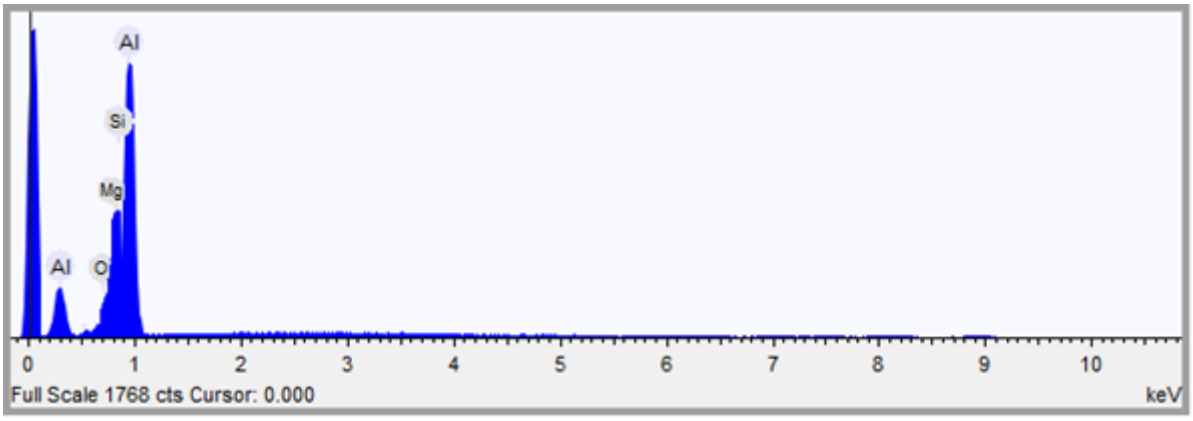

Figure 4.5 (d): EDX analysis of worn Al-F with 6% flyash sample.

Figure 4.5 (a), (b), (c) represents the SEM images of the wear area on the three samples. It is seen from Figure 4.5 (a) that the wear surface of the flyash content sample has many grooves, wedge sections and some plastic yielding on it, 2% flyash content sample clearly indicates the abrasive wear of the surface. These grooves, wedge sections and plastic yielding are also visible in a very limited amount in the 4% flyash content sample. The sample with 6 % flyash contents indicates the very low amount of wedge sections, grooves, and ploughing as visible from Figure 4.5 (c).

Figure 4.5 (d) presents the EDX analysis of the worm Al-F composite. The wear debris on the surface of the worn surface indicates the abrasive wear and flyash contents along with Al_2O_3 layer which was developed due to atmospheric air helped in keeping the surface particles together and increases the wear resistance.

4.1.2 Aluminium Graphite Composite

4.1.2.1 Wear Analysis

The three pin specimens with 2-4-6 wt. % graphite in aluminium were tested against mild steel on a pin on disc tribometer. The wear was recorded with the help of a wear sensor in micrometer units as a function of the length of the pin and plotted for sliding distance (Figure 4.6). Initially, the sensor indicates some negative wear, and after that a transition to abrupt wear because of the breakdown of the wear particle deposits between the pin and disc surfaces.

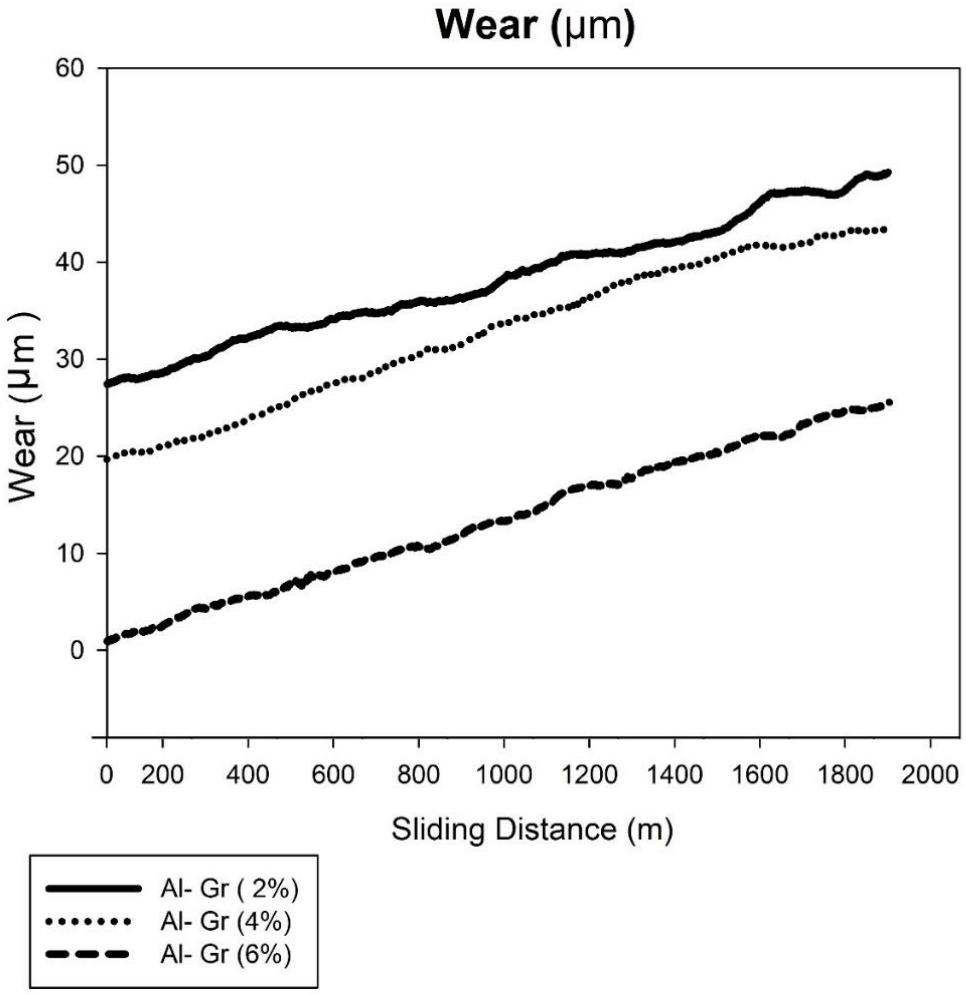

Figure 4.6: Variation of wear for Al-Gr composites.

Figure 4.6 also represents that as the graphite content increases in the aluminium melt, the amount of wear decreases. This decrease in the wear of the Al-Gr composite is due to the reinforcement of graphite particles. The graphite particles behave like a lubricant between the

pin and disc surface and form a very thin layer, thus prevents the metal to metal contact. This nature of wear from the Al-Gr is in good agreement with the results reported by Krishan and Rohatgi (1984).

In the second method, the wear in gram was measured by weighing the pin samples before and after the experimentations. This wear loss was later converted to specific wear rate. Figure 4.7 represents the specific wear loss for the three pin samples and it represents a decrease in specific wear loss with increases in graphite contents.

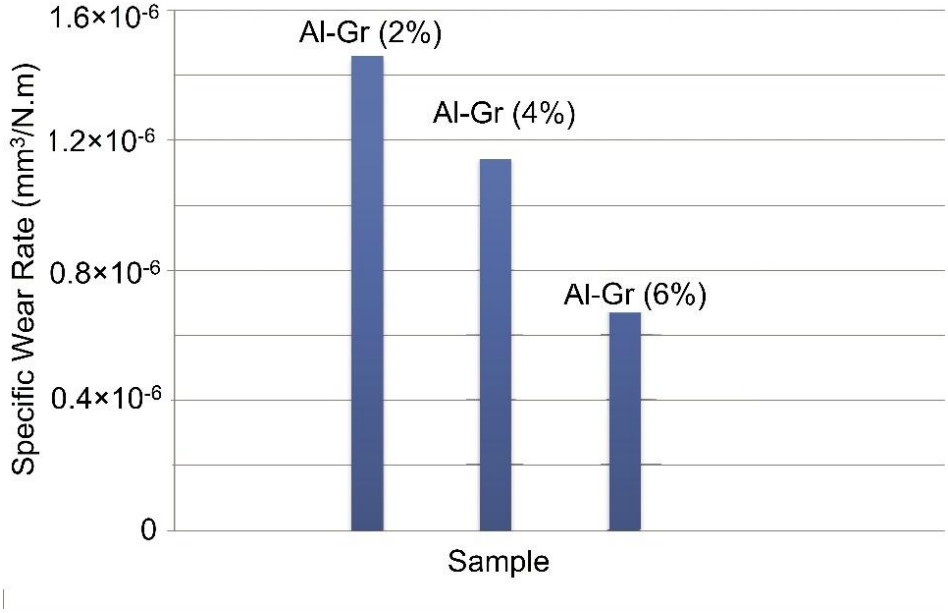

Figure 4.7: Variation of specific wear rate for Al-Gr composite.

4.1.2.2 Coefficient of friction

The variation of coefficient of friction for the three Al-Gr composite materials can be observed from Figure 4.8. Initially, an increase in the value of friction coefficient is observed for all the composite specimens. After the starting running distance of about 200 m, the friction coefficient stabilizes. The specimen with the highest graphite content resulted in the lowest friction coefficient value, followed by medium graphite content specimen and low graphite content specimen resulted in maximum friction coefficient value.

The smeared graphite particles layer which acts as a solid lubricant between the pin and disc surfaces is the possible reason for this decreases in friction coefficient values with increase in graphite contents. Also some protective layer of Al_2O_3 helped in improveing the tribological nature of the developed material. For the composite with 2 wt% graphite particles, the

smeared layer developed is very thin which may cause some metal to metal contact and hence the friction coefficient values is high and as the graphite particles are increasing in the aluminium matrix, the smeared layer of graphite plays a significant role in decreasing the friction coefficient.

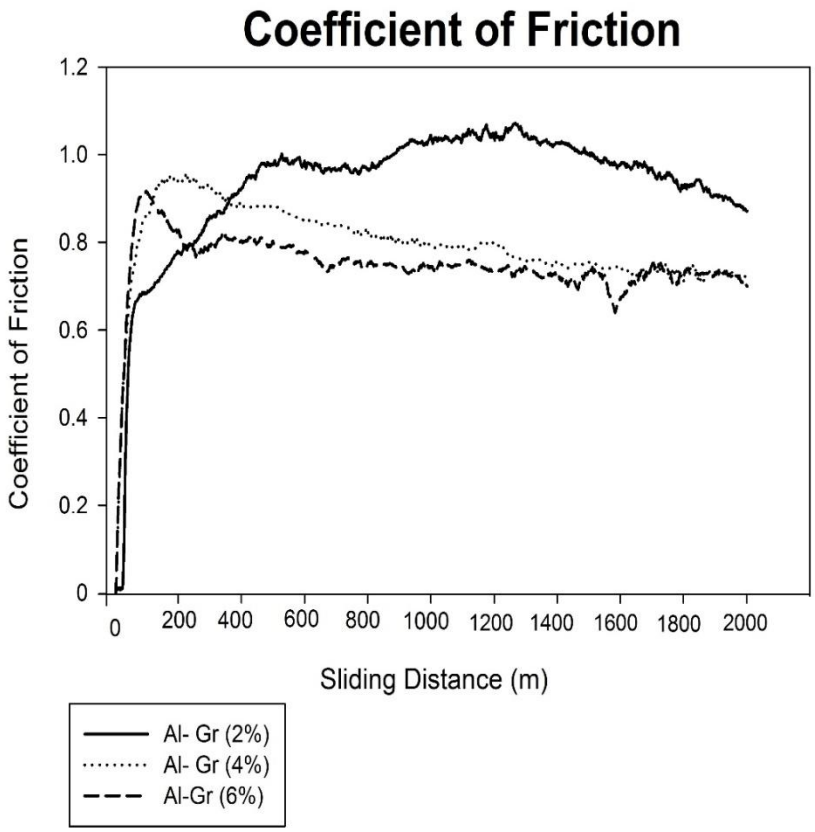

Figure 4.8: Variation of the coefficient of friction for Al-Gr composite.

Table 4.1: Experimental results values for friction coefficient and Sp. Wear rate for tribological testing

S. no.	Pin Specimen	Disc Specimen	Friction coefficient	Sp. Wear Rate (mm^3/N.m)
1	Al-Gr (2%)	Mild Steel	0.815	1.480×10^{-6}
2	Al-Gr (4%)	Mild Steel	0.722	1.155×10^{-6}
3	Al-Gr (6%)	Mild Steel	0.712	0.643×10^{-6}

Table 4.1 represents the average value of the friction coefficient and specific wear rate values for the three Al-Gr composites. There is a 21. 9% decrease in the specific wear rate of Al-Gr

(4%) as compared to Al-Gr (2%) composite material and 11.4 % decreases in the value of friction coefficient.

For comparing the Al-Gr (6%) with Al-Gr (4%), there is 44.3% decrease in the specific wear rate of Al-Gr (6%) as compared to Al-Gr (4%) composite material and 1.3% decreases in the value of friction coefficient.

4.2.1.3 Surface Analysis

Figure 4.9 (a, b, c) represents the scanning electron microscope images for the worn samples of the Al-Gr composites. Figure 4.9 (a) shows the wear area for the low graphite content Al-Gr (2%), composite. The wear marks are visible on the images for the whole area with small debris and wear wedges.

Figure 4.9 (b) depicts the wear area for medium graphite content composite. Al-Gr (4%), samples resulted in less wear as compared to the low graphite content composite. Figure 4.9 (c) represents the wear area Al-Gr (6%), composite. There are very less wear marks visible on the surface of the specimens, which indicates less wear from the composite surface. All the SEM images were obtained at working voltage of 15kV.

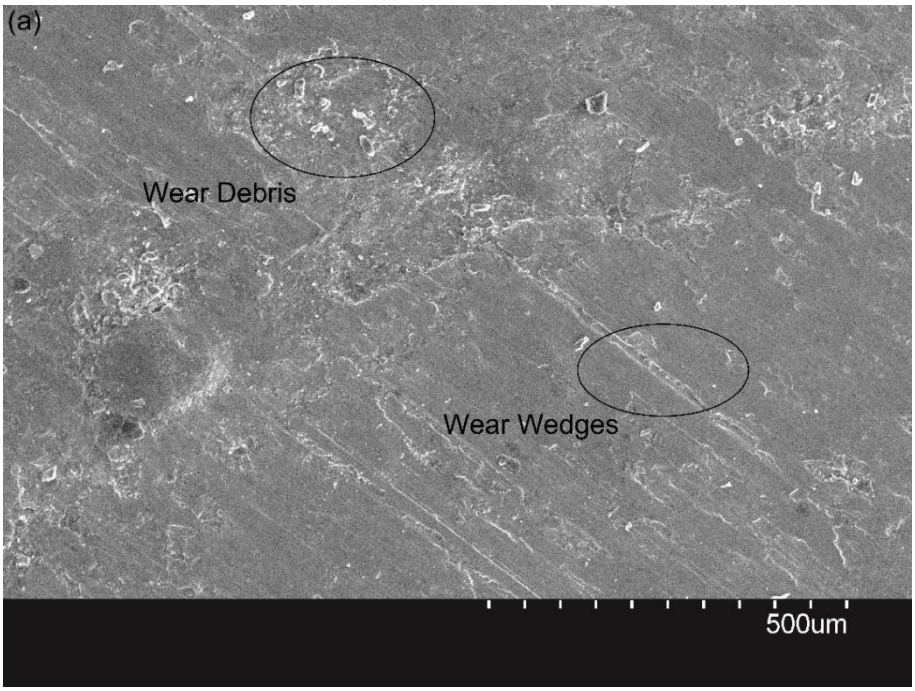

Figure 4.9 (a): SEM images for Al-Gr (2%) composite after the wear testing.

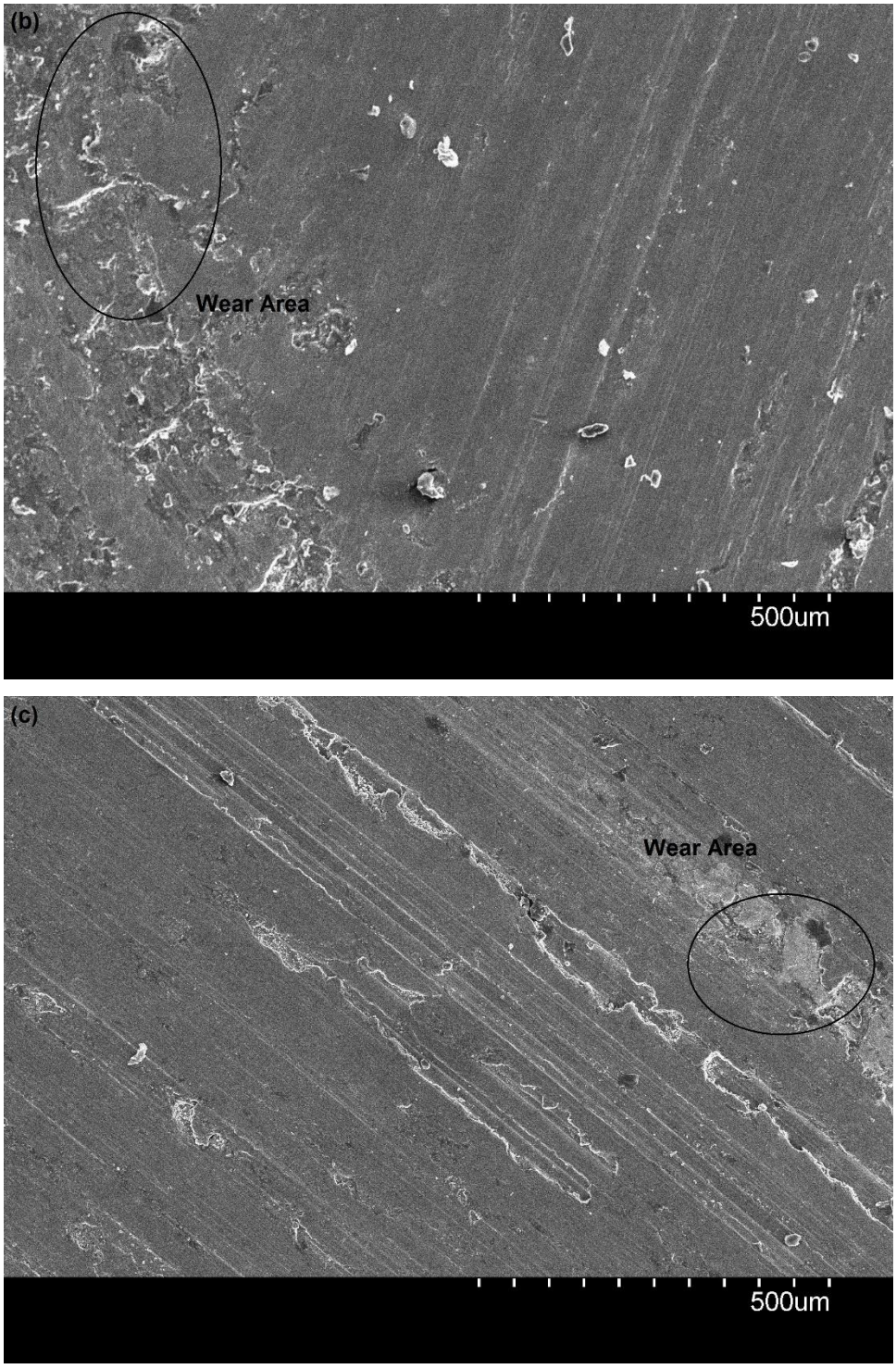

Figure 4.9 (b,c) SEM image Al-Gr (4%), Al-Gr (6%) composite after the wear testing.

After analysis the dry sliding behaviour of the Aluminum-flyash and Aluminium-Graphite composites, it is observed that coefficient of friction value decreases with addition of graphite and flyash particles in the aluminium. The graphite being the solid lubricant decreases the coefficient of friction with increasing graphite contents, which is not in the case of flyash

particles. The composite sample with 4% flyash content yields minimum coefficient of friction value. By comparing the two fabricated aluminium composites, it is observed that aluminium flyash composite resulted in low values of coefficient of friction. Based on this analysis, aluminium flyash composite was considered for further study.

4.1.3 Copper composites

After fabricating and testing the aluminium based composites, two copper-based materials were fabricated and compared with the conventional copper-lead journal bearing material for the tribological properties. Copper (Cu) with Nickel (Ni) and Aluminium (Al) as major alloying elements and copper (Cu) with phosphorous (P) and Aluminium (Al) were fabricated. These fabricated materials were tested for wear and friction properties and compared with copper (Cu)-Lead (Pb) journal bearing material.

4.1.3.1 Wear and Friction Properties

The friction sensor installed on a pin on disc machine measures the friction force between the pin and disc samples. The measured friction force from the sensors is used to calculate the coefficient of friction. The friction sensor records the friction force for a complete run of the sliding distance (4000 m). These continuous measurements were analyzed and average COF values were calculated and plotted against the sliding speed in Figure 4.10 (b-d). The coefficient of friction contains three basic parts as ‘running in’, ’steady state’, and ‘wear out’. For explaining these three parts, Figure 4.10 (a) presents the COF with sliding distance at 0.31 MPa pressure and 4.39 m/s sliding speed values under starved lubrication regime. At the beginning of the running in the stage, the surface asperities of the mating parts generate the substantial friction. The coefficient of friction increases and reaches a maximum value. In the running-in stage, the surface asperities get removed from the mating surfaces and the surfaces become smooth at the steady-state stage. An intermediate stage of the mixed zone is also observed during the testing. This mixed zone represents the transition of the coefficient of friction from running in stage to the steady-state region. During the steady state, the coefficient of friction is nearly constant and minimum. It is desirable for the mating parts to run in the steady-state region. This helps in increasing the life of the components. The wear out stage starts after the steady-state region. In this the coefficient of friction again starts increasing, indicating the massive wear between the mating parts.

The frictional behavior of the three materials is presented in Figure 4.10 (b-d), which shows the variation of COF as a Stribeck curve obtained from the experimental data. For the Stribeck curve, the experiments were performed at three sliding speed values and COF is plotted against the lubrication parameter. For low sliding speed values the COF values are maximum in all the lubrication regimes, and with an increase in sliding speed, the COF starts reducing. It is seen from Figure 4.10 (b) that the average coefficient of friction in fully flooded condition reaches to 0.02 for Cu-Pb, 0.016 for Cu-NiAl and 0.015 for the Cu-PAl material at 4.39 m/s sliding speed value. With further increase in the sliding speed, the COF reduces for all the three considered materials. The Cu-PAl material resulted in least amount of coefficient of friction. The range of COF (0.009-0.020) indicates that the contacts were in hydrodynamic lubrication regime. The presence of aluminium in the copper matrix for Cu-NiAl and Cu-PAl helps in maintaining the low values of COF. The oxygen in SAE 15W-40 lubricating oil combines with aluminium and makes a layer of Al_2O_3 which protects the material from wearing and reduces the COF. This Al_2O_3 oxide layer is also reported by Basumatary and Wood (2017) in the NaCl solution.

Figure 4.10 (c) presents the average COF values for the starved lubrication condition. In starved condition, a single layer of oil was applied on the disc surface and experiments were performed. In this, the lubricating oil prevents the metal to metal contact for some-time after which, a heavy amount of wearing was observed during the experimentation. This leads to higher COF for all three materials. Cu-NiAl resulted in the maximum amount of COF and Cu-PAl performs slightly better than the Cu-Pb material at all sliding speed values. However, for a particular material, the COF value reduces considerably at higher sliding speeds. The soft phases of lead and phosphorous helped in reducing the COF for Cu-PAl and Cu-Pb materials. The soft phases in the Cu-PAl and Cu-Pb detached themselves from the copper matrix and leave behind microvoids. These microvoids act as the lubricant reservoir and provide the lubricant oil in case of scarcity of lubricating oil.

The dry sliding results for COF with a varying sliding speed are presented in Figure 4.10 (d). The presence of lead and phosphorous in Cu-Pb and Cu-PAl helps in reducing the COF values. Figure 4.11 (a-c) shows a transfer of metal layer on the disc surface, which prevents the wear of the pin and disc surfaces and hence the two surfaces remain smooth and resulted in low COF values.

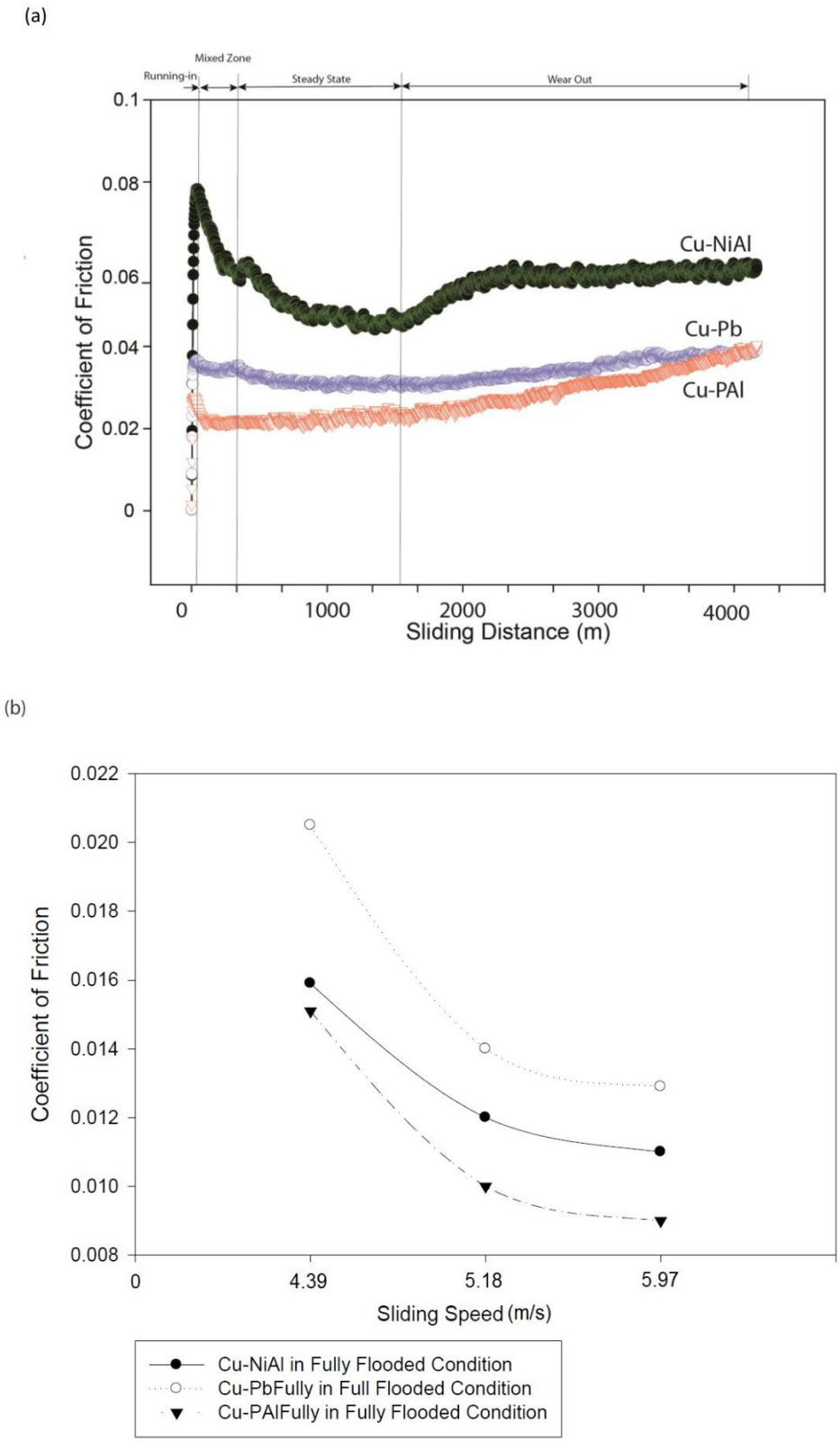

Figure 4.10: (a) Variation of the coefficient of friction at 0.31 Pa and 4.29 m/s in starved condition (b) COF with sliding speed in fully flooded lubrication condition

(c)

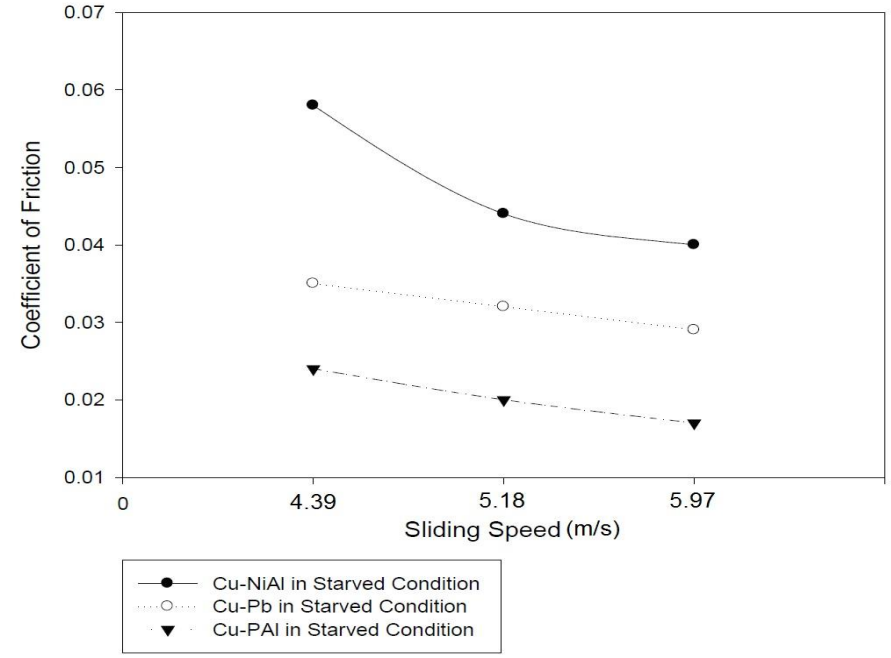

(d)

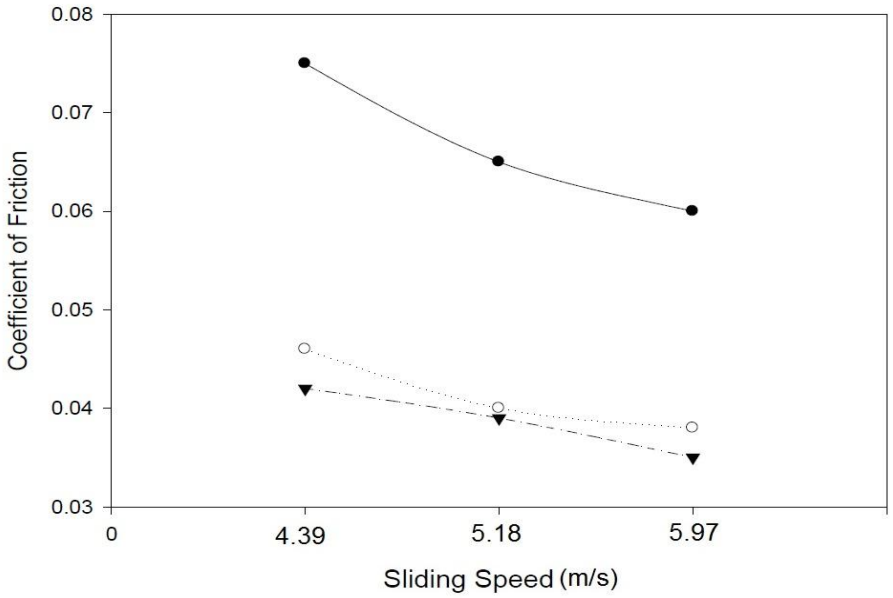

Figure 4.10: (c) COF with sliding speed in Starved lubrication condition (d) COF with sliding speed in unlubricated condition

During the testing of the wear, the change in weight of the pin samples was recorded to evaluate the specific wear rate. Equation (3.1) was used to calculate it. It is seen from Figure 4.13 (a,b,c) that, in case of fully flooded condition the Cu-NiAl resulted in low specific wear

rate as compared to Cu-Pb and Cu-PAl for all the considered sliding speed values. Formation of the aluminium oxide layer due to the presence of oxygen in lubricating oil on the surface of the material could be a reason for this improvement in wear properties [Prasad (2000), Hutchings (1992)]. The oxide film formed on the Cu-NiAl materials consists of alumina-rich inner layer and copper oxide film as an outer layer. During the initial sliding of the pin on disc specimen, the alumina oxide layer transfers and adheres itself to the steel disc. This phenomenon forms a stable layer on the steel disc surface and a stable copper-rich oxide layer remain on the pin surface. This stable combination of two oxide layers on the disc and pin provides the excellent wear resistance to the Cu-NiAl. The oxygen present in the lubricant oil helps in maintaining the continuous formation of this oxide layer [Prasad (1997)]. Since aluminium oxide is a very hard compound, so it works as a load carrying phase. The presence of zinc in the material also forms an oxide as zinc oxide which helps the material in lubrication [Torabian et al. (1994)].

In the case of starved and unlubricated conditions, Cu-NiAl resulted in the maximum amount of SWR. In the absence of lubricating oil, the lead and phosphorous in Cu-Pb and Cu-PAl transfer a thin layer on the disc surface and promotes the easy shearing between the layer particles. This also ensures a low friction coefficient in the absence of lubricating oil as well. The formation of this layer is a significant characteristic of the Cu-Pb and Cu-PAl material.

These two-layers were clearly visible during the tribological testing of the Cu-Pb and Cu-PAl. Figure 4.11 shows these layers on the surface of disc specimens. The Cu-PAl resulted in lowest SWR for starved as well as unlubricated conditions.

The presence of lead and phosphorous particles was also verified by the EDX analysis of the disc. Figure 4.12 (a,b,c) presents the EDX results for the disc specimens used for wear and friction testing of Cu-NiAl, Cu-Pb, and Cu-PAl materials. The EDX results were obtained at 10 keV with nearly 1700 counts. Small peaks of Cu with other alloying elements are visible on the EDX pattern clearly. The EDX analysis of the disc samples revealed the presence of lead and phosphorous elements on the surface of the disc. These layers helped in reducing the wear from the pin specimens.

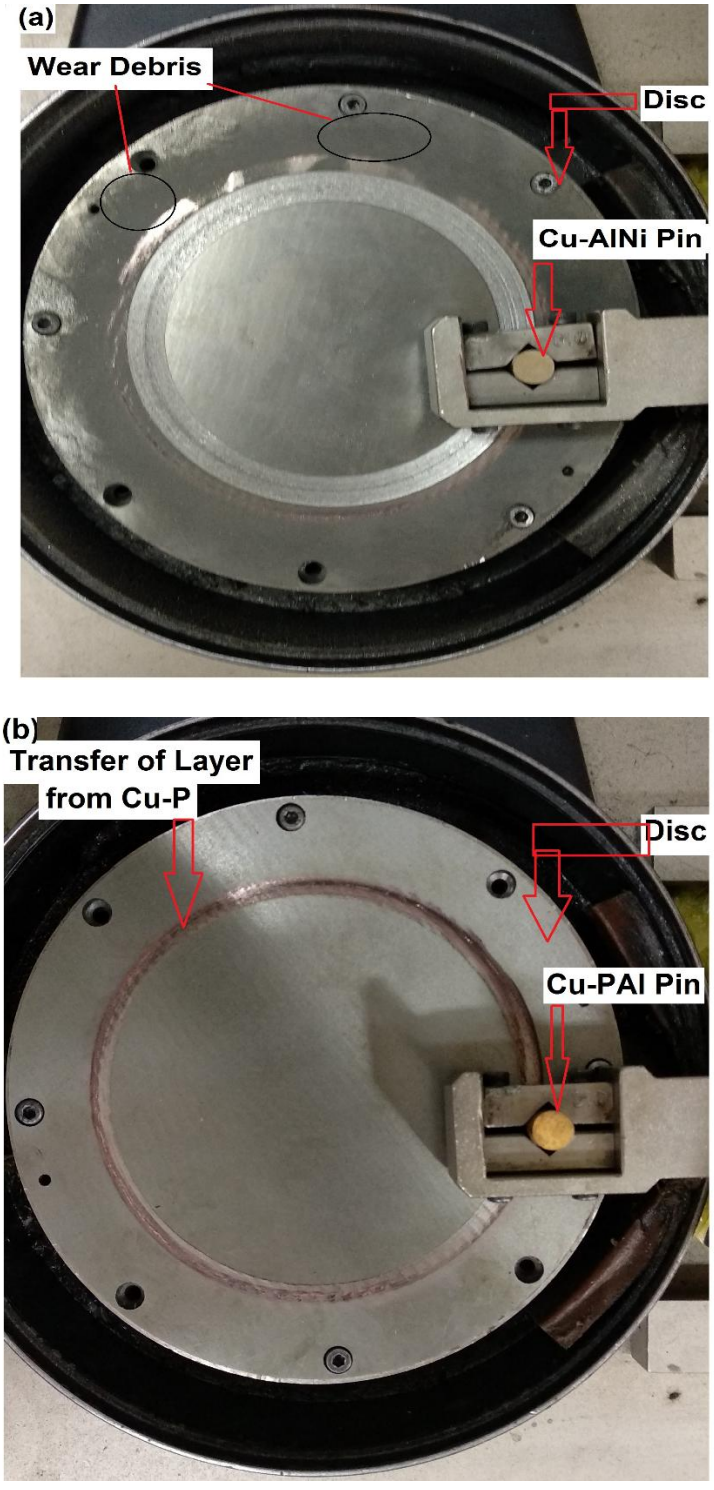

Figure 4.11: Presentation of layers on the disc surface of (a) for Cu-NiAl (b) Cu-PAl material

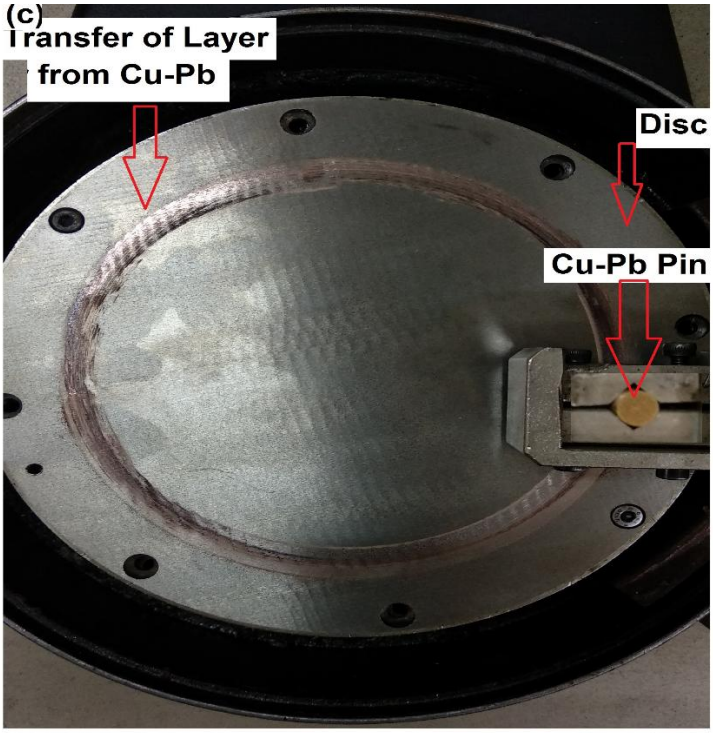

Figure 4.11: (c) Presentation of layers on the disc surface of Cu-Pb material.

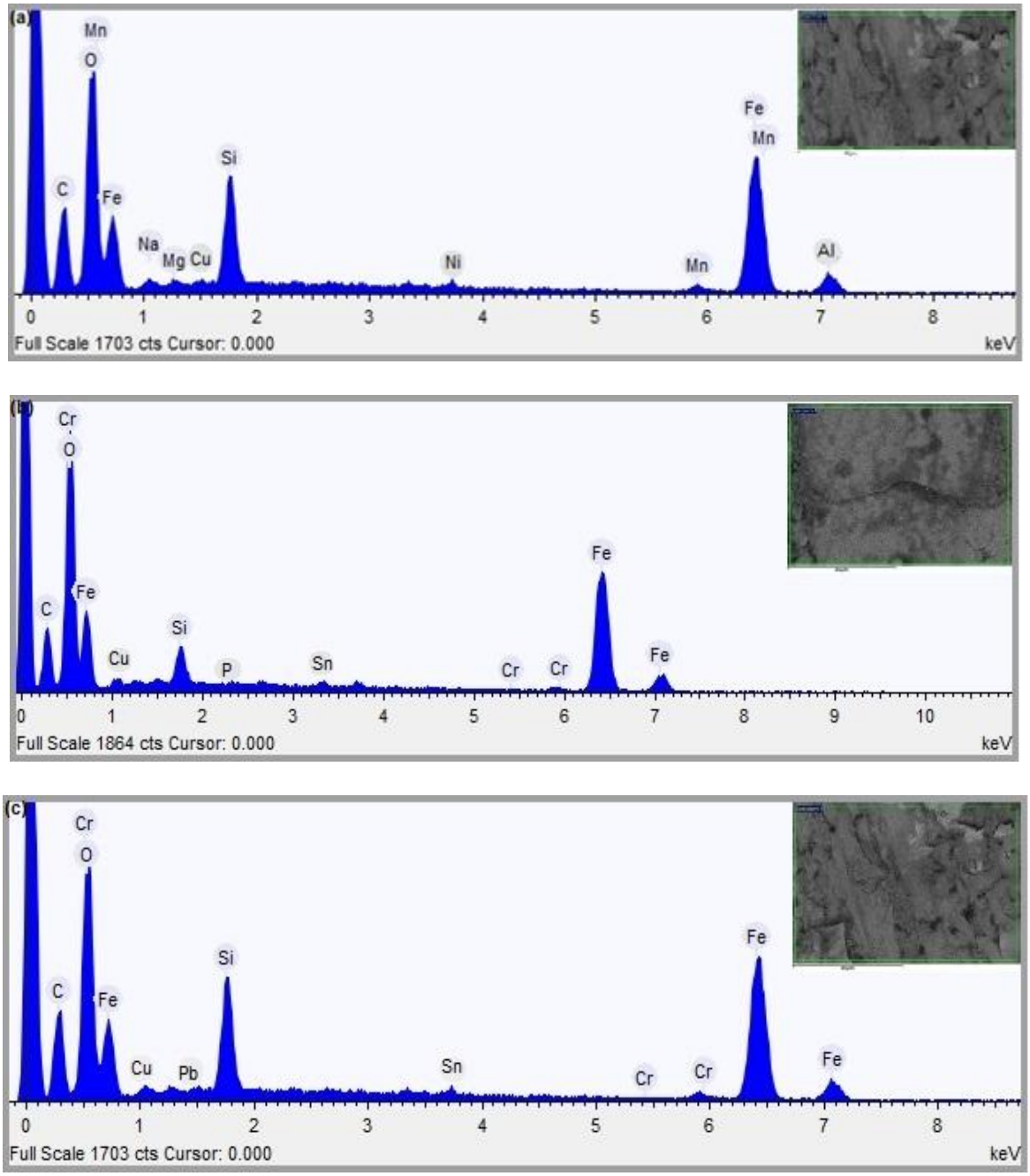

Figure 4.12: EDX analysis for the worn disc surface obtained by mating with (a) Cu-NiAl material (b) Cu-PAl material (c) Cu-Pb material.

(a)

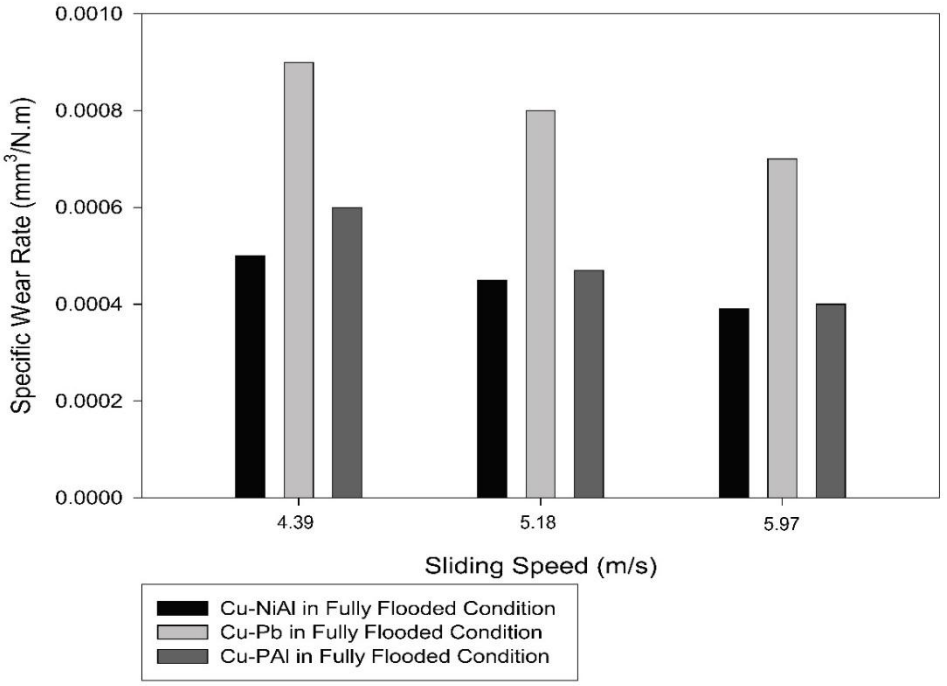

(b)

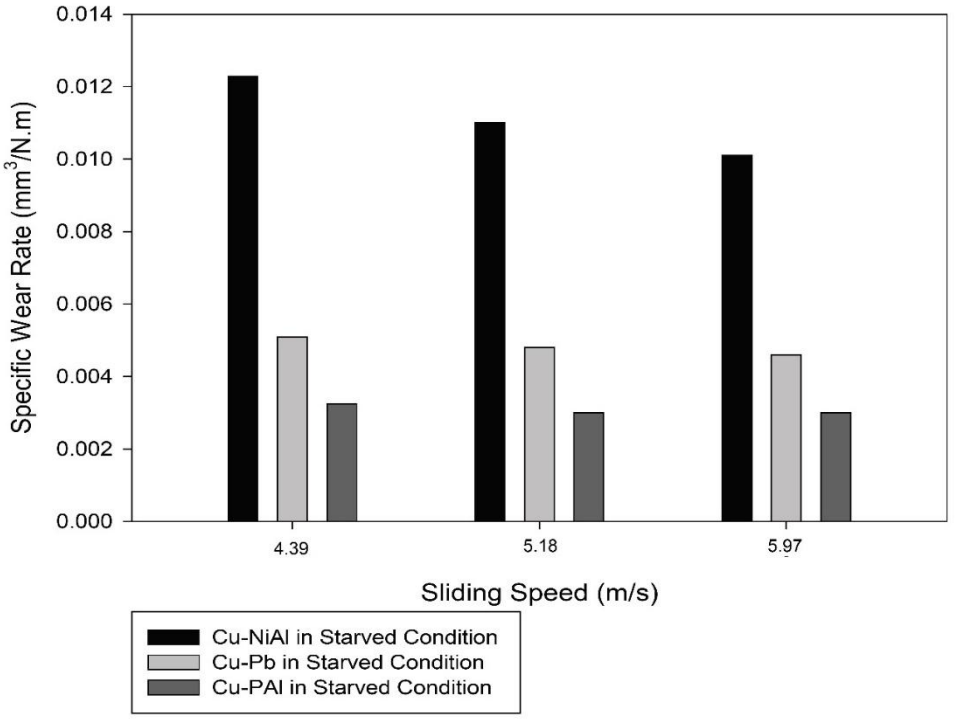

Figure 4.13: Variation of specific wear rate for the pin samples in (a) fully flooded lubrication (b) starved lubrication

(c)

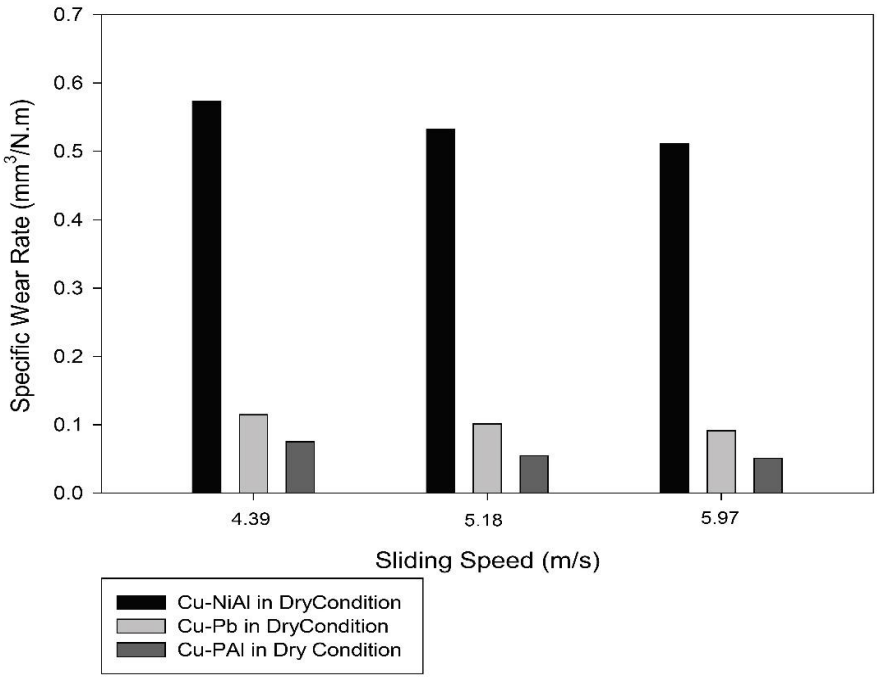

Figure 4.13: Variation of specific wear rate for the pin samples in unlubricated condition.

4.1.3.2 Surface Analysis

Figure 4.14 (a) presents the scanning electron microscopy (SEM) image of the worn Cu-NiAl pin sample. The SEM images show the deep grooves and wear a wedge section on the worn pin sample. The large friction coefficient on the Cu-NiAl surface promotes the formation of the damaged layer which undergoes plastic deformation. The Cu-NiAl suffered heavy wear in unlubricated condition, which is evidenced by deep grooves on the worn pin surfaces. Figure 4.14 (b) presents the SEM image of the worn Cu-PAl pin sample. Flat wear areas were observed on the Cu-PAl worn pin samples. Some thin wear wedges are also visible on the surface of the worn sample. Thin wear lines are also visible on the optical micrograph obtains at 10X magnification. The presence of iron particle (Fe) is also visible on the worn surface of the Cu-Pb material. The embed-ability property of the copper material plays a significant role in entrapping the iron particles in the copper matrix. Some amount of the carbon layer is also visible on the wear surfaces of both the materials. Figure 4.14 (c) presents the SEM image of the worn Cu-Pb pin sample. Some shallow grooves are visible on the surface of the worn sample. These shallow grooves are also visible on the optical micrograph obtained at 10X magnification.

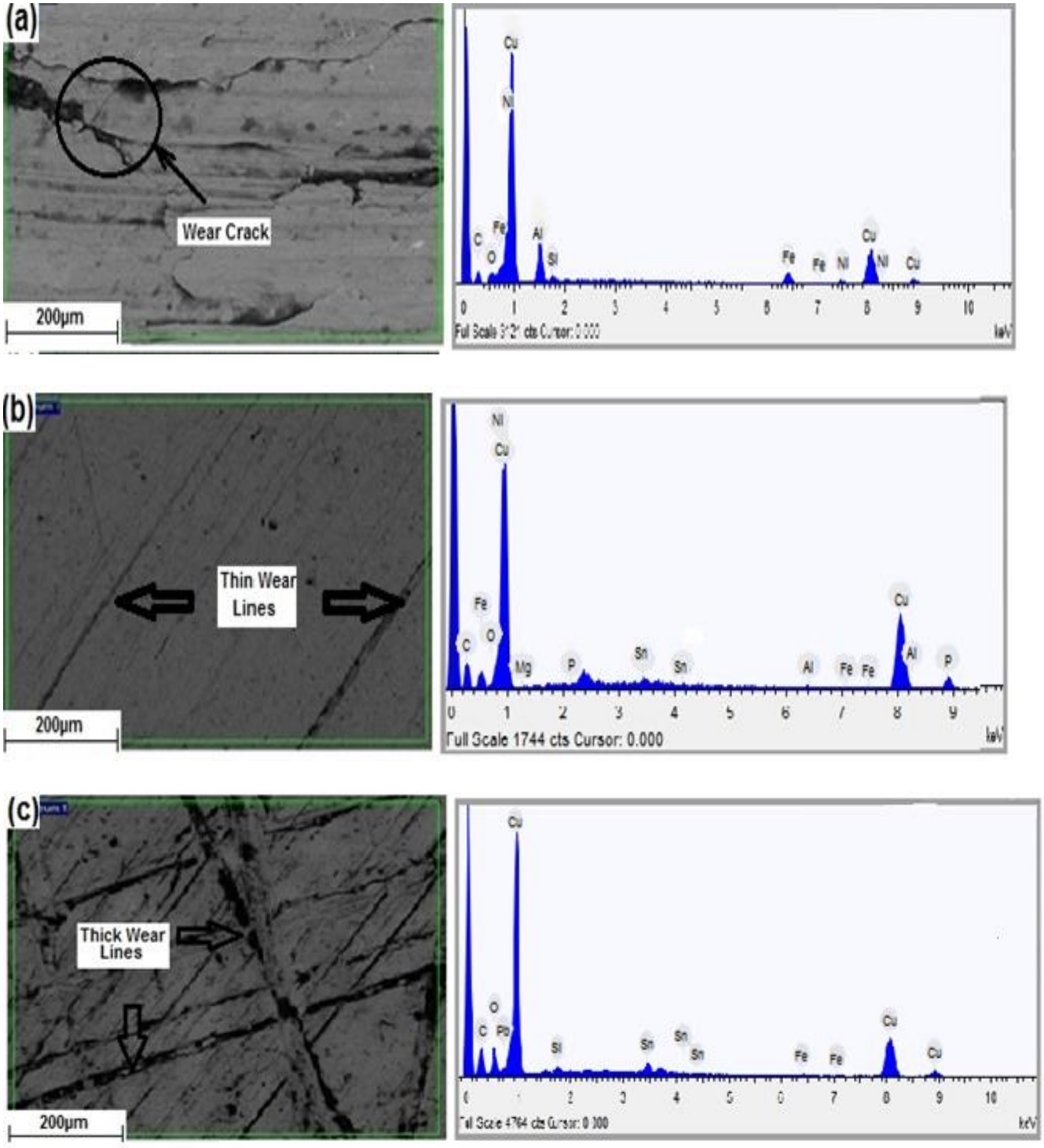

Figure 4.14: (a) SEM and EDX analysis image for the worn Cu-NiAl material after unlubricated tests, (b) SEM and EDX analysis image for the worn Cu-PAl material after unlubricated tests, (c) SEM and EDX analysis image for the worn Cu-Pb material after unlubricated tests.

The presence of iron particles (Fe) is also visible on the worn surface of the Cu-Pb material. The embed-ability property of the copper material plays a significant role in entrapping the iron particles in the copper matrix.

4.1.3.3 Microscopic Study

The microscopic images of Cu-NiAl, Cu-PAl, and Cu-Pb are shown in Figure 4.15. An optical microscope was used to obtain the optical micrographs at 10X magnification. It is seen from Fig. 3 (a) that the Cu-NiAl has copper-rich solid solution α phases and retained β phases throughout the matrix. The overall distribution is uniform and homogeneous. Some areas of very fine precipitates in the α phase are iron-rich and are termed as k_{iv} phase (precipitates of Ni-Fe-Al). The microstructure of Cu-Pb indicates the large evenly distributed lead particles. The lead is practically insoluble in copper, as the mixture freezes, the copper particles freeze first and lead make the globules shape in the copper matrix. In Figure 4.15 (a), the δ phase is shown in dark color and lead is seen as light globules. Figure 4.15 (b) presents the distribution of alloying elements for Cu-PAl material. Aluminium is seen distributed throughout the matrix of the copper.

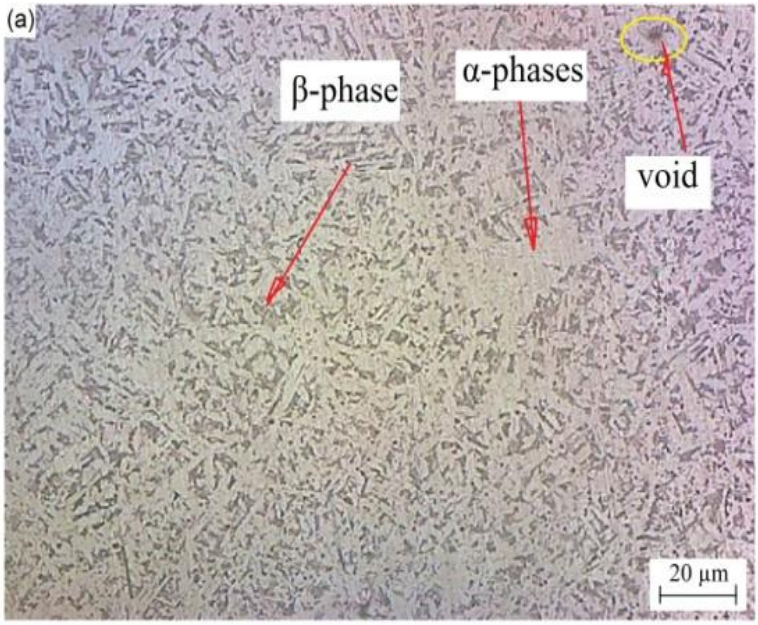

Figure 4.15: (a) Optical micrographs for Cu-NiAl

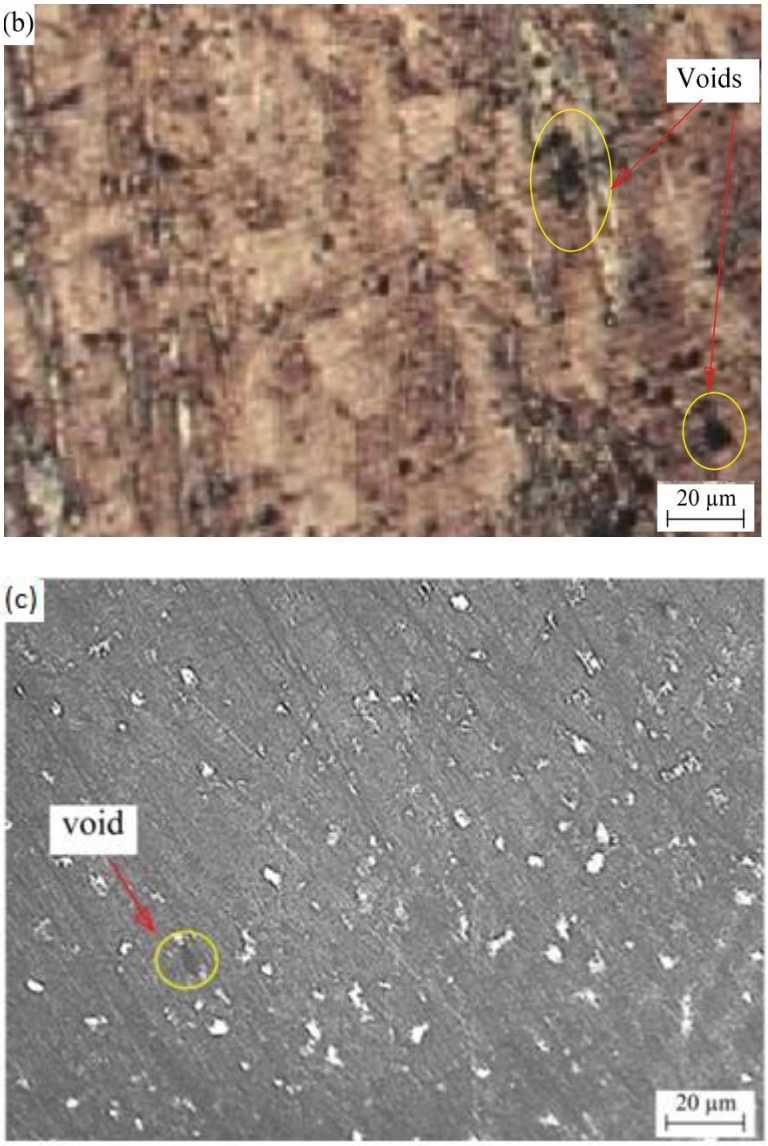

Figure 4.15: Optical micrographs for (b) Cu-Pal (c) Cu-Pb

Table 4.2 presents the mechanical properties of the prepared materials. For the evaluation of microhardness of the fabricated materials, a Fischer made microhardness tester was used. The instrument facilitates digital measurement and control. In its procedure, the head of the system is lowered until the indenter touches the material surface, after this the loading and unloading of the force is carried out. A diamond indenter of square base pyramid shape was used to indent on a cleaned surface of the specimens at a load of 3000 mN for 20 seconds. For each specimen, three hardness values were measured and the average of three was taken for the analysis. The tensile and yield strength were measured by using an INSTRON universal tensile testing machine. Specimens were prepared as ASTM-E8M for strength testing. The testing was with a tension rate of 1mm/min.

The Cu-NiAl has the maximum hardness value as 243.6. The precipitation of the α phase into the β phase helped in achieving the higher hardness value. The soft globules of lead particles limited the hardness of Cu-Pb material to 116.6 HV. The Cu-NiAl had a maximum tensile strength of 610 MPa and yield strength of 430 MPa. The presence of high amount of Al and Ni provides the strength to the copper matrix.

Table 4.2: Mechanical properties of fabricated materials

Property/Material	Tensile Strength(MPa)	Yield Strength(MPa)	Vicker Hardness (Hv)
Cu-NiAl	610	430	243.6
Cu-PAl	550	450	212.9
Cu-Pb	269	207	116.6

4.1.4 **Comparison of Copper composites with Aluminium Flyash Composite**

In this section, the selected aluminium flyash composite was compared with the copper alloys different lubrication regimes.

4.1.4. 1 **Wear analysis in Starved Lubrication Regime**

The wear from the pin surfaces was measured in the form of mass loss (g). The wear sensor installed on the pin on disc machine also measured the wear from the pin in the form of a decrease in length of the pin (μm). The variation of wear in mass loss for the Al-F, Cu-NiAl, Cu-Pb and Cu-PAl materials is represented in Figure 4.16. It is clearly seen that Cu-PAl material resulted in the least amount of wear (0.0007 g) as compared to other materials and Al-F composite material gives the maximum wear (0.0042 g). The Cu-PAl material gave 36% less wear as compared to the conventional journal bearing material (Cu-Pb).

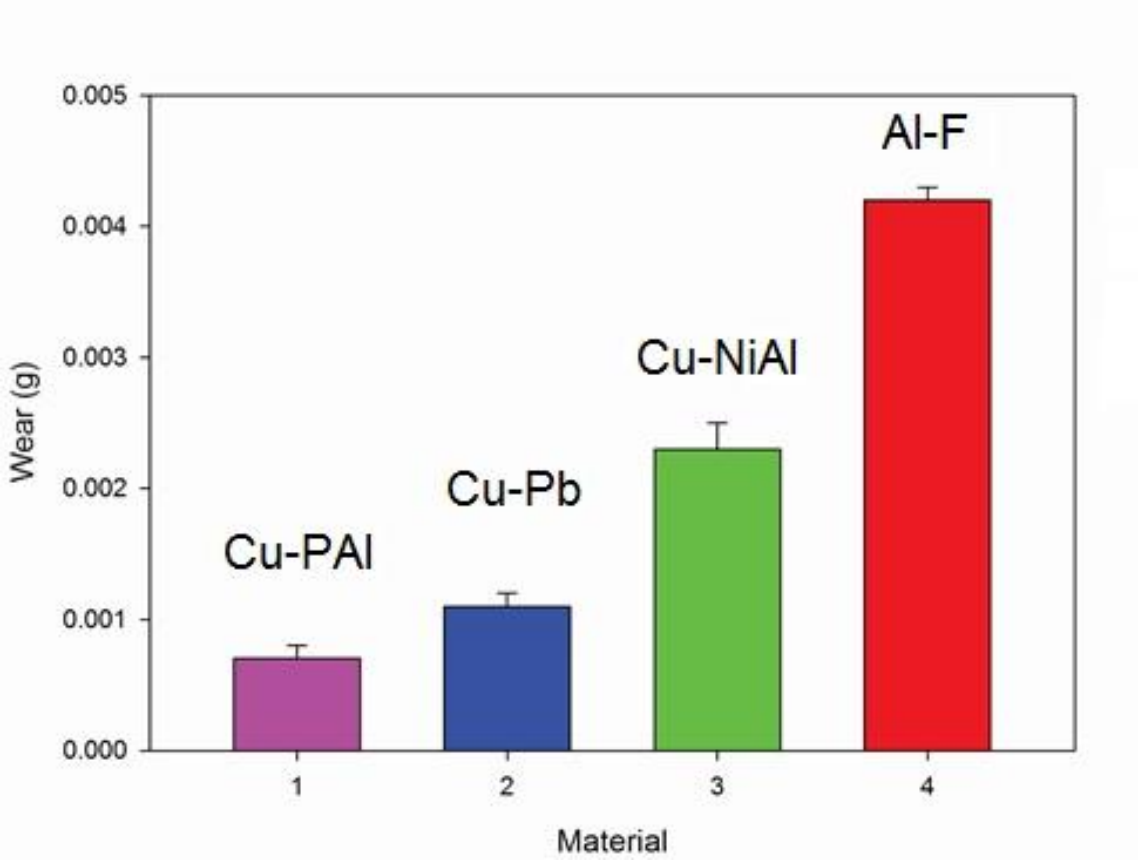

Figure 4.16: Variation of wear (g) of material after the testing

Figure 4.17 represents the wear loss from the pin surface as recorded by the wear sensor of the pin on disc machine. Because of the initial asperities on the surface of pins, the wear increases sharply for the initial sliding distance and after that, it attains a maximum value and stabilizes itself. The Al-F wears more as compared to other materials and Cu-PAl resulted in the smallest wear scar on the pin.

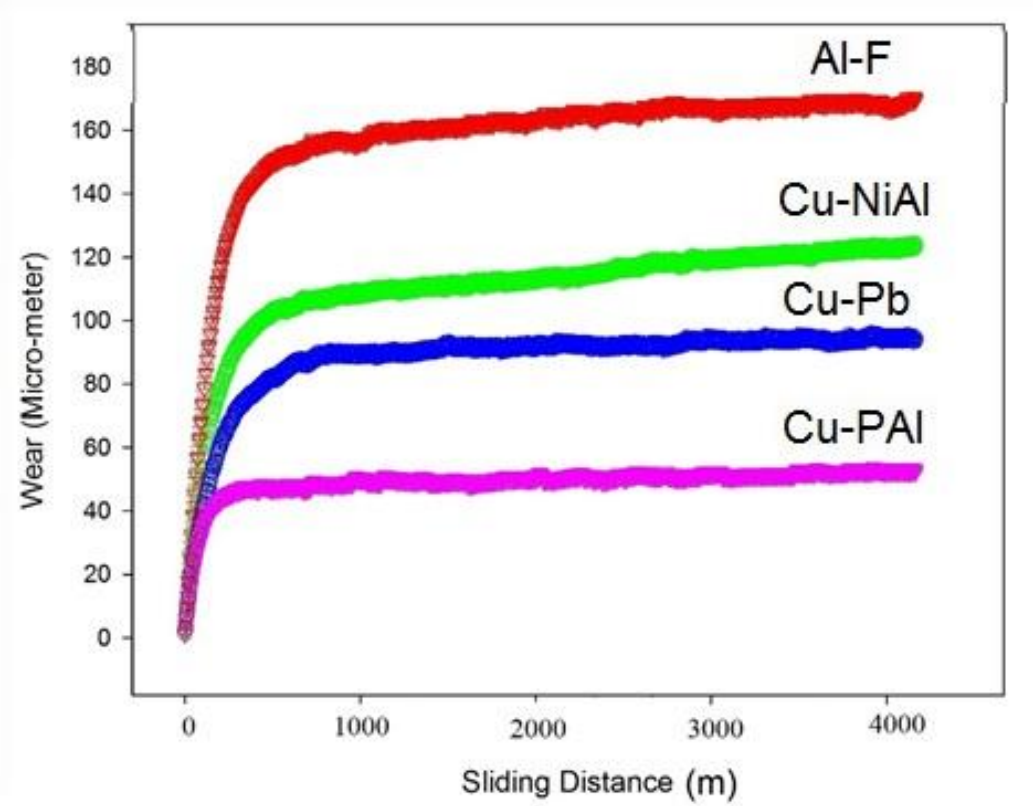

Figure 4.17: Variation of wear in pin length of material after the testing

4.1.4.2 Surface Analysis

For the better understanding of the wear pattern, scanning electron microscope (SEM) images and energy dispersive X-Ray (EDX) analysis of the worn pin samples were conducted. The SEM images of the worm pin samples are shown in Figure 4.18 (a, b, c, d). The SEM images were obtained at 1500X magnification, 15000 V accelerating voltage and 1750 mA filament current settings.

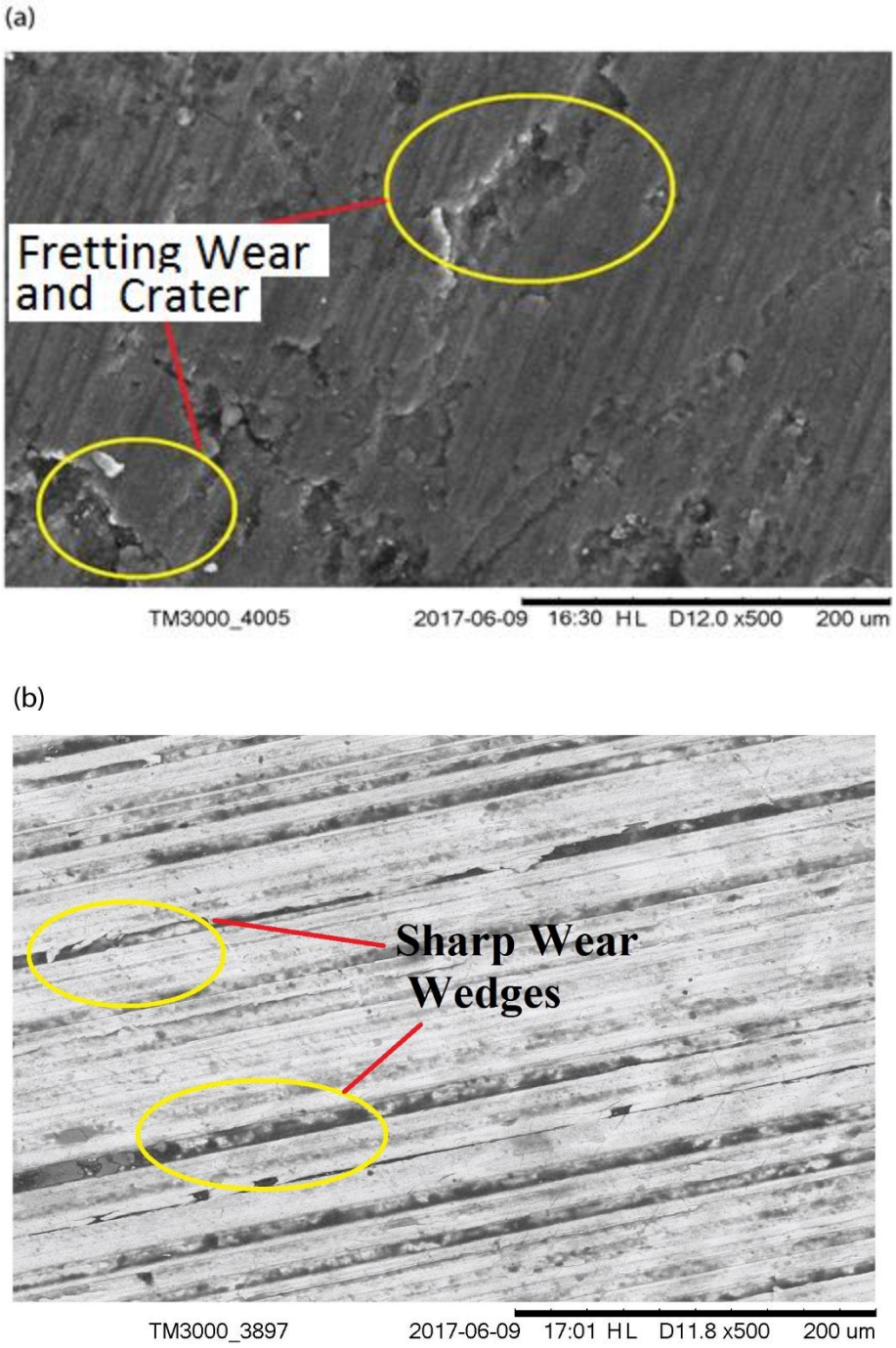

Figure 4.18: (a) SEM image for Aluminium-Flyash (Al-F) composite (b) SEM image for Copper-Aluminium (Cu-NiAl)

(c)

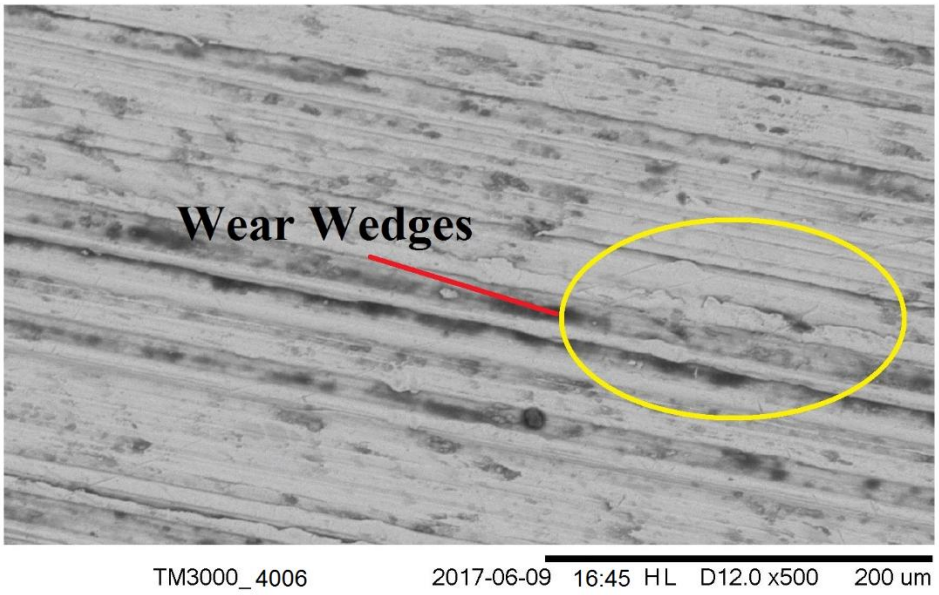

(d)

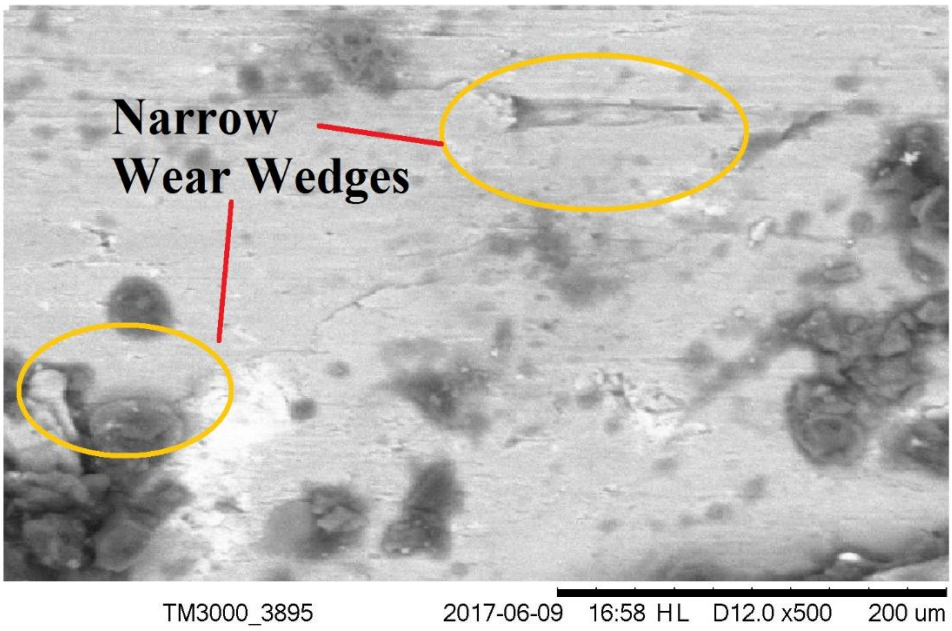

Figure 4.18: (c) SEM image for Copper-Lead (Cu-Pb) (d) SEM image for Copper-Phosphorous (Cu-PAl) material.

The SEM image for AL-F composite material indicates the wear tracks with fretting wear and crater. The bulk of the material from the pin surface is removed due to the heavy wearing. The SEM image of Cu-NiAl represents the sharp wear wedges throughout the whole surface of the material with predominantly abrasive wear with fretting. Similarly, for Cu-Pb material, wear wedges with some plastic yielding are clearly seen from the SEM images. The SEM

images of the Cu-PAl shows some narrow wear wedges in some areas and slight crater at upper side with not much wear on the other areas. The deposition of carbon particles on the surface of all the materials is also visible from the SEM images.

Figure 4.19 (a, b) shows the EDX analysis of Al-F and Cu-PAl materials respectively. The EDX analysis of Cu-PAl materials represents the presence of some iron (Fe) particles which might be embedded into the matrix of Cu from the disc surface (mild steel) during the pin on disc testing. Similar trends were obtained for Cu-NiAl and Cu-Pb materials as represented in Figure 4.20 (a, b).

(a)

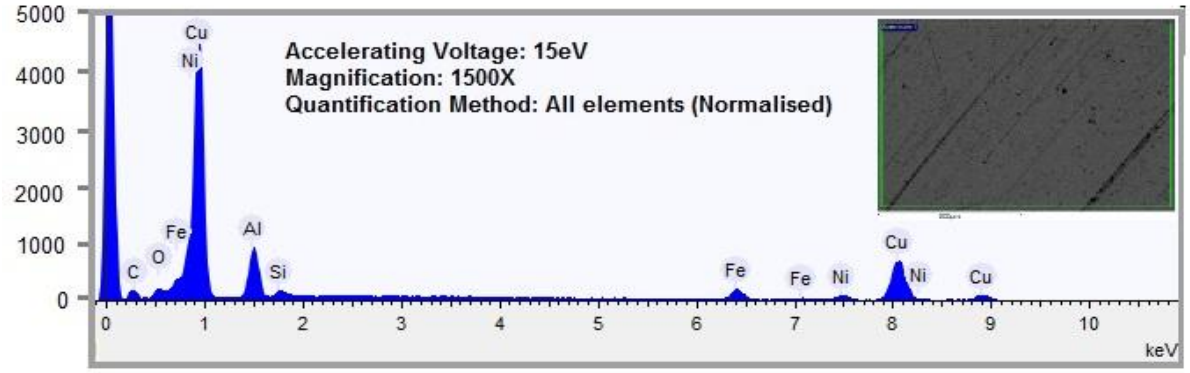

(b)

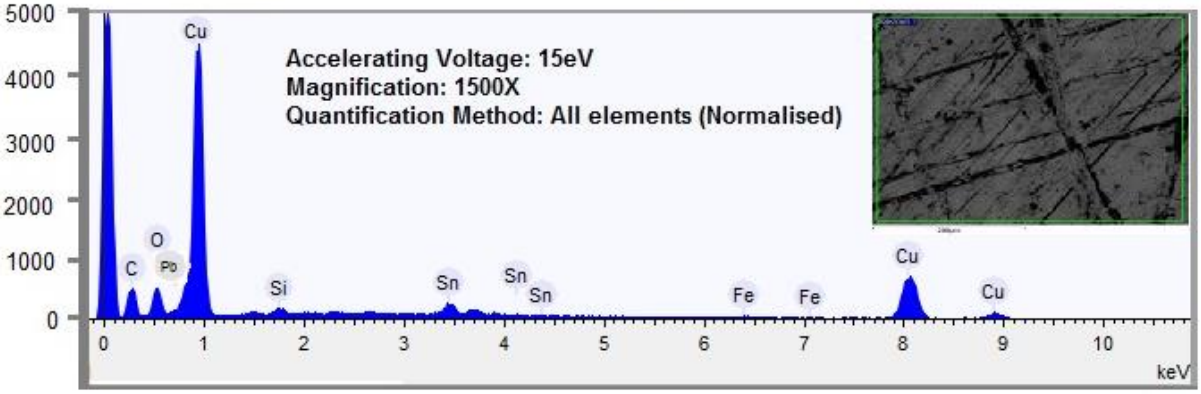

Figure 4.19: (a) EDX analysis for aluminium flyash (Al-F) composite (b) EDX analysis for Copper- Phosphorous (Cu-PAl) material

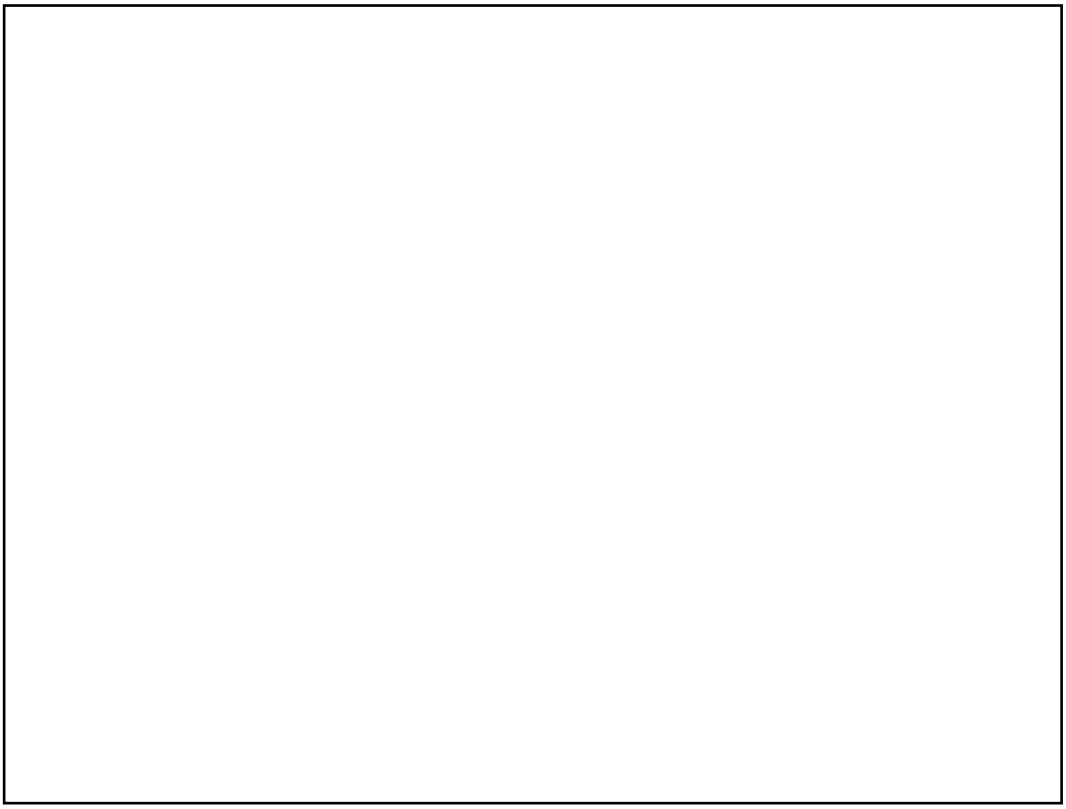

Figure 4.20: (a) EDX analysis for Copper- Aluminium (Cu-NiAl) material (b) EDX analysis for Copper- Lead (Cu-Pb) material.

4.1.4.3 Coefficient of Friction

The pin on disc machine recorded the friction force for the Al-F, Cu-PAl, Cu-NiAl and Cu-Pb materials. The measured friction force is used to calculate the coefficient of friction as presented in Figure 9. The coefficient of friction for all the materials upsurges sharply to 0.02 for Al-F, 0.025 for Cu-PAl, 0.038 for Cu-Pb and 0.079 for Cu-NiAl. After attaining the maximum value of the coefficient of friction, it decreases and acquires a near constant value. This region of constant coefficient of friction as presented in Figure 4.21 is the 'steady state' region. The steady state region starts at 100 m of sliding distance and runs for almost 1600 m.

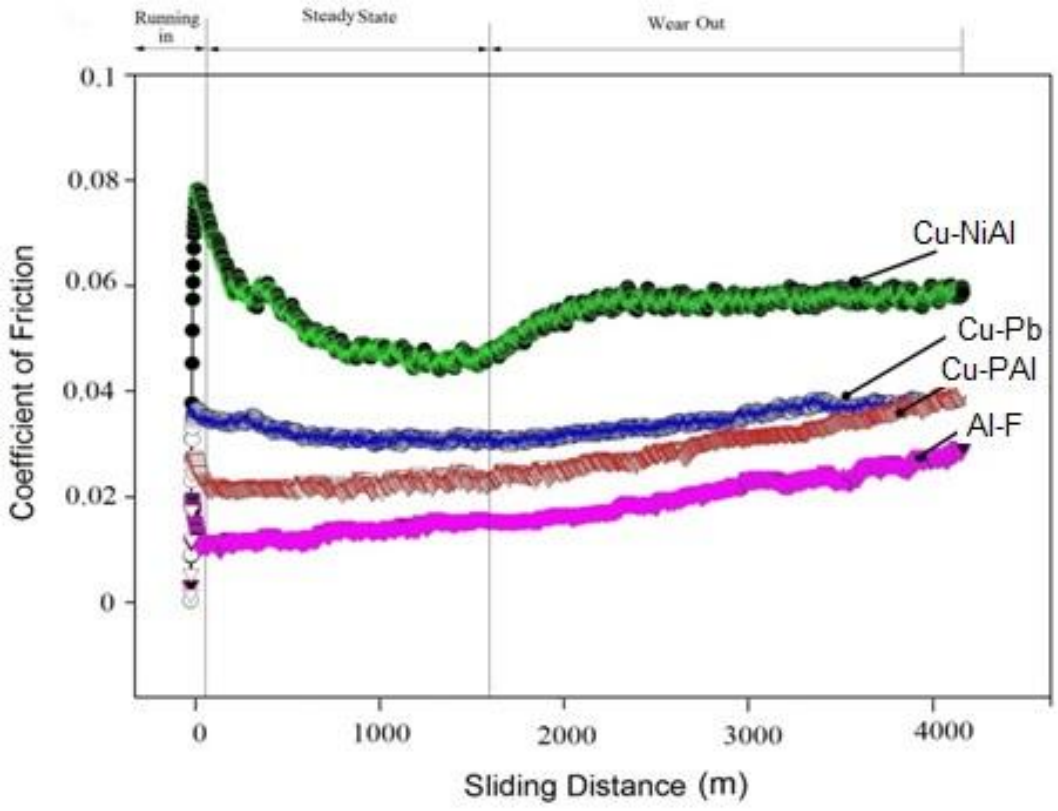

Figure 4.21: Variation of the coefficient of friction

It is seen that Al-F composite material results in the lowest coefficient of friction value. The flyash contents of the composite provide the anti-friction properties to the aluminium material which decreases the coefficient of friction. The coefficient of friction for Al-F was 32% less as compared to the average coefficient of friction for the conventional journal bearing material (Cu-Pb). The maximum friction coefficient was obtained between the Cu-NiAl and mild steel tribopairs.

4.1.4.4 Comparison in Unlubricated Condition

For the complete understanding of the tribological behaviour of the journal bearing materials, it is equally important to evaluate and calculate the wear and friction properties of the prepared materials in unlubricated conditions as well.

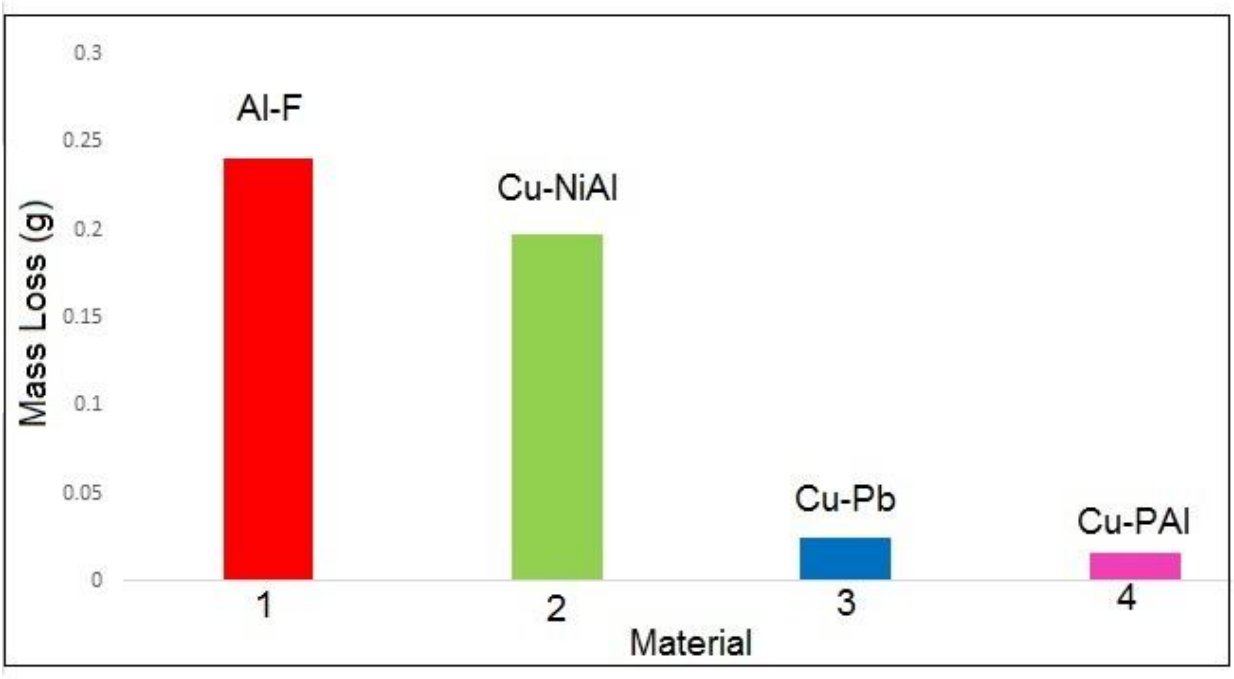

Figure 4.22: Mass loss (g) for the fabricated materials.

Figure 4.22 represents the mass loss from the pin samples during the wear testing. The Al-Flyash pin experienced maximum mass loss as compared to other materials. The presence of soft phases may have resulted in more wear. The Cu-NiAl also exhibits more wear as compared to the conventional journal bearing material (Cu-Pb). However, Cu-PAl material behaved slightly better than the Cu-Pb material. The presence of a smooth layer on the disc surface is the possible reason for this lower wearing of the Cu-Pb and Cu-PAl material.

The variation of coefficient of friction is presented in Figure 4.23, the presence of flyash particles in aluminium matrix helped in lowering the friction coefficient values for the Al-Flyash composite. The Cu-NiAl material resulted in maximum friction coefficient values. The Cu-PAl has a better friction coefficient values as compared to the Cu-Pb material. The average values of friction coefficient are presented in Table 4.3.

This lowest coefficient of friction value for the Al-F composite is mainly attributed due to the nature of the flyash particles, the flyash particles are generally spherical in shape which makes the surface of aluminium smooth and hence the coefficient of friction value decreases. However, the presence of aluminium and low hardness value of the Al-F composite as compared to the other copper composite materials resulted in high mass loss.

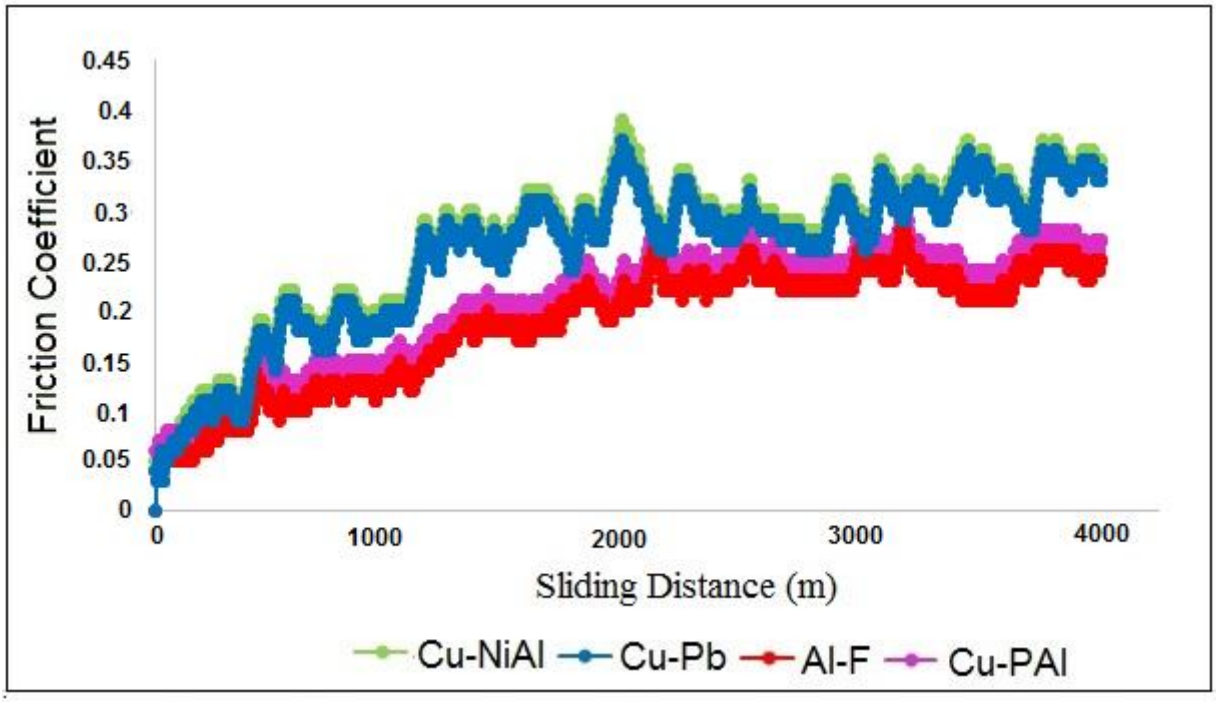

Figure 4.23: Variation of the coefficient of friction in unlubricated condition

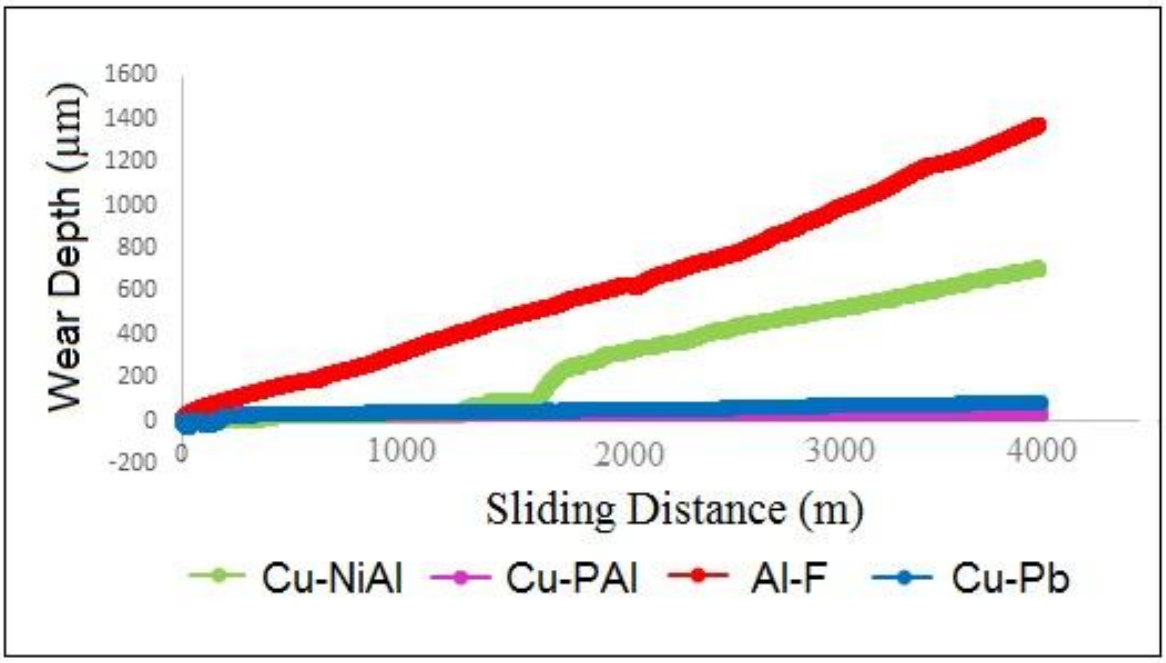

Figure 4.24: Wear scar depth in unlubricated condition

For further understanding of the wear of the material, the wear depth in the form of length of pin is plotted against the time. Figure 4.24 presents this wear depth for the considered materials. for the initial sliding of the materials, the Cu-NiAl, Cu-Pb and Cu-PAl material has almost similar wear depth. After that, the wear depth for Cu-NiAl increases with more sliding, the hard particles of the Cu-NiAl may have resulted in three body wear. With further

sliding, the Cu-PAl material resulted in the least amount of wear. The elements like aluminium and phosphorous in the bronze matrix help in reducing the wear (Figure 4.25).

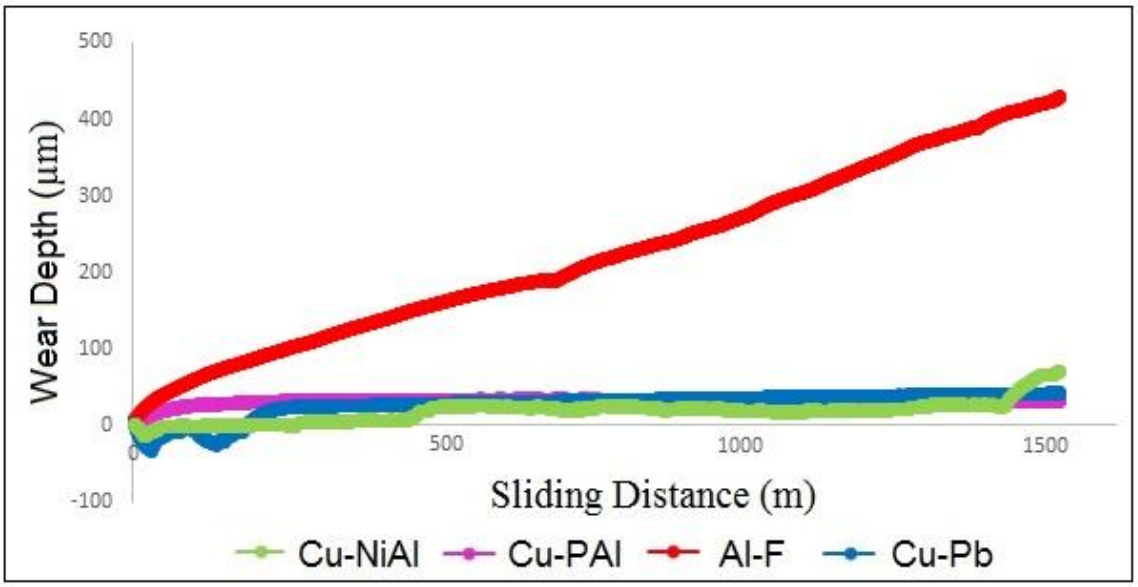

Figure 4.25: Wear scar depth in unlubricated condition (For 1500 m sliding distance)

Table 4.3: Average wear scar depth and friction force

Material	**Avg Wear Scar Depth (Micro-meter)**	**Coefficient of Friction**
Al-Flyash	641.6	0.24
Cu-NiAl	286.5	0.30
Cu-Pb	49.3	0.29
Cu-PAl	31.1	0.26

4.2 Journal Bearing Performance

The performance of a journal bearing system directly depends on the lubricant oil type, the load on the shaft and rotational speed of the shaft. In the present analysis, the journal bearing performance has been evaluated by incorporating surface textures on the bearing surface. In this section of the chapter, the effects of surface textures on the friction torque between the bearing and journal have been evaluated for starved as well as hydrodynamic lubrication regimes. In the last part of the section, the maximum oil film pressure due to the surface textures has also been studied.

4.2.1 Friction Torque in Starved Lubrication

The whole experimental work was divided into two phases. In the first phase, journal bearing test rig experiments were performed by using the conventional bearing at different load and rotational speeds of the journal. In the second phase, the surface textures of half-spherical shape were produced on the bearing surface and frictional torque was measured at the same input parameters of load and speed as used in the first phase. The results of the conventional bearing testing and textured bearing are evaluated and compared.

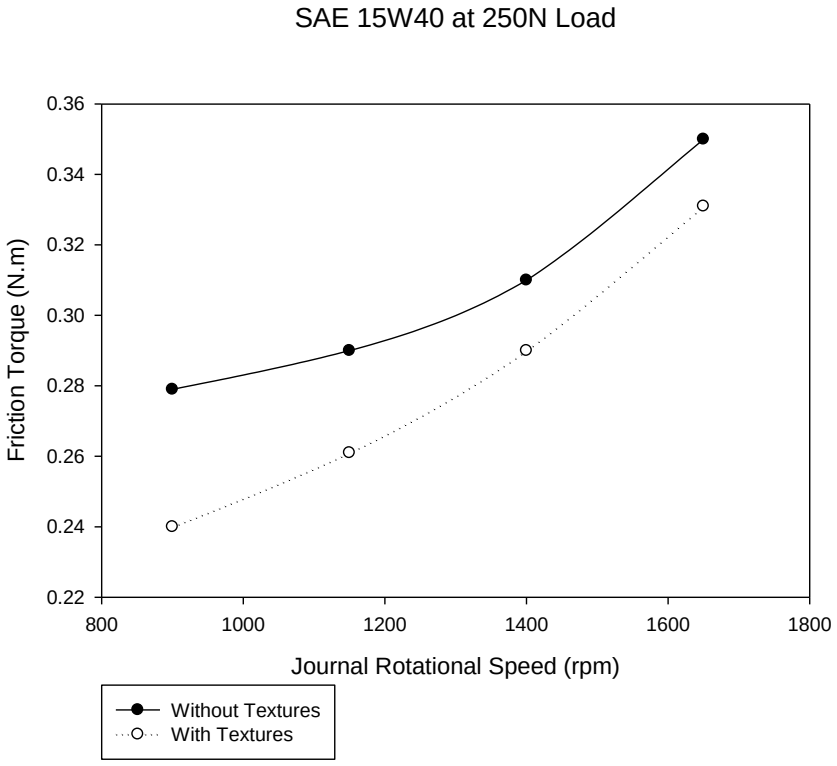

Figure 4.26: (a) Variation of friction torque at 250N load.

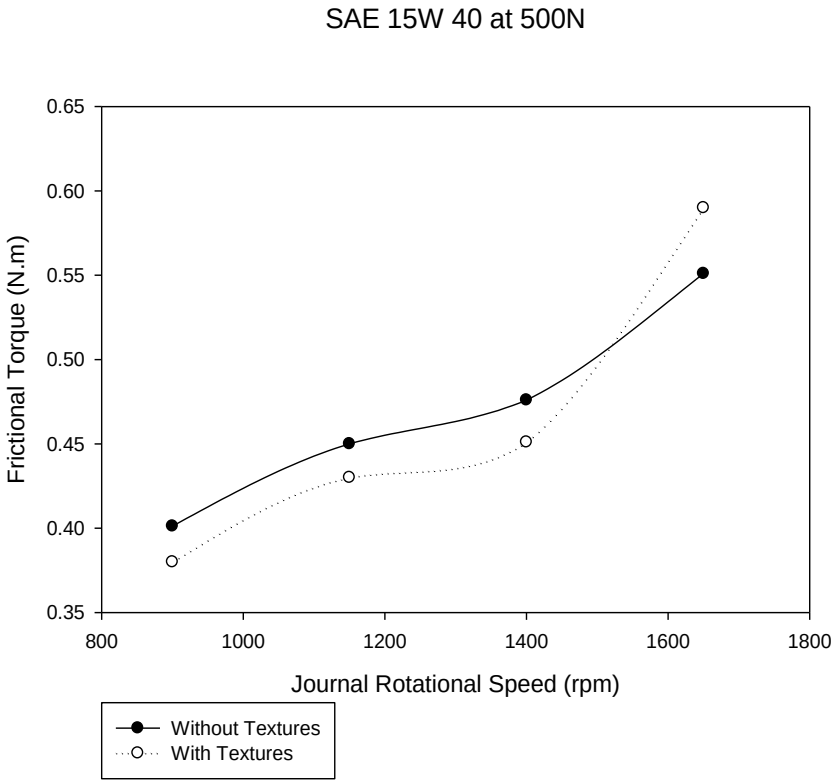

Figure 4.26: (b) Variation of friction torque at 500N load.

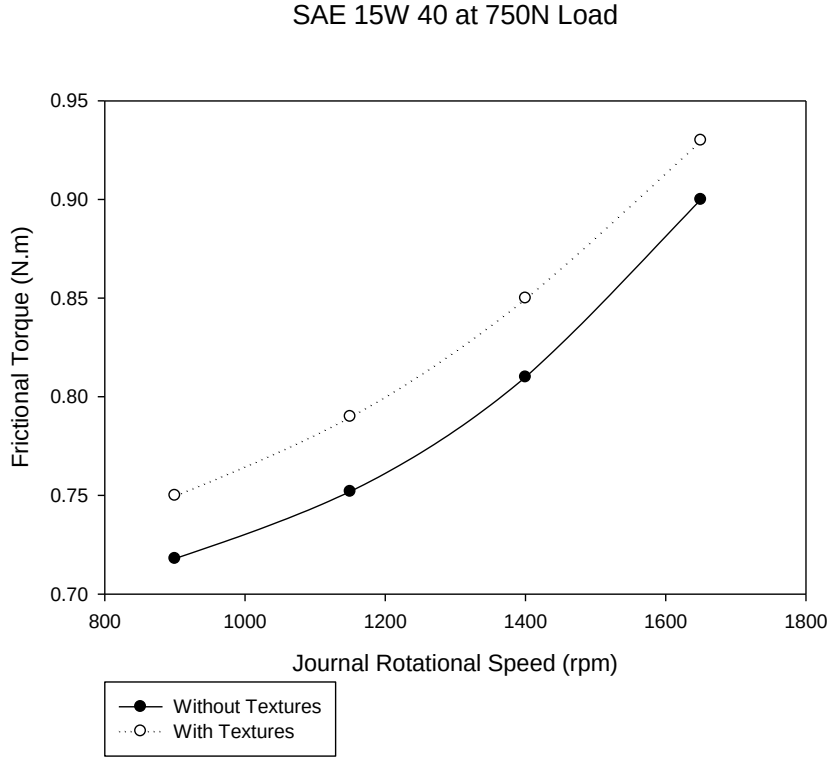

Figure 4.26: (c) Variation of friction torque at 750N load.

Figure 4.26 (a-c) presents the variation of frictional torque for conventional and textured bearing system during the starved lubrication regime. It is seen that at lower speeds (910 rpm), the average frictional torque is minimum as compared to the frictional torque at 1150, 1400, 1650 rpm speed of journal. At higher speeds, a fluid film layer thickness between the bearing and shaft becomes very thin which may result in higher frictional torque.
This rise indicates the low strength of the fluid film at higher journal speeds and represents the scarcity of the lubricating oil.

It is also observed that as the load on the shaft of the system increases, the frictional torque values also increase. This increased load on the shaft may result in a decrease in thickness of the lubricating oil which increases the frictional torque.

For the textured bearing system, the average friction torque for the 250N and 500N considered cases reduces significantly (except at 1650rpm, 500N). This reduction in frictional torque helps in improving the performance of the journal bearing system. The surface textures on the inner surface of the bearing act as the reservoir and hold the lubricating oil in it. This lubricating oil present in the surface textures help in reducing the frictional torque between the journal and the bearing. However, with further increase in the load value to 750N, the lubricant film get very thin, and surface texture burrs may have contacted with the shaft surfaces as well. This phenomenon, increases the frictional torque.

4.2.2 Frictional Torque in Hydrodynamic Lubrication

In this work, attempts have been made to evaluate the effects of partial surface textures on the frictional torque of the journal bearing. For these several experiments were conducted a varying journal speed and loading conditions. In the first section of the experimental work, three synthetic lubricating oils SAE 10W-40, SAE 15W-40 and SAE 20W-40 were used and compared for friction torque measurements. Figure 4.27 (a-d) presents the variation of frictional torque with the rotational speed of journal at loads 250N-1000N under the hydrodynamic effect of SAE 10W 40 lubricating oil. These graphs were obtained by measuring the average frictional torque values for the considered rotational speed and load values in fully flooded hydrodynamic lubrication condition. The theoretical values of the frictional torque were also calculated for the comparison using equation (1.3). It is observed that with increase in journal speed the friction torque value also gets increased for all the

loading values. The low viscosity of the lubricating oil resulted in shear thinning of the oil which raises the frictional torque values. With increases in load the friction torque values get reduced, the possible cause for this reduction would be higher eccentricity ratio which is produced due to an increase in applied load. These variations in the results are consistent with the findings observed by Lu (2006). Figure 4. 27 (e-h), presents the friction torque with SAE 15W 40 and Figure 4. 27 (i-l) shows the variation with SAE 20W 40 lubricating oil. From the figures 4.27 (a-l), it is observed that, the variation of friction torque was in the range of 2.8-23 % for the textured bearing as compared to theoretical value. There was an improvement in the average friction torque from textured bearing was in the range of 2.7 % - 13.5 % compared to the non-textured bearing.

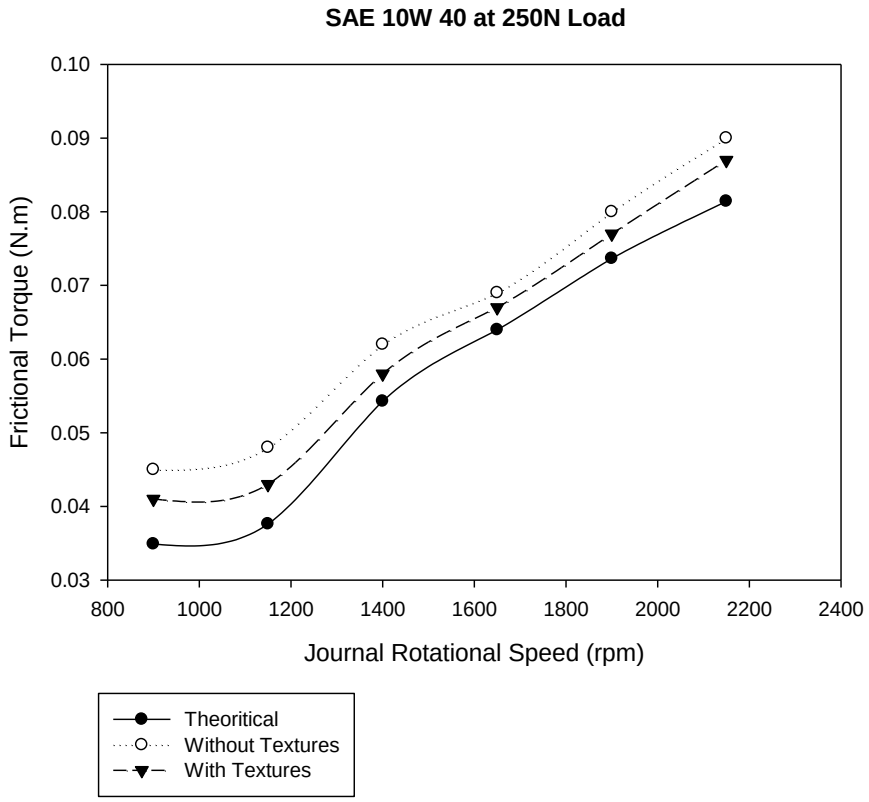

Figure 4.27 (a): Friction torque variation with SAE 10W 40 lubricating oil at 250N load

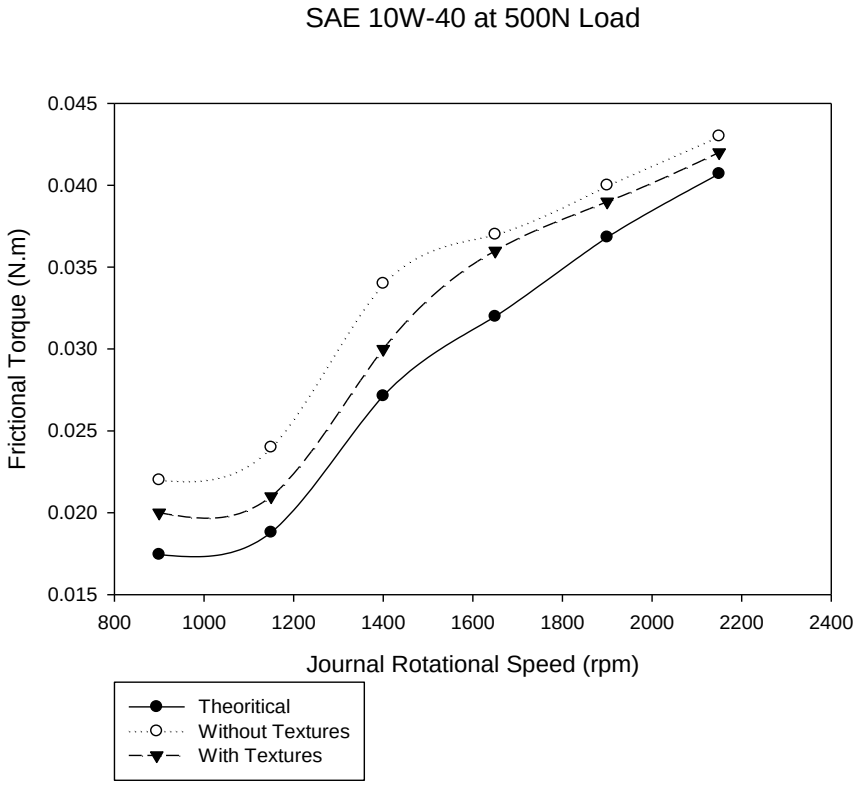

Figure 4.27 (b): Friction torque variation with SAE 10W 40 lubricating oil at 500N load

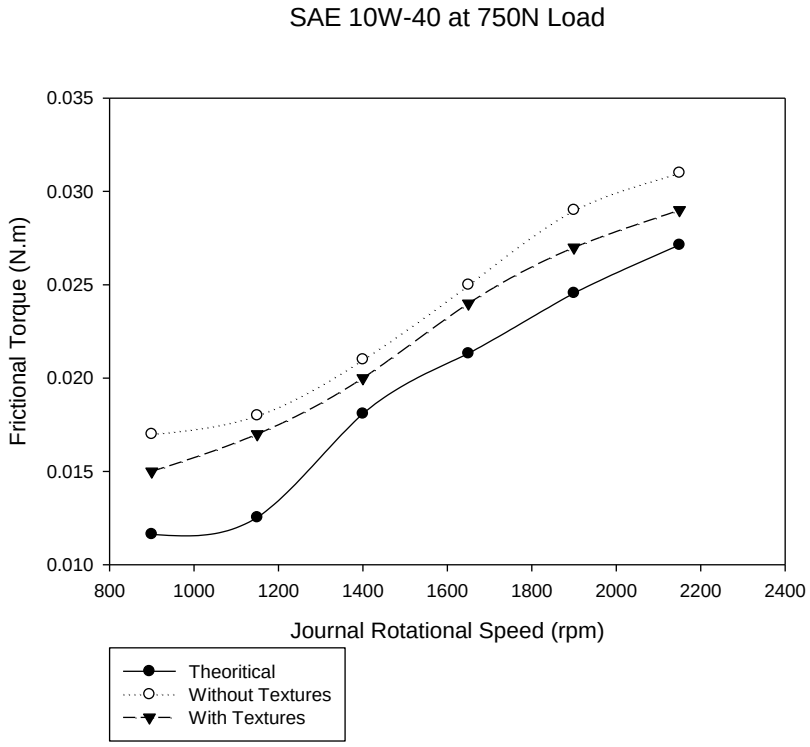

Figure 4.27 (c): Friction torque variation with SAE 10W 40 lubricating oil at 750N load

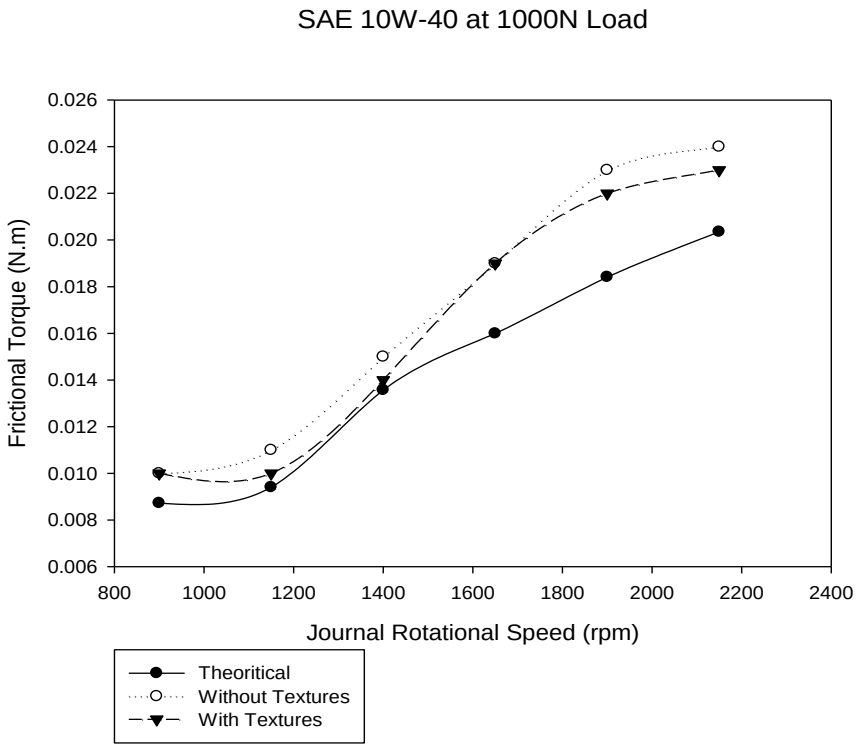

Figure 4.27 (d): Friction torque variation with SAE 10W 40 lubricating oil at 1000N load

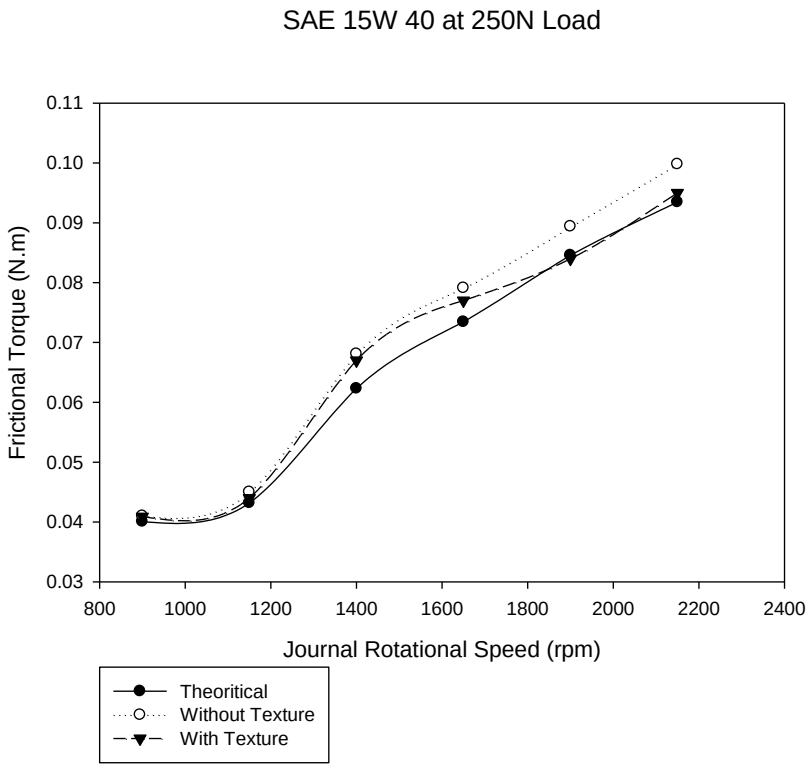

Figure 4.27 (e): Friction torque variation with SAE 15W 40 lubricating oil at 250N load

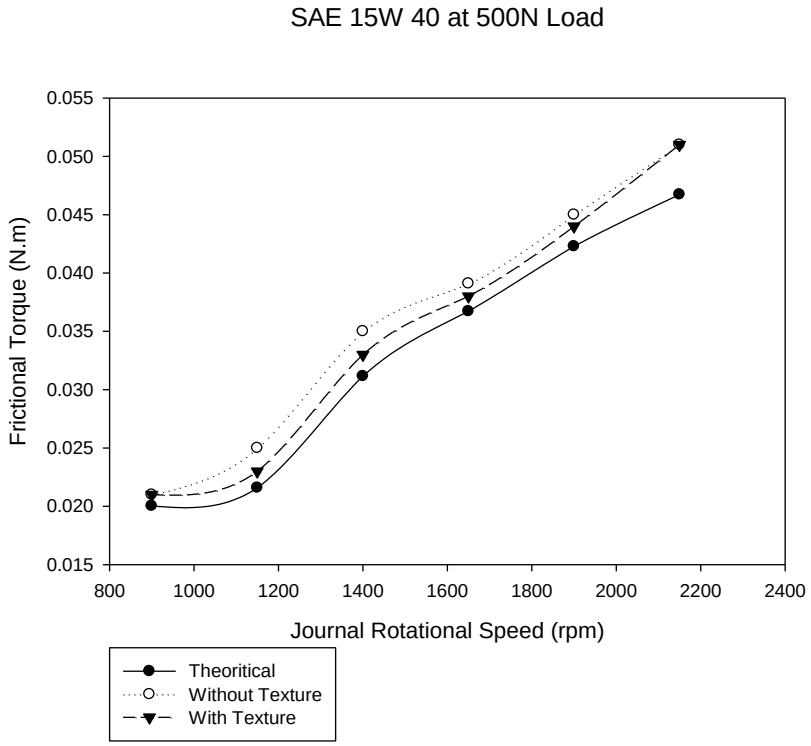

Figure 4.27 (f): Friction torque variation with SAE 15W 40 lubricating oil at 500N load

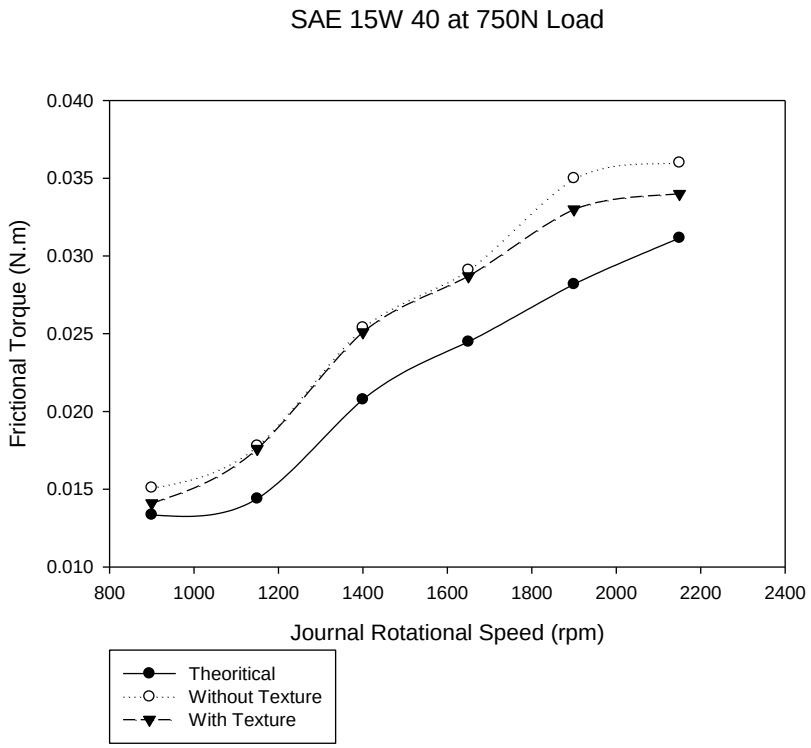

Figure 4.27 (g): Friction torque variation with SAE 15W 40 lubricating oil at 750N load

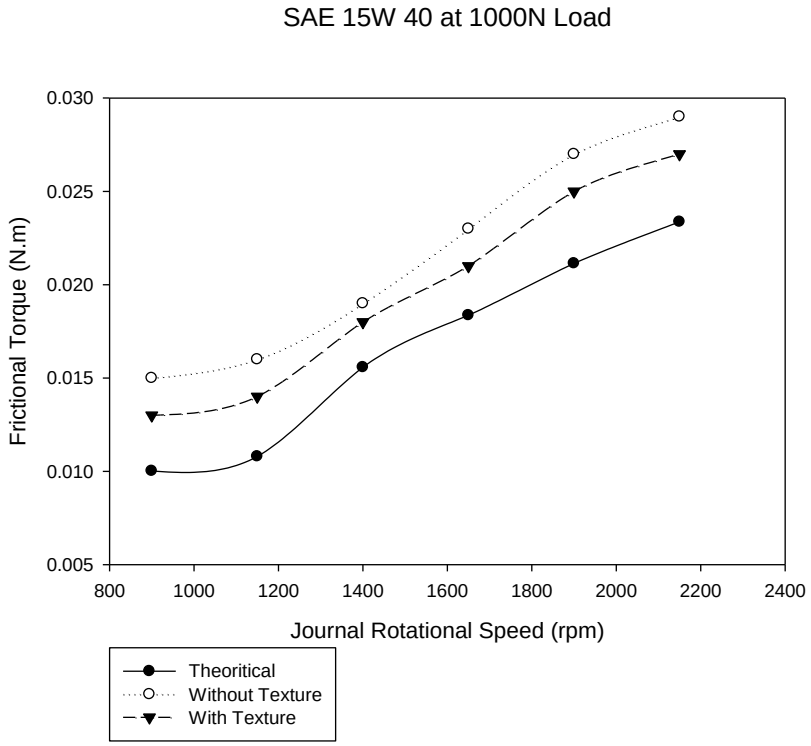

Figure 4.27 (h): Friction torque variation with SAE 15W 40 lubricating oil at 1000N load

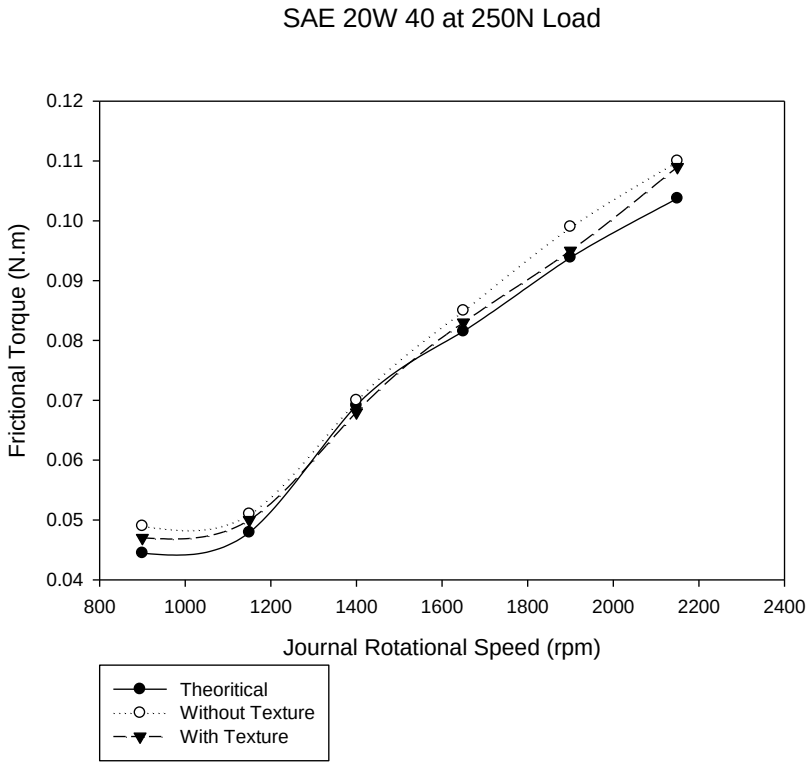

Figure 4.27 (i): Friction torque variation with SAE 20W 40 lubricating oil at 250N load

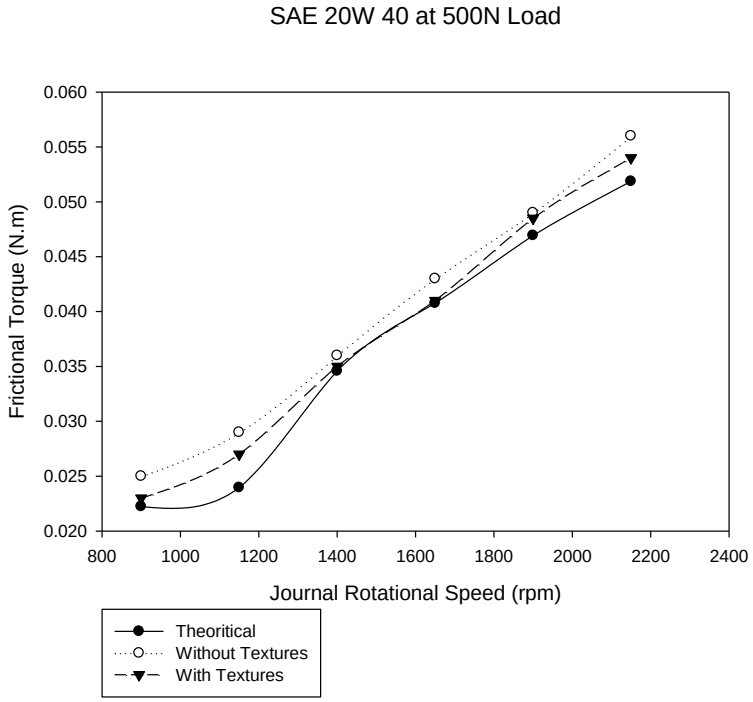

Figure 4.27 (j): Friction torque variation with SAE 20W 40 lubricating oil at 500N load

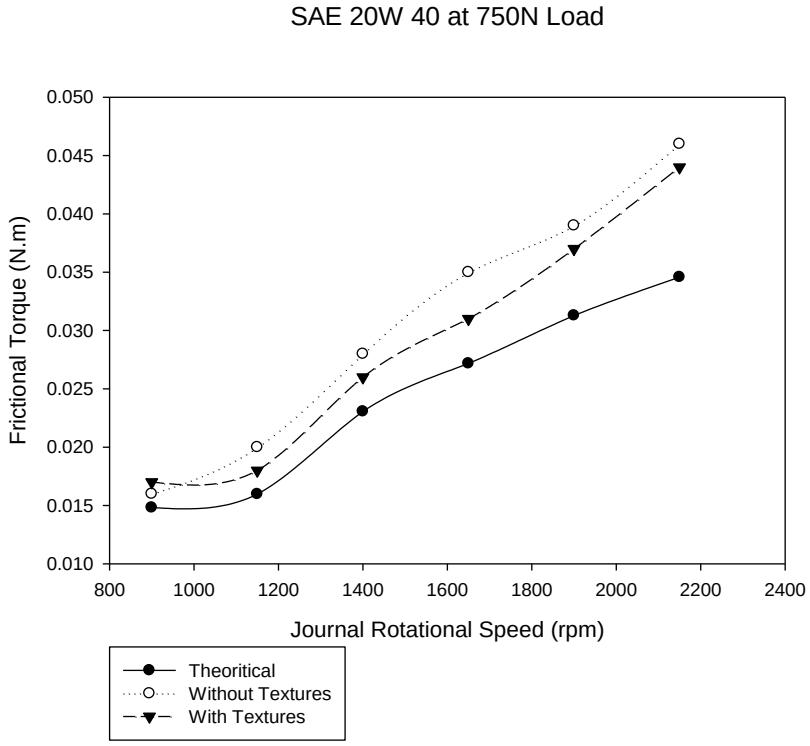

Figure 4.27 (k): Friction torque variation with SAE 20W 40 lubricating oil at 750N load

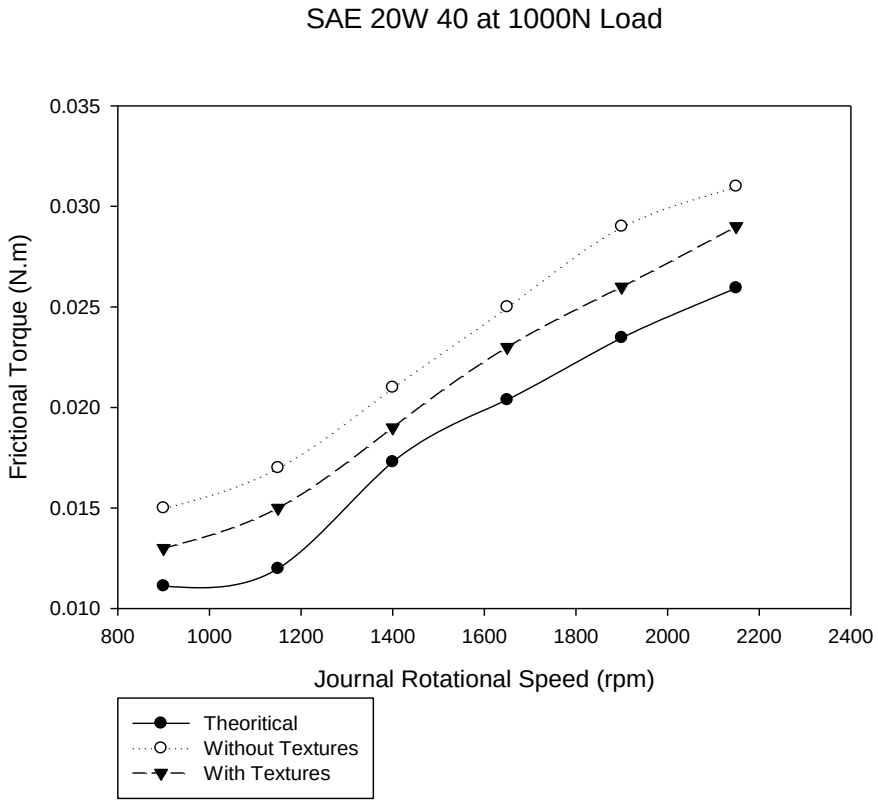

Figure 4.27 (l): Friction torque variation with SAE 20W 40 lubricating oil at 1000N load

In order to understand the effects of load and viscosity, graphs were obtained at varying rotational speeds. Figure 4.28 (a) presents the effect of applied load on the frictional torque. It is observed that, with the increase in the applied load the friction torque value reduces. In hydrodynamic lubrication conditions, the higher loads may have resulted in higher eccentricity ratio and at low loading conditions, the chances of journal misalignment may occur, which might result in higher friction torque values. The average friction torque values achieved are 0.067 N.m, 0.036 N.m, 0.025 N.m and 0.019 N.m for 250N, 500N, 750N and 1000N load. Figure 4.28 (b) presents the variation of friction torque with journal speed at 250 N load. Three lubricating oil were used. It is observed that with the increase in oil viscosity, the frictional torque value also increases. The viscosity of the oil played an important role in increasing the frictional torque value.

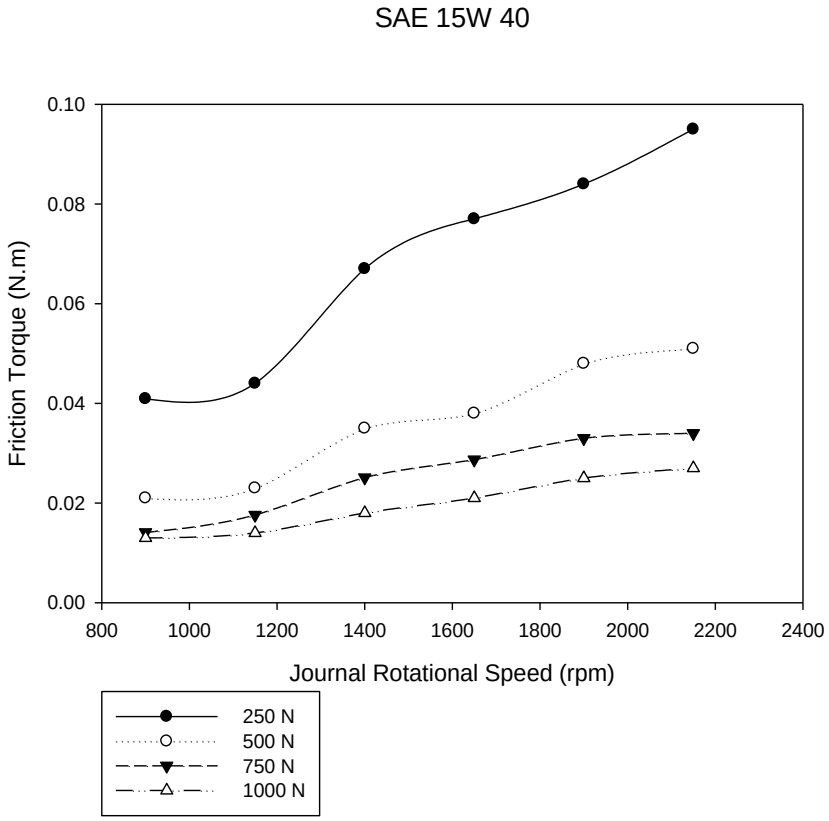

Figure 4.28 (a): Variation of friction torque with applied load with SAE 15W 40 lubricating oil

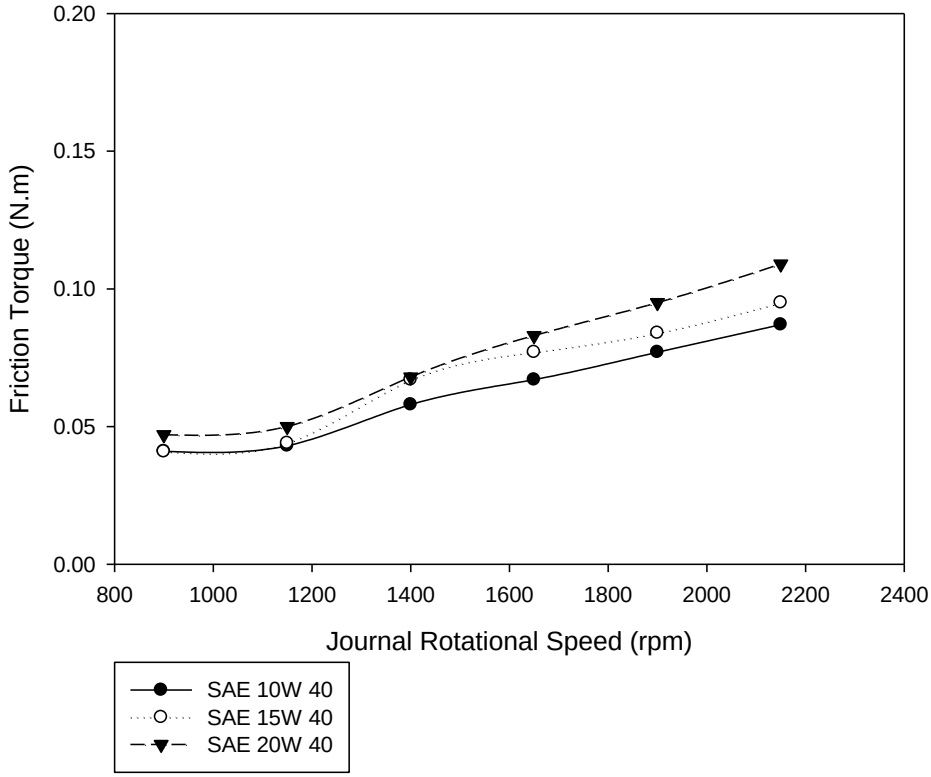

Figure 4.28 (b): Variation of friction torque with different lubricating oils at 250 N load.

4.2.3 Oil Film Pressure

The pressure around the periphery of the bearing surface was measured with the help of pressure sensors. The maximum pressure obtained at a particular load and rotational speed of the journal is plotted in Figure 4.29 to Figure 4.33. Figure 4.29 is obtained at 250N of applied load with variable rotational speeds of the journal with SAE 10W40 lubricants. It is observed that maximum pressure value increases with the increased rotational speed. The increased speed of the journal helped in providing an extra force on the lubricating oil which increases the pressure generation. However, at 1900rpm and 2150 rpm rotational speed, the maximum pressure values decrease slightly. This reduction in pressure is obtained because of low viscosity of the SAE 10W40 lubricating oil and very light loading. Due to these conditions, at higher speeds, the lubricant film may get weak and thus reduces the maximum pressure.

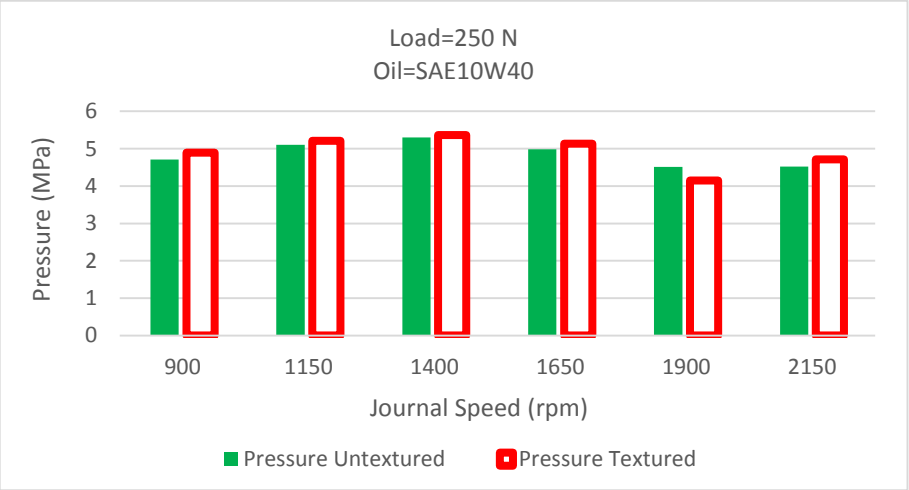

Figure 4.29: Pressure variation with rotational speed at 250N with SAE 10W 40 lubricant

Figure 4.30 is obtained at 250N with variable journal speed values. SAE 15W40 lubricating oil was used for the experiments. With SAE 15W40 lubricating oil, the lubricating film pressure increases slightly as compared to the SAE 15W40. It is also seen that there is no reduction in the maximum pressure value even at higher journal speeds. The high viscosity of lubricating oil helps in maintaining sufficient lubricant film thickness. Similarly, Figure 4.31 presents the lubricant film pressure with SAE 20W40 lubricating oil. SAE 20W40 maintains the higher pressure values and lubricating oil film does not get rupture at higher speeds as well.

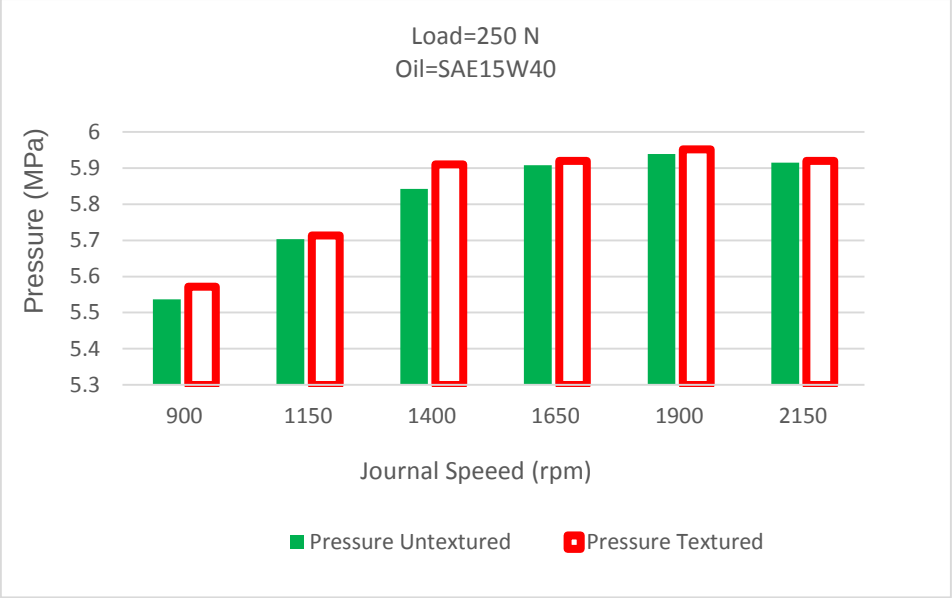

Figure 4.30: Pressure variation with rotational speed at 250N with SAE 15W 40 lubricant

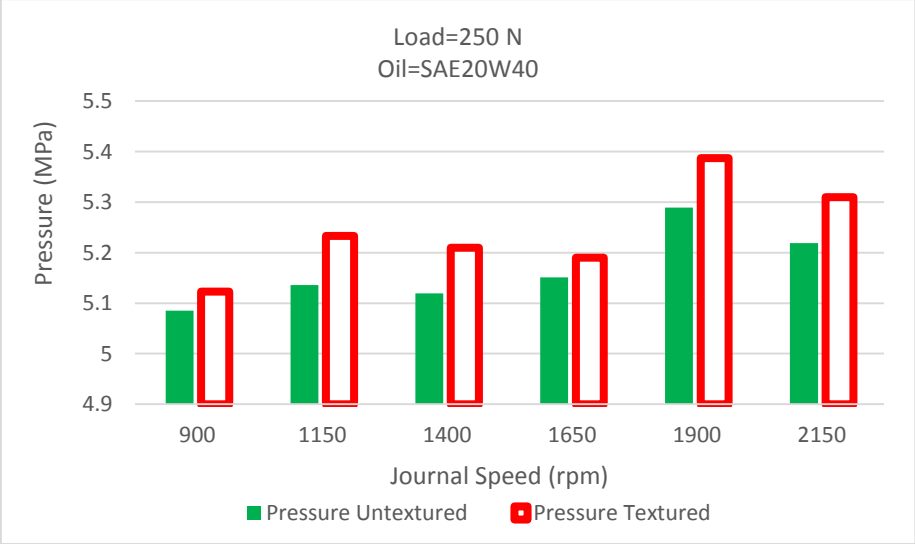

Figure 4.31: Pressure variation with rotational speed at 250N with SAE 20W 40 lubricant

Figure 4.32 presents the maximum lubricant film pressure at 500N load with SAE 10W40 lubricating oil. The oil film pressure increases with the increases in journal speed and achieves a maximum value at 2150 rpm. No oil film rupture was reported during the experimentation.

For SAE 15W40 oil, the oil film pressure also gets increases and the oil film becomes more stable and support the applied load.

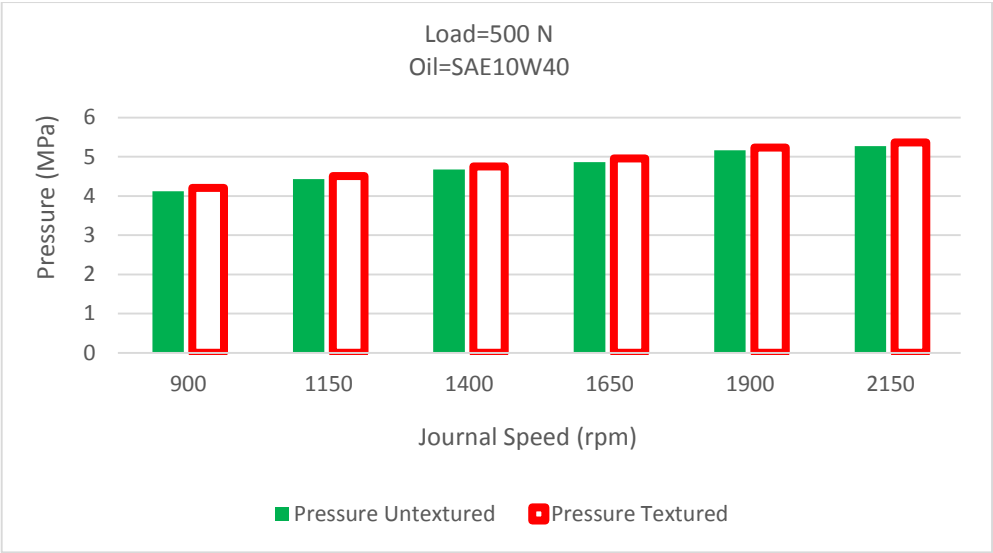

Figure 4.32: Pressure variation with rotational speed at 500N with SAE 10W 40 lubricant

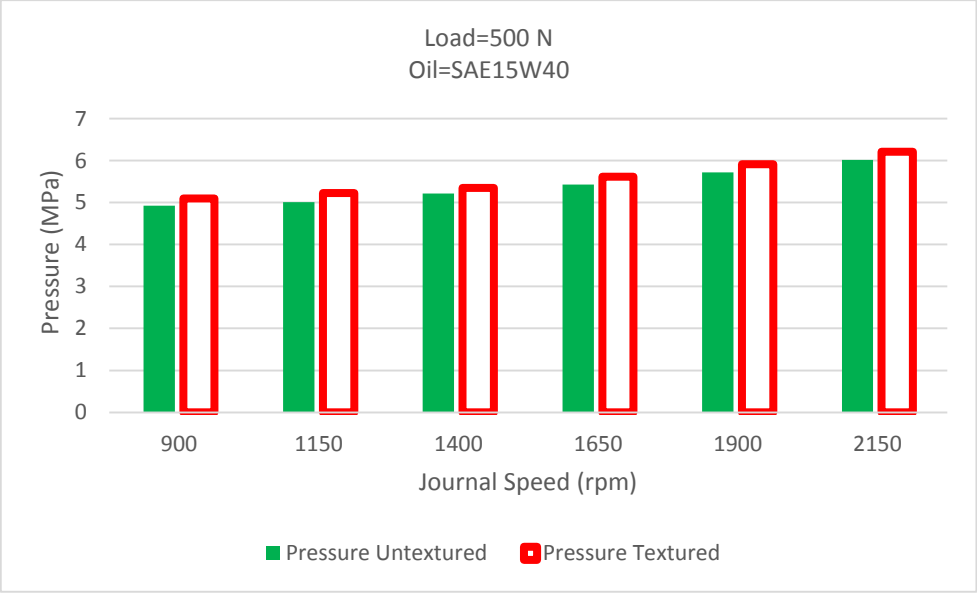

Figure 4.33: Pressure variation with rotational speed at 500N with SAE 15W 40 lubricant

With further increase in the lubricant viscosity, not much rise in the oil film pressure was reported. For SAE 20W40 oil, the maximum oil film pressure gets a slight decrease and fluctuates at higher journal speeds (Figure 4.34).

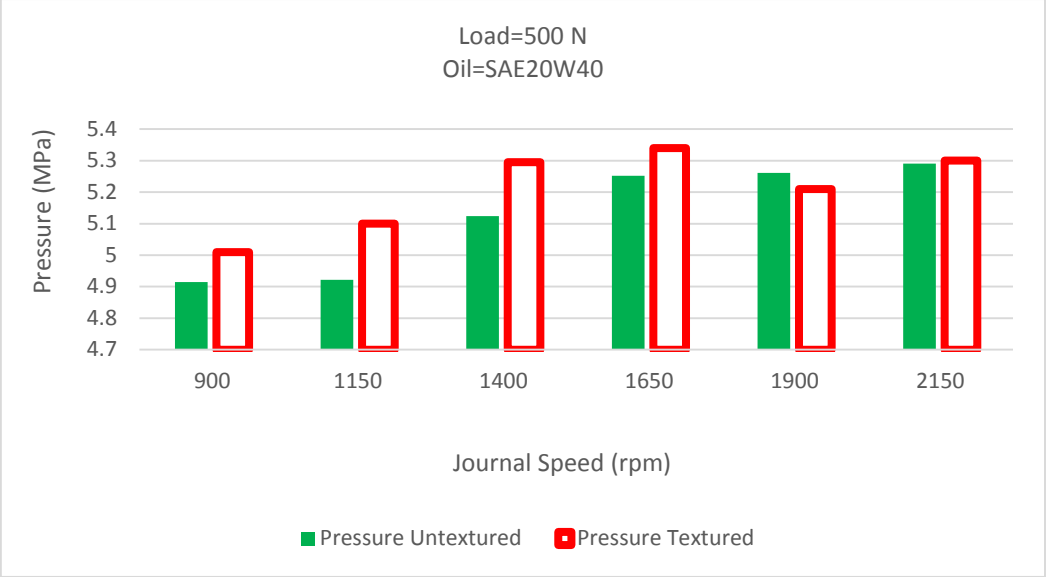

Figure 4.34: Pressure variation with rotational speed at 500N with SAE 20W 40 lubricant

4.3 Simulation

Figure 4.34 shows the variation of oil film pressure for the non-textured bearing surface. The red zone indicates the maximum pressure area whereas a blue part shows the minimum pressure area. The usually the pressure in the blue part is negative because of the cavitation region. The maximum pressure value achieved in the red zone is 10.97 MPa.

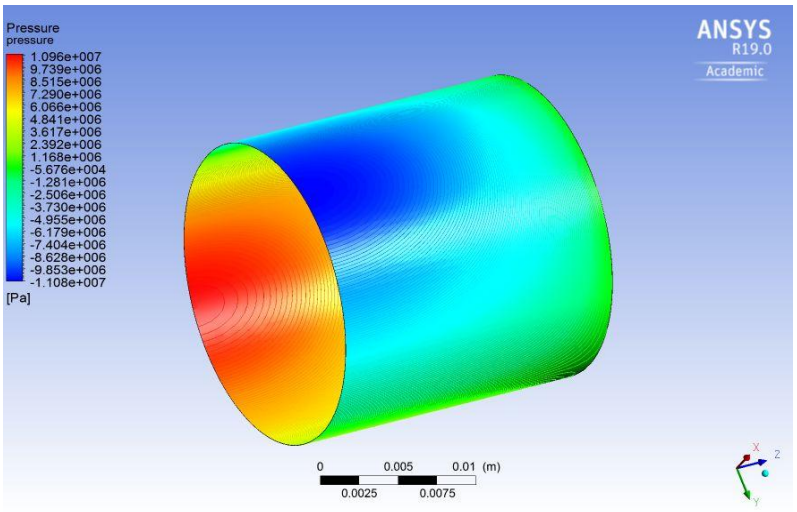

Figure 4.35: Oil film pressure for non-textured bearing surface.

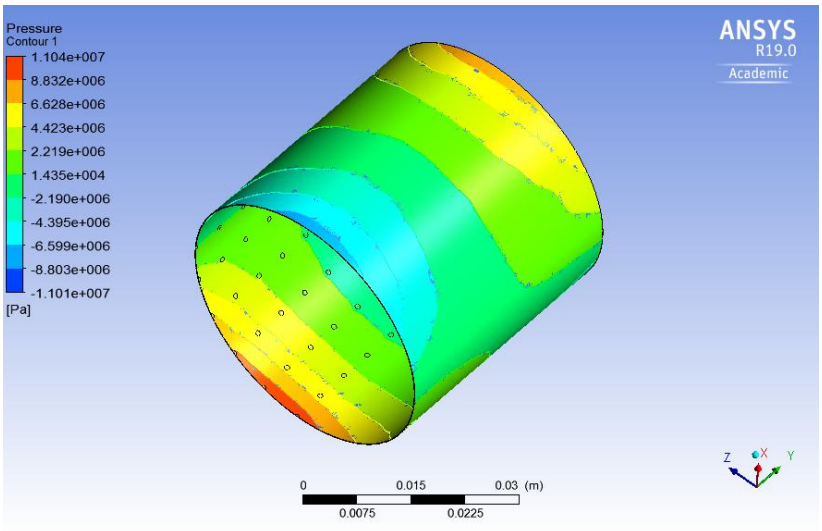

Figure 4.36: Oil film pressure variation for textured bearing surface.

Figure 4.35 shows the oil film pressure variation for the textured bearing surfaces. The textures present on the bearing surface produces some extra pressure which helps in improving the performance of the journal bearing system. The region of maximum pressure and negative pressure are similar to the non-textured bearing. The maximum oil film pressure achieved in case of the textured bearing surface is 11.04 MPa. The distribution of oil film

pressure is also a non-uniform in nature. The small textures on the surface of the bearing act as small bearing surfaces and produce the extra pressure in-between them. This extra pressure help in improving the performance of the journal bearing system.

Chapter 5 Conclusions and Future Works

5.1 Conclusions

In the present thesis work, attempts have been made to improve the performance parameters of a journal bearing. The designing of the bearing surface and material of the bearing were considered and worked upon for the possible improvement in the journal bearing performance. Four bearing materials were fabricated and experimentally tested and compared with the conventional journal bearing material. The main conclusions drawn from this thesis work are given below.

- Two aluminium based composites were prepared by using flyash and graphite as the reinforcing agents. The flyash and graphite both have proved to improve the wear and friction properties of the aluminium material. Two copper based material, namely, copper-aluminium (Cu-NiAl) and copper-phosphorous (Cu-PAl) were fabricated and tested for mechanical properties. It is observed that the addition of aluminium to the copper matrix have improved the properties of the copper, however, higher amounts of aluminium may have produced some negative results. The prepared aluminium composite and copper alloys were compared for the wear and friction properties with the conventional lead bronze (Cu-Pb) bearing material and it is observed that copper-phosphorous (Cu-PAl) resulted in the lowest amount of wear and friction in starved and unlubricated conditions. Cu-NiAl performed better under fully flooded lubrication regime.

- In fully flooded tribological studies, the three copper based fabricated materials resulted in very low amounts of specific wear rate and coefficient of friction. The presence of aluminium and nickel contents in Cu-NiAl helped in maintaining low specific wear rate and coefficient of friction values as compared to Cu-PAl and Cu-Pb.

- During the starved and unlubricated condition, Cu-PAl has shown better results with low specific wear rate and coefficient of friction as compared to Cu-NiAl and Cu-Pb. A soft layer of copper and phosphorous-rich elements formed on the disc surface,

which reduces the coefficient of friction and specific wear rate. However, Aluminium Flyash composite exhibits lowest coefficient of friction and largest specific wear rate.

- The scanning electron microscopy examination of the unlubricated pin samples reveals thick wear lines and wear grooves on the surface of Cu-NiAl material. Smaller and thin wear lines were visible for Cu-PAl material which indicates low wear.

- The EDX analysis of worn disc samples indicates the presence of copper-phosphorous layer for Cu-PAl and copper-lead layer for Cu-Pb, which reduces the wear and coefficient of friction. No such permanent layer was visible for Cu-NiAl material, rather wear debris were seen scattered around the disc surface.

- It is also observed that Flyash particles and graphite particles mix very well in the aluminium and makes an aluminium metal matrix composite. These particles help in improving the tribological properties of the aluminium, however, for heavy duty work in journal bearing, these were not suitable materials to operate.

- Surface texturing technique was used to improve the operating performance of the journal bearing system. A specific pattern of concave surface textures was designed and produced on the inner surface of the bearing. The maximum pressure zone of the bearing circumference was selected as the area for fabricating the surface textures and Electric Discharge Machining (EDM) process was used to generate the designed texture pattern. A specialized electrode was fabricated for this purpose. The textured journal bearing performed better as compared to the conventional journal bearing system for the considered operating parameters of the journal bearing in hydrodynamic lubrication regime.

- A simple, Computational fluid dynamics (CFD) methodology was applied to inspect the pressure profile of the lubricating film for a non-textured and textured bearing surface. This model could be utilized to inspect the behaviour of the lubricating film at different rotational speeds and lubricant properties.

5.2 Future Scope of work

- This thesis work presents the insights about the tribological properties of the lead-free journal bearing material and compared their properties with the conventional lead bronze material. Other properties of the bearing materials could be evaluated further for the broad analysis of the lead-free bearing materials.

- The effects of surface textures have found to improve the performance of the journal bearing. However, further study on the effects of different surface texture shapes and sizes could be conducted to inspect their effects.

References

1. Abhijeet, G Chavan, D.G., Thombare, N.K., Chhapkhane.Eexperimental investigation of effect of lubricant viscosity on vibrations of plain hydrodynamic journal bearing system. International journal for research & development in technology **3** (4), 31-36 (2015).

2. Ahmad, M. A., Kasolang, S. & Dwyer-Joyce, R. S. Experimental study on the effects of oil groove location on temperature and pressure profiles in journal bearing lubrication. *Tribol. Int.* **74,** 79–86 (2014).

3. Akhlaghi, F. & Zare-Bidaki, A. Influence of graphite content on the dry sliding and oil impregnated sliding wear behavior of Al 2024–graphite composites produced by in situ powder metallurgy method. *Wear* **266,** 37–45 (2009).

4. Al-Qutub, A. M., Allam, I. M. & Qureshi, T. W. Effect of sub-micron Al2O3 concentration on dry wear properties of 6061 aluminum based composite. *J. Mater. Process. Technol.* **172,** 327–331 (2006).

5. Anil, P. M., Kumar, R. & Sethuramiah, A. Effect of initial roughness and oxidation on the running-in wear of machined surfaces under dry sliding. *Int. J. Surf. Sci. Eng.* **11,** 45 (2017).

6. ASTM Standard D4052. *Standard Test Method for Density and Relative Density of Liquids by Digital Density Meter*. (ASTM International, West Conshohocken, PA, United States, 1984).

7. ASTM Standard D445. *Standard Method of Test for Viscosity of Transparent and Opaque Liquids (Kinematic and Dynamic Viscosities)*. (ASTM International, West Conshohocken, PA, United States., 1970).

8. ASTM Standard E387. in (ASTM International, West Conshohocken, PA, United States., 2017).

9. ASTM Standard G99. in (ASTM International, West Conshohocken, PA, United States., 2005).

10. Ausas, Roberto, Ragot, Patrick, Leiva, Jorge, Jai, Mohammed, Bayada, Guy & C. Gustavo. Buscaglia . The Impact of the Cavitation Model in the Analysis of Microtextured Lubricated Journal Bearings. *J. Tribol.* **129,** 868 (2007).

11. Baradeswaran, A. & Perumal, A. E. Wear and mechanical characteristics of Al 7075/graphite composites. *Compos. Part B Eng.* **56,** 472–476 (2014).

12. Basavarajappa, S., Chandramohan, G. & Paulo Davim, J. Application of Taguchi techniques to study dry sliding wear behaviour of metal matrix composites. *Mater. Des.* **28,** 1393–1398 (2007).

13. Basavarajappa, S., Chandramohan, G. & Paulo Davim, J. Application of Taguchi techniques to study dry sliding wear behaviour of metal matrix composites. *Mater. Des.* **28,** 1393–1398 (2007).

14. Basumatary, J. & Wood, R. J. K. Synergistic effects of cavitation erosion and corrosion for nickel aluminium bronze with oxide film in 3.5% NaCl solution. *Wear* **376–377,** 1286–1297 (2017).

15. Bhansali, K. J. & Mehrabian, R. Abrasive Wear of Aluminum-Matrix Composites. *JOM* **34,** 30–34 (1982).

16. Blau, P. J. Investigation of the nature of micro-indentation hardness gradients below sliding contacts in five copper alloys worn against 52100 steel. *J. Mater. Sci.* **19,** 1957–1968 (1984).

17. Bompos, D. A. & Nikolakopoulos, P. G. Tribological design of a multistep journal bearing. *Simul. Model. Pract. Theory* **68,** 18–32 (2016).

18. Bouyer, J. & Fillon, M. Experimental measurement of the friction torque on hydrodynamic plain journal bearings during start-up. *Tribol. Int.* **44,** 772–781 (2011).

19. Brizmer, V. & Kligerman, Y. A Laser Surface Textured Journal Bearing. *J. Tribol.* **134,** 031702 (2012).

20. Candan, E., Ahlatci, H. & Çïmenoğlu, H. Abrasive wear behaviour of Al–SiC composites produced by pressure infiltration technique. *Wear* **247,** 133–138 (2001).

21. Chen, J. K. & Huang, I. S. Thermal properties of aluminum–graphite composites by powder metallurgy. *Compos. Part B Eng.* **44,** 698–703 (2013).

22. Chmura, W. & Gronostajski, Z. Bearing composites made from aluminium and aluminium bronze chips. *J. Mater. Process. Technol.* **178,** 188–193 (2006).

23. Christensen, H. & Tonder, K. The Hydrodynamic Lubrication of Rough Journal Bearings. *J. Lubr. Technol.* **95,** 166 (1973).

24. Costa, H. L. & Hutchings, I. M. Hydrodynamic lubrication of textured steel surfaces under reciprocating sliding conditions. *Tribol. Int.* **40,** 1227–1238 (2007).

25. Cupillard, S., Glavatskih, S. & Cervantes, M. J. Computational fluid dynamics analysis of a journal bearing with surface texturing. *Proc. Inst. Mech. Eng. Part J J. Eng. Tribol.* **222,** 97–107 (2008).

26. Davim, J. P., Marques, N. & Baptista, A. M. Effect of carbon fibre reinforcement in the frictional behaviour of Peek in a water lubricated environment. *Wear* **251,** 1100–1104 (2001).

27. Dhande, D. Y. & Pande, D. W. Multiphase flow analysis of hydrodynamic journal bearing using CFD coupled Fluid Structure Interaction considering cavitation. *J. King Saud Univ. - Eng. Sci.* **30,** 345–354 (2018).

28. Dinaharan, I., Kalaiselvan, K., Akinlabi, E. T. & Davim, J. P. Microstructure and wear characterization of rice husk ash reinforced copper matrix composites prepared using friction stir processing. *J. Alloys Compd.* **718,** 150–160 (2017).

29. Ding, Y., Lv, Yuting, Chen, Kai, Zhao, Bingjai, Han, Yuanfei, Wang, Liqiang, Lu, Weijie. Effects of microstructure on the stress corrosion cracking behavior of nickel-aluminum bronze alloy in 3.5% NaCl solution. *Mater. Sci. Eng. A* **733,** 361–373 (2018).

30. Edalati, K., Ashida, M., Horita, Z., Matsui, T. & Kato, H. Wear resistance and tribological features of pure aluminum and Al–Al2O3 composites consolidated by high-pressure torsion. *Wear* **310,** 83–89 (2014).

31. Elrod, H. G. and A. A computer program for cavitation and starvation problems. Technical report 190. *1st LEEDS LYON Symp. Cavitation Relat. Phenom. Lubr. I.M.E.* 37–41 (1974).

32. Equey, S., Houriet, A. & Mischler, S. Wear and frictional mechanisms of copper-based bearing alloys. *Wear* **273,** 9–16 (2011).

33. Equey, S., Houriet, A. & Mischler, S. Wear and frictional mechanisms of copper-based bearing alloys. *Wear* **273,** 9–16 (2011).

34. Etsion, I. Improving Tribological Performance of Mechanical Components by Laser Surface Texturing. *Tribol. Lett.* **17,** 733–737 (2004).

35. Ettles, C. M., Seyler, J. & Bottenschein, M. Some Effects of Start-Up and Shut-Down on Thrust Bearing Assemblies in Hydro-Generators. *J. Tribol.* **125,** 824 (2003).

36. Feyzullahoğlu, E. & Şakiroğlu, N. The wear of aluminium-based journal bearing materials under lubrication. *Mater. Des.* **31,** 2532–2539 (2010).

37. Fowell, M., Olver, A. V., Gosman, A. D., Spikes, H. A. & Pegg, I. Entrainment and Inlet Suction: Two Mechanisms of Hydrodynamic Lubrication in Textured Bearings. *J. Tribol.* **129,** 336 (2007).

38. Gao, F., Liu, R. & Wu, X. J. Tribaloy alloy reinforced tin–bronze composite coating for journal bearing applications. *Thin Solid Films* **519,** 4809–4817 (2011).

39. Gao, G., Yin, Z., Jiang, D. & Zhang, X. Numerical analysis of plain journal bearing under hydrodynamic lubrication by water. *Tribol. Int.* **75,** 31–38 (2014).

40. Gao, L. L. & Cheng, X. H. Microstructure and dry sliding wear behavior of Cu–10%Al–4%Fe alloy produced by equal channel angular extrusion. *Wear* **265,** 986–991 (2008).

41. Gebretsadik, D. W., Hardell, J. & Prakash, B. Tribological performance of tin-based overlay plated engine bearing materials. *Tribol. Int.* **92,** 281–289 (2015).

42. Gebretsadik, D. W., Hardell, J. & Prakash, B. Friction and wear characteristics of different Pb-free bearing materials in mixed and boundary lubrication regimes. *Wear* **340–341,** 63–72 (2015).

43. Goodman John. Recent advances in Friction. *Proc. Inst. Civ. Eng* **85,** 376–392 (1886).

44. Harnoy, A. Model-Based Investigation of Friction During Start-Up of Hydrodynamic Journal Bearings. *J. Tribol.* **117,** 667 (1995).

45. Hsu, T.-C., Chen, J.-H., Chiang, H.-L. & Chou, T.-L. Lubrication performance of short journal bearings considering the effects of surface roughness and magnetic field. *Tribol. Int.* **61,** 169–175 (2013).

46. Huei-Long, L., Wun-Hwa, L. & Sammy Lap-Ip Chan. Abrasive wear of powder metallurgy Al alloy 6061-SiC particle composites. *Wear* **159,** 223–231 (1992).

47. I M Hutchings. in *Tribology: Friction and Wear of Engineering Materials* (Edward Arnold, London, 1992).

48. İzciler, M. & Muratoglu, M. Wear behaviour of SiC reinforced 2124 Al alloy composite in RWAT system. *J. Mater. Process. Technol.* **132,** 67–72 (2003).

49. J. Paulo DavimNuno Marques. Evaluation of Tribological Behaviour of Polymeric Materials for Hip Prostheses Application. *Tribol. Lett.* **11,** 91–94 (2001).

50. Kandavel, T. K., Panneerselvam, T. & Mohan, V. Experimental investigation on wear characteristics of sintered Fe-C-Cr low alloy steels. *Int. J. Surf. Sci. Eng.* **11,** 381 (2017).

51. Kango, S., Singh, D. & Sharma, R. K. Numerical investigation on the influence of surface texture on the performance of hydrodynamic journal bearing. *Meccanica* **47,** 469–482 (2012).

52. Kango, S., Sharma, R. & Pandey, R. Comparative analysis of textured and grooved hydrodynamic journal bearing. *Proc. Inst. Mech. Eng. Part J J. Eng. Tribol.* **228,** 82–95 (2014).

53. Kaplan, M. & Yildiz, A. K. The effects of production methods on the microstructures and mechanical properties of an aluminum bronze. *Mater. Lett.* **57,** 4402–4411 (2003).

54. Keogh, P. S., Gomiciaga, R. & Khonsari, M. M. CFD Based Design Techniques for Thermal Prediction in a Generic Two-Axial Groove Hydrodynamic Journal Bearing. *J. Tribol.* **119,** 428 (1997).

55. Khatri, C. B. & Sharma, S. C. Influence of textured surface on the performance of non-recessed hybrid journal bearing operating with non-Newtonian lubricant. *Tribol. Int.* **95,** 221–235 (2016).

56. Khatri, C. B. & Sharma, S. C. Influence of textured surface on the performance of non-recessed hybrid journal bearing operating with non-Newtonian lubricant. *Tribol. Int.* **95,** 221–235 (2016).

57. Kim, H. G. & Jeon, S. I. Effect on friction of engine oil seal with engine oil viscosity. *Int. J. Automot. Technol.* **9,** 601–606 (2008).

58. Kim, S. S., Park, D. C. & Lee, D. G. Characteristics of carbon fiber phenolic composite for journal bearing materials. *Compos. Struct.* **66,** 359–366 (2004).

59. Kim, S. S., Yu, H. N., Hwang, I. U. & Lee, D. G. Characteristics of wood–polymer composite for journal bearing materials. *Compos. Struct.* **86,** 279–284 (2008).

60. Krishnan, B. P. & Rohatgi, P. K. Modification of Al–Si alloy melts containing graphite particle dispersions. *Met. Technol.* **11,** 41–44 (1984).

61. Krithivasan, R. & Khonsari, M. M. Thermally Induced Seizure in Journal Bearings During Startup and Transient Flow Disturbance. *J. Tribol.* **125,** 833 (2003).

62. Li, W. S., Wang, Z.P., Lu, Y., Jin, Y.H., Yuan, L.H., Wang, F. Mechanical and tribological properties of a novel aluminum bronze material for drawing dies. *Wear* **261,** 155–163 (2006).

63. Li, Y., Ngai, T. L. & Xia, W. Mechanical, friction and wear behaviors of a novel high-strength wear-resisting aluminum bronze. *Wear* **197,** 130–136 (1996).

64. Lin, C. B., Chang, R. J. & Weng, W. P. A study on process and tribological behavior of Al alloy/Gr. (p) composite. *Wear* **217,** 167–174 (1998).

65. Linjamaa, A., Lehtovaara, A., Larsson, R., Kallio, M. & Söchting, S. Modelling and analysis of elastic and thermal deformations of a hybrid journal bearing. *Tribol. Int.* **118,** 451–457 (2018).

66. 7Lu, X. & Khonsari, M. M. An Experimental Investigation of Dimple Effect on the Stribeck Curve of Journal Bearings. *Tribol. Lett.* **27,** 169–176 (2007).

67. Luo, Q., Wu, Z., Qin, Z., Liu, L. & Hu, W. Surface modification of nickel-aluminum bronze alloy with gradient Ni-Cu solid solution coating via thermal diffusion. *Surf. Coatings Technol.* **309,** 106–113 (2017).

68. Mathavan, J. J. & Patnaik, A. Analysis of wear properties of aluminium based journal bearing alloys with and without lubrication. *IOP Conf. Ser. Mater. Sci. Eng.* **149,** 012052 (2016).

69. Mazahery, A. & Shabani, M. O. Experimental Investigation on the Aging Response, Hardness and Total Impact Energy Absorption of Sr-Modified Heat-Treatable Cast Automotive Aluminum Alloys. *Trans. Indian Inst. Met.* **67,** 753–759 (2014).

70. Mazahery, A. & Shabani, M. O. Tribological behaviour of semisolid–semisolid compocast Al–Si matrix composites reinforced with TiB2 coated B4C particulates. *Ceram. Int.* **38,** 1887–1895 (2012).

71. McCarthy, D. M. C. & Glavatskih, S. B. Assessment of polymer composites for hydrodynamic journal-bearing applications. *Lubr. Sci.* **21,** 331–341 (2009).

72. Meng, F. M., Zhang, L., Liu, Y. & Li, T. T. Effect of compound dimple on tribological performances of journal bearing. *Tribol. Int.* **91,** 99–110 (2015).

74. Muzakkir, S., Lijesh, K., Hirani, H. & Thakre, G. Effect of cylindricity on the tribological performance of heavily loaded slow-speed journal bearing. *Proc. Inst. Mech. Eng. Part J J. Eng. Tribol.* **229,** 178–195 (2015).

75. Petrov., P. N. Friction in machines and the effect of the lubricant. *Inzhenernii Zhurnat St. Petersbg.* **1,** 71–140 (1883).

76. Panagopoulos, C. N., Georgiou, E. P. & Simeonidis, K. Lubricated wear behavior of leaded α+β brass. *Tribol. Int.* **50,** 1–5 (2012).

77. Panda, J. N., Bijwe, J. & Pandey, R. K. Role of treatment to graphite particles to increase the thermal conductivity in controlling tribo-performance of polymer composites. *Wear* **360–361,** 87–96 (2016).

78. Patel, N. S., Vakharia, D. P., Deheri, G. M. & Patel, H. C. Experimental performance analysis of ferrofluid based hydrodynamic journal bearing with different combination of materials. *Wear* **376–377,** 1877–1884 (2017).

79. Pathak, J. P. & Mohan, S. Tribological behaviour of conventional Al-Sn and equivalent Al-Pb alloys under lubrication. *Bull. Mater. Sci.* **26,** 315–320 (2003).

80. Pathak, J. P., Torabian, H. & Tiwari, S. N. Antiseizure and antifriction characteristics of Al-Si-Pb alloys. *Wear* **202,** 134–141 (1997).

81. Petrica, M., Duscher, B., Koch, T. & Archodoulaki, V. M. Impact of surface roughness and contact pressure on wear behaviour of PEEK, POM, and PE-UHMW. *Int. J. Surf. Sci. Eng.* **11,** 65 (2017).

82. Pistner, C. A. Some Effects of Start-Up Transient Loads on Shoe Bearings for Large Hydraulic Pump/Turbines. *Tribol. Trans.* **39,** 93–98 (1996).

83. Poddar, S. & Tandon, N. Detection of journal bearing vapour cavitation using vibration and acoustic emission techniques with the aid of oil film photography. *Tribol. Int.* **103,** 95–101 (2016).

84. Prasad, B. K. Effects of Silicon Addition and Test Parameters on Sliding Wear Characteristics of Zinc-Based Alloy Containing 37.5% Aluminium. *Mater. Trans. JIM* **38,** 701–706 (1997).

85. Prasad, B. K., Patwardhan, A. K. & Yegneswaran, A. H. Factors controlling dry sliding wear behaviour of a leaded tin bronze. *Mater. Sci. Technol.* **12,** 427–435 (1996).

86. Prasad, B. . Effect of microstructure on the sliding wear performance of a Zn–Al–Ni alloy. *Wear* **240,** 100–112 (2000).

87. Qin, Z. *et al.* Improving corrosion resistance of nickel-aluminum bronzes by surface modification with chromium ion implantation. *Surf. Coatings Technol.* **334,** 402–409 (2018).

88. Qiu, Y. & Khonsari, M. M. On the Prediction of Cavitation in Dimples Using a Mass-Conservative Algorithm. *J. Tribol.* **131,** 041702 (2009).

89. Rahimipour, M. R., Tofigh, A. A., Mazahery, A. & Shabani, M. O. Strategic developments to improve the optimization performance with efficient optimum solution and produce high wear resistance aluminum–copper alloy matrix composites. *Neural Comput. Appl.* **24,** 1531–1538 (2014).

90. RF, S. *ASM Specialty Handbook Copper and Copper Alloys*. (ASM International, 1992).

91. Rohatgi, P. K., Sobczak, J., Asthana, R. & Kim, J. K. Inhomogeneities in silicon carbide distribution in stirred liquids—a water model study for synthesis of composites. *Mater. Sci. Eng. A* **252,** 98–108 (1998).

91. Sahin, Y. Wear behaviour of aluminium alloy and its composites reinforced by SiC particles using statistical analysis. *Mater. Des.* **24,** 95–103 (2003).

92. Sahoo, B., Kumar, R., Joseph, J., Sharma, A. & Paul, J. Preparation of aluminium 6063-graphite surface composites by an electrical resistance heat assisted pressing technique. *Surf. Coatings Technol.* **309,** 563–572 (2017).

93. Santos, E. N., Blanco, C. J. C., Macêdo, E. N., Maneschy, C. E. A. & Quaresma, J. N. N. Integral transform solutions for the analysis of hydrodynamic lubrication of journal bearings. *Tribol. Int.* **52,** 161–169 (2012).

94. Sastry, C. V. S. H. S. R. & Janardhana, G. R. Influence of process and test parameters on the dry sliding wear behaviour of Al-Pb alloys produced by mechanical alloying. *Int. J. Surf. Sci. Eng.* **4,** 377 (2010).

95. SAUD, S. N., HAMZAH, E., ABUBAKAR, T. & BAKHSHESHI-RAD, H. R. Correlation of microstructural and corrosion characteristics of quaternary shape memory alloys Cu–Al–Ni–X (X=Mn or Ti). *Trans. Nonferrous Met. Soc. China* **25,** 1158–1170 (2015).

96. Scaraggi, M., Mezzapesa, Francesco, Carbone, Giuseppe, Ancona, Antonia, Sorgente, Donato, Lugara, Pietro M. Minimize friction of lubricated laser-microtextured-surfaces by tuning microholes depth. *Tribol. Int.* **75,** 123–127 (2014).

97. Shabani, M. O., Mazahery, A., Davami, P. & Razavi, M. Silicon morphology modelling during solidification process of A356 Al alloy. *Int. J. Cast Met. Res.* **25,** 53–58 (2012).

98. Shamsipour, M., Pahlevani, Z., Shabani, M. O. & Mazahery, A. Optimization of the EMS process parameters in compocasting of high-wear-resistant Al-nano-TiC composites. *Appl. Phys. A* **122,** 457 (2016).

99. Sharma, S. C., Girish, B. M., Kamath, R. & Satish, B. M. Graphite particles reinforced ZA-27 alloy composite materials for journal bearing applications. *Wear* **219,** 162–168 (1998).

100. Shi, Z., Sun, Y., Bloyce, A. & Bell, T. Unlubricated rolling-sliding wear mechanisms of complex aluminium bronze against steel. *Wear* **193,** 235–241 (1996).

101. Shinde, A. B. & Pawar, P. M. Multi-objective optimization of surface textured journal bearing by Taguchi based Grey relational analysis. *Tribol. Int.* **114,** 349–357 (2017).

102. Sinanoğlu, C., Nair, F. & Karamış, M. B. Effects of shaft surface texture on journal bearing pressure distribution. *J. Mater. Process. Technol.* **168,** 344–353 (2005).

103. Singh, M., Prasad, B. ., Mondal, D. . & Jha, A. . Dry sliding wear behaviour of an aluminium alloy–granite particle composite. *Tribol. Int.* **34,** 557–567 (2001).

104. Song, Q. N., Zheng, Y. G., Jiang, S. L., Ni, D. R. & Ma, Z. Y. Comparison of Corrosion and Cavitation Erosion Behaviors Between the As-Cast and Friction-Stir-Processed Nickel Aluminum Bronze. *CORROSION* **69,** 1111–1121 (2013).

105. Sriram, S. B. and G. No Title. *IEEE-International Conf. Adv. Eng. Sci. Manag.* 132–135 (2012).

106. Tala-Ighil, N., Fillon, M. & Maspeyrot, P. Effect of textured area on the performances of a hydrodynamic journal bearing. *Tribol. Int.* **44,** 211–219 (2011).

107. Taya, M., Lulay, K. E. & Lloyd, D. J. Strengthening of a particulate metal matrix composite by quenching. *Acta Metall. Mater.* **39,** 73–87 (1991).

108. Thapliyal, S. & Dwivedi, D. K. Study of the effect of friction stir processing of the sliding wear behavior of cast NiAl bronze: A statistical analysis. *Tribol. Int.* **97,** 124–135 (2016).

109. Thurston Robert H. *Friction and Lubrication*. (Railroad Gazette Publication Co, 1879).

110. Torabian, H., Pathak, J. P. & Tiwari, S. N. Wear characteristics of Al-Si alloys. *Wear* **172,** 49–58 (1994).

111. Tower Beauchamp. 1st report on Friction Experiments. *Proc. Inst. Mech. Eng.* **1,** 632–666 (1891).

112. Tzeng, S. T. & Saibel, E. On the effects of surface roughness in the hydrodynamic lubrication theory of a short journal bearing. *Wear* **10,** 179–184 (1967).

113. Vettivel, S. C., Selvakumar, N. & Ponraj, P. V. Mechanical Behaviour of Sintered Cu-5%W Nano Powder Composite. *Procedia Eng.* **38,** 2874–2880 (2012).

114. Vijayaraghavan, D. & Brewe, D. E. Effect of Rate of Viscosity Variation on the Performance of Journal Bearings. *J. Tribol.* **120,** 1 (1998).

115. Von Pauli, F.A. Uber den Widerstand der Zapfenreibung, Kunst und Gewerbeblatt des Polytechnischen Verein des Konigreich Bayern. **8/9,** 452–469 (1849).

116. Voong, M., Neville, A. & Castle, R. The Compatibility of Crankcase Lubricant–Material Combinations in Internal Combustion Engines. *Tribol. Lett.* **15,** 431–441 (2003).

117. W., B. *Materials Technology for Technicians*. (Butterworth, 1981).

118. Wang, A. & Rack, H. J. Transition wear behavior of SiC-particulate- and SiC-whisker-reinforced 7091 Al metal matrix composites. *Mater. Sci. Eng. A* **147,** 211–224 (1991).

119. Wang, H., Liu, Z., Zou, L. & Yang, J. Influence of both friction and wear on the vibration of marine water lubricated rubber bearing. *Wear* **376–377,** 920–930 (2017).

120. Wang, Q. Seizure failure of journal-bearing conformal contacts. *Wear* **210,** 8–16 (1997).

121. Wang, W., Huang, Z., Shen, D., Kong, L. & Li, S. The Effect of Triangle-Shaped Surface Textures on the Performance of the Lubricated Point-Contacts. *J. Tribol.* **135,** 021503 (2013).

122. Wert, J. J., Singerman, S. A., Caldwell, S. G. & Quarles, R. A. The role of stacking fault energy and induced residual stresses on the sliding wear of aluminum bronze. *Wear* **91,** 253–267 (1983).

123. Wu, Z., Cheng, Y. F., Liu, L., Lv, W. & Hu, W. Effect of heat treatment on microstructure evolution and erosion–corrosion behavior of a nickel–aluminum bronze alloy in chloride solution. *Corros. Sci.* **98,** 260–270 (2015).

124. Yan, J., Lindo, A., Schwaiger, R. & HODGE, A. M. Sliding wear behavior of fully nanotwinned Cu alloys. *Friction* (2018). doi:10.1007/s40544-018-0220-z

125. Yang, L. J. The transient and steady wear coefficients of A6061 aluminium alloy reinforced with alumina particles. *Compos. Sci. Technol.* **63,** 575–583 (2003).

126. Zhang, H., Zhang, D. Y., Hua, M., Dong, G. N. & Chin, K. S. A Study on the Tribological Behavior of Surface Texturing on Babbitt Alloy under Mixed or Starved Lubrication. *Tribol. Lett.* **56,** 305–315 (2014).

Appendix-I

A1: Specifications of Journal bearing rig TR-660

Table A1.1: Specification of machine

S.No.	Test Parameters	Details
1	Pressure	Digital Pressure Sensor
2	Friction Factor	
3	Oil Flow Rate	
4	Temperature of Inlet of Bearing	Thermocouple
5	Bearing Specifications	Cylindrical Bearing, id=40mm, length=40mm, wall thickness 10mm, c/r=0.0015, hole dia for oil supply=6mm, 10 holes for pressure data
6	Load Applied	3000N
7	Speed Range	40 to 8000 rpm
8	Permissible Error in Performance	Thermocouple= ± 1°C Pressure= ± 1% Mpa Frictional Torque= ± 2%Nm Shaft Speed= ± 0.1% rpm Flow Rate= ± 0.5%lit/min

Table A1.2: Electrical Specification

S.No.	Part Detail		Range
1	AC Induction motor	Make	Seimens 2.2 kw
		Specifications	2.2 kw, 1435 rpm 415V/ 3 ph/ 50 Hz, 4.4 A, foot mounted
2	Variable frequency drive	Make	TB woods
		Output supply	415V, 5.8 A, 3 ph
		Specifications	2.2 kw, 5.8 A, 415 V, 3 ph
3	AC motor for lubrication	Make; Capacity	SEF Induction motor
		Specifications	0.37 kw, 1350 rpm, 1.2 A, flange mounted, 230 V
		Input supply	230 V/ 50 Hz/ 1 ph, 0.5 A
4	Power Required		2.5 KVA

Table A1.3: Sensor Specifications

S.No.	Part Detail		Specifications
1	Speed	Sensor	Output from drive
		Range	Min ;40 rpm, Max 8000 rpm
		Least Count	1 rpm
		Accuracy	(1 ± 2% measured speed) rpm
2	Temperature	Type	PT 100, make ; Hot set
		Range	Max 200°C
		Least Count	0.1°C
		Accuracy	(0.1 ± 1% measured temp) °C
3	Pressure	Sensor	Digital stainless steel isolated pressure sensor, make ; measurement specialties
		Range	10 Mpa, or 100 bar
		Least Count	0.001 Mpa (1 Kpa)
		Accuracy	(0.001 ± 1% measured value) Mpa
4	Frictional Torque	Sensor	Beam type load cell make ; sensortronics, cap 30 kg
		Range	15 Nm
		Least Count	0.01 Nm
		Accuracy	(0.1 ± 1% measured value) Nm

Table A1.4: Mechanical Specification

SI NO.	Part detail		Range
1.	Shaft detail		22 ± 0.005mm
	Journal outer diameter fitted on shaft		40 -0.005/0.006mm
	Journal inner diameter fitted on shaft		22.035mm
2.	Bearing	Inner dia	40 +0.050/006mm
		Width	40.04mm
3.	Radial clearance		0.027mm
4.	Length/ dia (l/d) ratio		1
	c/r ratio		0.00135
5.	Base plate height from floor		800mm
6.	Journal height from base plate		150mm
7.	Loading bracket height from base plate		760mm
8.	Maximum load		3000N
	Loading ratio		1:5
	Frictional torque distance		51mm
9.	Spindle speed	Min speed	40
		Max speed	8000rpm
10.	Pulley ratio	Speed upto 300 rpm	4:1
		Speed above 300rpm	1:4
11.	Overall size of the machine L*W*H		100*750*1560mm
12.	Weight of the machine		240kg
	Weight of controller		11kg
	Total weight		60kg
13.	Floor size L*W		2000*1500mm
14.	Lubrication unit	Make	Cenlube system
		Oil pressure	5 to 10 bar
		Tank capacity	25 lit
		Size l*b*h	370*290*300mm

Appendix-II

A2: Specifications of Pin on Disc Tribometer

Table A2.1: Pin on Disc tribometer specifications

Parameter	Value	
Disc speed	Range (rpm)	200-2000
	Sensor	Drive output
	Least count (rpm)	1
Load Parameters	Range (N)	0-200
	Specification	20 Kg Beam type load cell
	Least count (N)	0.1
Machine Parameters	Range (mm)	2
	Sensors specs	LVDT, make: Syscon
	Least count (μm)	0.1
Wear Track Diameter (mm)		150-50

A Brief Biographical Sketch

Vipin Kumar Sharma

Mr. Vipin Kuamr Sharma received his B.Tech degree in Mechanical Engineering from Amritsar College of Engineering and Technology, (Affiliated to Punjab Technical University), Punjab, India and M.E. Degree from Delhi College of Engineering (Delhi University), Delhi, India. He is working as an Assistant Professor in the Department of Mechanical and Automation Engineering at Maharaja Agrasen Institute of Technology, Delhi, India. He is actively engaged in teaching and research. As a recognition of his academic achievements, He was awarded the first rank merit certificate by Delhi Technological University for securing 1st rank in ME (Production Engineering) course. He has many research publications in reputed journals/conference proceedings. He is currently working in the area of tribology and advanced materials.